

**ANALYSIS OF AGGREGATE IMAGING SYSTEM (AIMS) MEASUREMENTS
AND THEIR RELATIONSHIP TO ASPHALT PAVEMENT SKID RESISTANCE**

A Thesis

by

ANTHONY DAVID LUCE

Submitted to the Office of Graduate Studies of
Texas A&M University
in partial fulfillment of the requirements for the degree of

MASTER OF SCIENCE

December 2006

Major Subject: Civil Engineering

**ANALYSIS OF AGGREGATE IMAGING SYSTEM (AIMS) MEASUREMENTS
AND THEIR RELATIONSHIP TO ASPHALT PAVEMENT SKID RESISTANCE**

A Thesis

by

ANTHONY DAVID LUCE

Submitted to the Office of Graduate Studies of
Texas A&M University
in partial fulfillment of the requirements for the degree of

MASTER OF SCIENCE

Approved by:

Chair of Committee,	Eyad Masad
Committee Members,	Dallas Little
	Bruce Herbert
Head of Department,	David Rosowsky

December 2006

Major Subject: Civil Engineering

ABSTRACT

Analysis of Aggregate Imaging System (AIMS) Measurements and Their Relationship
to Asphalt Pavement Skid Resistance. (December 2006)

Anthony David Luce, B.S., Texas A&M University

Chair of Advisory Committee: Dr. Eyad Masad

This thesis consists of two parts. The first part includes analyses of the correlation between the results of two Aggregate Imaging System (AIMS) units. These analyses have led to refinements of the AIMS analysis methods of angularity and texture, which resulted in reduced variability in the results and better correlation between the two AIMS units. The refined analysis methods were used to establish a database of the shape characteristics of about 100 aggregate samples from the state of Texas and to propose a new method for the classification of aggregates based on their shape characteristics. This new method of classification is for use in the Texas Department of Transportation (TxDOT) wet weather accident reduction program (WWARP). The use of AIMS texture index and variability in texture within an aggregate source is proposed instead of the British Polish Value (BPV) for classifying aggregates used in pavement surfaces.

The second part of the thesis investigates the relationship between shape characteristics and asphalt pavement skid resistance. Many states have implemented wet weather accident reduction programs aimed at maintaining acceptable levels of

pavement skid resistance. Proper aggregate selection before construction aids in maintaining acceptable levels of skid resistance throughout the life of the pavement.

Several predictive models of pavement skid resistance have been developed over the years. Some of these models account for the influence of aggregate characteristics on pavement skid resistance, primarily through incorporating the results of the BPV test in the model. However, the BPV test is known to have high variability and dependence on experimental factors that are not related to the actual aggregate resistance to polishing. AIMS offers a method to measure aggregate shape characteristics directly in a relatively short period of time. The new method for relating aggregate shape characteristics to pavement skid resistance was verified by relating skid resistance measurements from field test sections to measured aggregate properties from the laboratory. This methodology is expected to be the basis for further study to form a more comprehensive and verified model for the prediction of pavement skid resistance that incorporates measured aggregate properties from the AIMS system.

DEDICATION

I dedicate this thesis to my loving wife Sarah and my parents, Marta and Dave Luce. Without their love and support, I would not be the person that I am today.

ACKNOWLEDGMENTS

First and foremost, I would like to thank Dr. Eyad Masad for all of the opportunities that he has given me throughout my time at Texas A&M University. I am grateful for his encouragement and his confidence in me throughout my research and course of study as well as the knowledge and passion for the subject that he passed on to me. Additionally, I would like to thank Dr. Bruce Herbert and Dr. Dallas Little for serving on my committee and for helping with the review of this thesis.

I would also like to thank the Texas Department of Transportation (TxDOT) and the National Cooperative Highway Research Program (NCHRP) for funding my research projects. I greatly appreciate the input and help of Dr. German Claro, Mr. Ed Morgan, Mr. Michael Dawidczik, and Ms. Caroline Herrera at TxDOT. I would also like to extend thanks to Ed Kaltenbaugh at Pine Instruments, who was instrumental in the revision made to the AIMS device.

I owe many thanks to fellow students who helped me with my research as well. First I would like to thank Dr. Taleb Al-Rousan, who first started working with me on AIMS, and Enad Mahmoud, who helped me with changes made to the system and getting it where it is today. Thanks also to those students who helped me with my research: Stephanie Paine, Genevieve Turco, and especially Patrick Miles, who kept me sane on the long days working together and on numerous trips to Austin to visit TxDOT.

TABLE OF CONTENTS

	Page
ABSTRACT	iii
DEDICATION.....	v
ACKNOWLEDGMENTS.....	vi
TABLE OF CONTENTS.....	vii
LIST OF TABLES.....	x
LIST OF FIGURES	xii
 CHAPTER	
I INTRODUCTION.....	1
Problem Statement.....	1
Objectives of the Study	2
Thesis Organization.....	3
II LITERATURE REVIEW	5
Overview	5
Pavement Skid Resistance.....	5
Pavement Texture Components of Skid Resistance	7
Force Components of Skid Resistance	9
Factors Affecting Skid Resistance.....	11
Pavement Variables.....	11
Traffic Variables	13
Weather Variables.....	13
Other Variables	14
Aggregate Polishing.....	14
Predictive Models for Skid Resistance	17
Summary	21
III DEVELOPMENT AND ANALYSIS OF TXDOT AGGREGATE DATABASE.....	23
Overview	23
Aggregate Tests and Procedures	24

CHAPTER	Page
Aggregate Consensus Properties.....	25
Crushed Face Count	25
Flat and Elongated Particles	26
Sand Equivalent Test	27
Flakiness Index	28
Durability and Deleterious Materials Tests.....	29
Micro-Deval	29
Los Angeles Abrasion	30
Magnesium Sulfate Soundness	30
British Polish Value	31
Aggregate Imaging System Data	32
Aggregate Angularity	32
Texture	34
Sphericity	35
Comparison Between TxDOT and TTI AIMS Results.....	35
Coarse Aggregate Angularity	36
Modification of Coarse Aggregate Angularity	37
Comparison of Modified and Original Angularity Methods for Database Aggregates.....	41
Comparison of AIMS Using Modified Angularity	43
Aggregate Particle Texture Comparison	46
Modification of Texture Method.....	48
Comparison of AIMS Units Using Average Texture Levels 4 and 5	55
Sphericity Comparison	57
Comparison of the Texture of Polishing Coupons.....	59
Comparison of Micro-Deval Results.....	62
Correlation of Micro-Deval and Magnesium Sulfate Soundness	65
Analysis of Accelerated Polishing Test	66
Summary	68
IV CLASSIFICATION OF AGGREGATES	69
Overview	69
Classification Using Clustering Analysis	70
Classification Using Quartile Analysis	73
Classification of Aggregates Used in Asphalt Pavement Surfaces	78
Summary	84

CHAPTER	Page
V RELATIONSHIP OF AGGREGATE TEXTURE TO PAVEMENT SKID RESISTANCE	85
Overview	85
Background	85
Experimental Methodology	87
Pavement Test Sections	87
Mix Design	89
Skid Measurements	90
Evaluation of Aggregate Polishing	91
AIMS	92
Micro-Deval Test	93
Statistical Model	93
Results	94
Summary	99
VI CONCLUSIONS AND RECOMMENDATIONS	102
Conclusions	102
Recommendations	106
REFERENCES	107
APPENDIX A	113
VITA	146

LIST OF TABLES

TABLE	Page
3.1 Summary of Tests Run Between the Two Laboratories.....	24
3.2 Weight Specifications for Micro-Deval Test.....	29
3.3 Summary of Varying the Number of Steps Used to Calculate the Gradient Angularity Index.....	39
3.4 Modified Angularity Regression Summary.....	45
3.5 Texture Level 6 Regression Results.....	48
3.6 Summary of Sample Names and TxDOT Lab Numbers.....	49
3.7 Summary of Texture Scale versus Magnification Level.....	50
3.8 Average of Texture Levels 4 and 5 Regression Results.....	57
3.9 Sphericity Regression Results.....	59
3.10 Aggregate Types Used in Coupons.....	60
3.11 Micro-Deval Analysis of Variability: Weight Loss Linear Model Results (All Data Points).....	63
3.12 Micro-Deval Analysis of Variability: Weight Loss Linear Model Results (Excluding Outliers).....	64
3.13 PSV Frequency Percentage Distribution.....	67
4.1 Summary of Aggregate Properties and Classifications.....	69
4.2 Bounds for Modified Gradient Angularity.....	72
4.3 Bounds for Average of Texture Levels 4 and 5.....	72
4.4 Bounds for Sphericity.....	72
4.5 Percentage of Particles Falling Within Each Category for Angularity.....	72
4.6 Percentage of Particles Falling Within Each Category for Texture.....	73

TABLE	Page
4.7 Percentage of Particles Falling Within Each Category for Sphericity	73
4.8 Individual Particle Angularity Quartiles	75
4.9 Individual Particle Texture Quartiles	75
4.10 Individual Particle Sphericity Quartiles	75
4.11 Average Angularity Quartiles	75
4.12 Average Texture Quartiles.....	76
4.13 Average Sphericity Quartiles.....	76
4.14 Aggregate Surface Classification Properties	81
4.15 Changes in Aggregate Classification	83
5.1 Mix Summary	88
5.2 Regression Coefficient Summary	94
5.3 Skid Measurements of Test Sections.....	97

LIST OF FIGURES

FIGURE	Page
2.1 Pavement Surface Profile (Kamel et al. 1982).....	7
2.2 Variation in Skid Resistance Due to Speed and Texture Scale (Jayawickrama and Graham 1995)	9
2.3 Schematic of Hysteresis and Adhesive Forces Acting on Tire-Pavement Interface (Bazlamit and Reza 2005).....	10
2.4 Aggregate Methods for Providing Pavement Texture (Dahir 1979).....	16
2.5 Decrease in Pavement Skid Resistance Due to Polishing of Traffic (Skeritt 1993).....	16
2.6 Decrease in Uncompacted Voids After Increased Time in LA Abrasion Test (Crouch et. al. 1996)	18
2.7 Mineral Composition Related to Skid Resistance (Mullen et al. 1974).....	20
3.1 Calculation Example to Compute Percent Flat and Elongated Particles (TxDOT 2006)	27
3.2 Coupon Before and After Polishing	32
3.3 Illustration of Angle Differences Between Gradients for Smooth and Angular Particles	34
3.4 Combined BMD and AMD Average Gradient Angularity Index Comparison	37
3.5 Comparison of COV versus Number of Steps in Angularity Analysis for 10 Test Aggregates	40
3.6 Comparison of Current and Proposed Angularity Methods	40
3.7 Combination of BMD and AMD Comparison between Modified and Original Angularity.....	41
3.8 BMD Comparison between Modified and Original Angularity COV	42
3.9 AMD Comparison between Modified and Original Angularity COV	43

FIGURE	Page
3.10 Modified Angularity Comparison BMD	44
3.11 Modified Angularity Comparison AMD	44
3.12 Modified Angularity Comparison Combined BMD and AMD	45
3.13 Texture Level 6 Comparison of BMD Aggregates	46
3.14 Texture Level 6 Comparison of AMD Aggregates.....	47
3.15 Texture Level 6 Comparison of Combined BMD and AMD Aggregates.....	47
3.16 Average Level 6 Texture Indices of Six Sandstones with Varying Magnification and Objective Lens	50
3.17 Comparison of Texture Levels of Six Sandstones, One Granite, One Highly Textured Limestone, One Quartzite, and One Low Textured Limestone	51
3.18 Texture Level Comparison for BMD Samples	53
3.19 Texture Level Comparison for AMD Samples	53
3.20 Coefficient of Variation Comparison for BMD Samples	54
3.21 Coefficient of Variation Comparison for AMD Samples.....	54
3.22 Average of Texture Levels 4 and 5 Comparison of BMD Samples	55
3.23 Average of Texture Levels 4 and 5 Comparison of AMD Samples	56
3.24 Average of Texture Levels 4 and 5 Comparison of Combined BMD and AMD Samples	56
3.25 Sphericity Comparison for BMD Samples	57
3.26 Sphericity Comparison for AMD Samples	58
3.27 Sphericity Comparison for Combined BMD and AMD Samples.....	58
3.28 Aggregate Polished Coupon Texture Results	61

FIGURE	Page
3.29 Micro-Deval Analysis of Variability: Weight Loss Results (All Data Points)	63
3.30 Micro-Deval Analysis of Variability: Weight Loss Results (Excluding Outliers)	64
3.31 Correlation of Percent Loss of Sulfate Soundness and Micro-Deval.....	66
3.32 PSV Percentages Histogram	67
4.1 Clustering Comparison Based on Mineralogy for BMD Samples.....	77
4.2 Clustering Comparison Based on Mineralogy for AMD Samples	77
4.3 Clustering Comparison Based on Mineralogy for Combined Samples	78
4.4 Surface Aggregate Classification for WWARP	79
4.5 Proposed Surface Aggregate Classification Method.....	82
5.1 AIMS Texture Index versus Time in the Micro-Deval Test with Regression Results for A) Texture Level 4, B) Texture Level 5, and C) Texture Level 6	95
5.2 Skid Results of IH-20 Test Sections	97
5.3 COV versus AIMS Texture Index for A) Texture Level 4, B) Texture Level 5, and C) Texture Level 6	100

CHAPTER I

INTRODUCTION

PROBLEM STATEMENT

The skid resistance of a pavement is the force that develops between the pavement-tire interface when a tire that is not rolling slides along the surface of the pavement. Adequate pavement skid resistance is required to ensure driver safety, especially under wet weather conditions. Pavement skid resistance is influenced by two main pavement texture components, namely microtexture, or harshness, and macrotexture, or stone projections. Aggregates that are polish resistant, angular, and cubical provide a pavement with high initial skid resistance and retain an acceptable level of skid resistance throughout the life of the pavement.

Throughout the last several decades, many different studies have attempted to develop predictive models that relate laboratory measurements of mix properties to asphalt pavement skid resistance. These studies have shown mixed results in the prediction of initial and/or long-term pavement skid resistance. Many of these predictive models had shortcomings such as only accounting for one of the two pavement texture scales that influence skid resistance, using indirect and highly variable methods for measuring aggregate properties, or using tests that did not characterize the polishing or abrasion of aggregates well.

This thesis follows the style and format of *Journal of Materials in Civil Engineering* (ASCE).

Recent studies at Texas A&M University have focused on using image analysis techniques to quantify aggregate shape properties: angularity, texture, and shape. These techniques allow direct measurement of aggregate properties and assessment of the change in these properties after the aggregates undergo mechanical forces that cause polishing, abrasion, and breakage.

This study therefore focuses on using image analysis techniques to measure aggregate resistance to polishing and relating this property to skid resistance of pavements. The Micro-Deval test was used to polish the aggregates for different time intervals and the Aggregate Imaging System (AIMS) was used to determine the changes in aggregate properties as a function of polishing time. The repeatability of the AIMS unit was also studied by comparing the results of tests conducted using AIMS units at the Texas Transportation Institute (TTI) and the Texas Department of Transportation (TxDOT). The properties of aggregates were measured using AIMS before and after Micro-Deval. The data collected for this study were used to determine refinements to AIMS analysis methods in order to reduce variability and to propose a new method for classifying aggregates as part of the TxDOT wet weather accident reduction program (WWARP).

OBJECTIVES OF THE STUDY

The main objectives of this study are as follows:

- Compare the results of two AIMS units, one at the TTI laboratory and one at the TxDOT laboratory.

- Make necessary changes to the AIMS analysis methods to improve sensitivity to changes in aggregate properties and reduce variability.
- Compile a database of aggregate properties that include the AIMS measurements of aggregate shape, angularity, and texture characteristics.
- Assess the variability in the AIMS measurements conducted at TxDOT and TTI.
- Develop a new method for classifying aggregates used in asphalt pavement surfaces as part of WWARP.
- Relate aggregate resistance to polishing measured using AIMS to pavement skid resistance.

THESIS ORGANIZATION

This thesis is organized in six chapters as follows:

- Chapter I introduces the main motivation of this study, followed by the objectives and the outline of the thesis.
- Chapter II contains a literature review that emphasizes the significance of aggregates in influencing the skid resistant of pavements. In addition, the literature review also discusses laboratory methods that have been used to predict the skid performance of pavements.
- Chapter III discusses development and analysis of an aggregate database using AIMS data and other laboratory results.

- Chapter IV describes a new method for classification of aggregates based on their shape characteristics.
- Chapter V describes the method used to evaluate aggregate resistance to polishing and the correlation between the results of this method and field skid data on nine pavement sections.
- Chapter VI includes the conclusions and recommendations of this thesis.

CHAPTER II

LITERATURE REVIEW

OVERVIEW

This literature review focuses on the definition of skid resistance and the pavement characteristics that influence this important property. This is followed by discussion of the mix design factors that constitute the pavement microtexture and macrotexture, which are considered the primary factors that influence skid resistance. One section of the literature review is devoted to discussion of the forces that constitute skid resistance and the relationship of these forces to pavement macrotexture and microtexture. The influence of aggregate resistance to polishing on pavement skid resistance is described in this chapter as well. The last section of this chapter presents available methods for measuring mix and aggregate properties in order to predict pavement skid resistance.

PAVEMENT SKID RESISTANCE

The skid resistance of a pavement is the force that develops between the pavement-tire interface when a tire slides along the surface of the pavement and is kept from rolling (Murad 2004). Forster (1989) noted that skid resistance is one of the major factors in determining the overall safety of a highway. Even though this is a widely accepted assessment, studies have shown that many states do not have guidelines for pavement friction as a design requirement (Jayawickrama et al. 1996, Murad 2004).

Jayawickrama et al. (1996) also found that most state agencies trust that proper pavement design alone will provide adequate skid resistance for a pavement.

Wet weather accidents account for 18 percent of all accidents. This accident rate can be reduced greatly by implementing pavement skid programs to actively study and evaluate problem areas that are in need of improved skid resistance. After a skid resistance monitoring program was implemented in the United Kingdom, the accident rate dropped by 35 percent and the skid resistance of the pavements increased by 30 percent (Murad 2004). Similar results were found in studies in the United States, whereby increasing the skid resistance of deficient pavements reduced wet weather accidents by 54 percent and total accidents by 29 percent (Kamel and Musgrove 1981).

Many different types of forces and stresses act upon a pavement to affect its durability and ability to retain adequate skid resistance. Slow grinding and abrasion by tires, fast grinding by studded tires, crushing and breakage of aggregate edges due to heavy truck loads, and physical and chemical weathering are all types of wear that a pavement is subjected to on a normal basis (Dahir 1979). Increased traffic and heavier truck loads have increased the rate at which aggregates are polished due to higher stresses present in the pavements, and therefore higher quality aggregates are being required for new pavements (Roque et al. 1995).

Overcautious specifications for use of polish-resistant aggregates in hot-mix asphalt (HMA) can result in increased pavement costs (Crouch et al. 1996). Many young pavements designed under state specifications perform poorly in skid resistance, indicating that current design methods and evaluation of aggregates are lacking (Roque

et al. 1995). Therefore, better methods to predict the performance of aggregates in HMA are required to ensure adequate skid resistance throughout the design life of the pavement.

PAVEMENT TEXTURE COMPONENTS OF SKID RESISTANCE

The skid resistance of a pavement is composed of two main texture scales, namely macrotexture and microtexture. Macrotexture is usually considered to represent those stone projections from the surface of the pavement greater than 0.5 mm, while microtexture are those projections smaller than 0.5 mm (Henry and Dahir 1979, Stroup-Gardner et al. 2004). Figure 2.1, from Kamel et al. (1982), shows a normal pavement surface profile indicating the microtexture and macrotexture of the pavement.

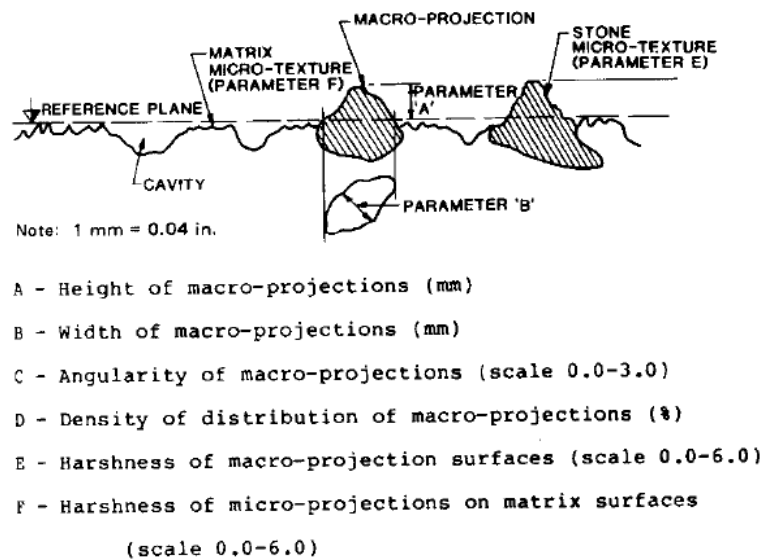


Figure 2.1. Pavement Surface Profile (Kamel et al. 1982)

Macrotexture is the large-scale roughness that is present on the surface of the pavement resulting from the arrangement of aggregate particles. The initial value of the macrotexture depends on the size, shape, and gradation of the coarse aggregates used in the asphalt mix (Jayawickrama et al. 1996). Kamel et al. (1982) also stated that the macrotexture of a pavement is a function of the height, width, and density of the macro-projections on the pavement surface. Macrotexture is considered to be a major component that affects the skid resistance of pavements at high speed, usually above 40 mph (Stroup-Gardner et al. 2004). The macrotexture provides drainage paths for water to escape from the tire-pavement interface (Henry and Dahir 1979, Kamel and Musgrove 1981). The stone projections also penetrate the water film that forms on the surface of the pavement and allows contact between the tire and pavement (Kamel and Musgrove 1981). This contact can cause excessive wear on the pavement, and the microtexture becomes the main provider of skid resistance (Diringer and Barros 1990).

Microtexture, or harshness, is composed of the small-scale projections on the aggregate surfaces as well as those exposed surfaces of the fine aggregates in the asphalt mix (Stroup-Gardner et al. 2004, Kamel and Musgrove 1981). The microtexture of a pavement is essential to penetrating the water layer that does not drain away due to the macrotexture and to generating friction forces between the pavement and tire (Do et al. 2000, Kamel and Musgrove 1981). The microtexture of a pavement is highly dependent upon the size, shape, and angularity of the micro-projections (Do et al. 2000) as well as the petrology and physical characteristics of the aggregates (Skeritt 1993). Microtexture is considered to be important at all speeds, but is most important at lower speeds (Kamel

and Musgrove 1981, Henry and Dahir 1979). Figure 2.2, from Jayawickrama and Graham (1995), shows the relationship between skid resistance and type of texture versus speed.

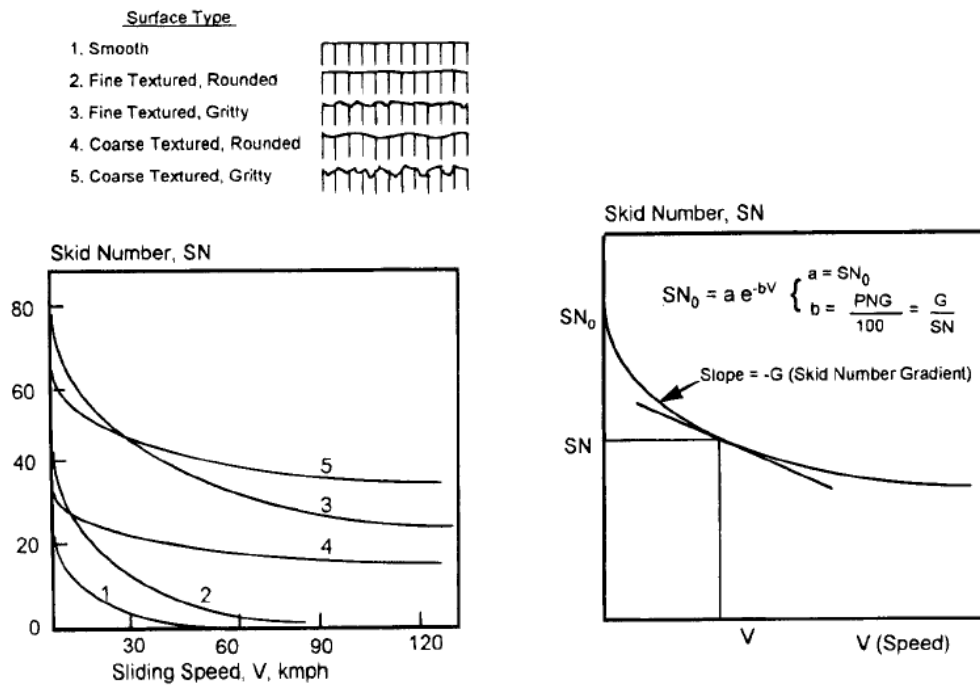


Figure 2.2. Variation in Skid Resistance Due to Speed and Texture Scale (Jayawickrama and Graham 1995).

FORCE COMPONENTS OF SKID RESISTANCE

Two primary forces combine to give a pavement its skid resistance, hysteresis and adhesion. These forces are the result of interaction between the different texture scales on the pavement surface and the tire. Figure 2.3, from Bazlamit and Reza (2005), shows the two different components acting between the tire and pavement.

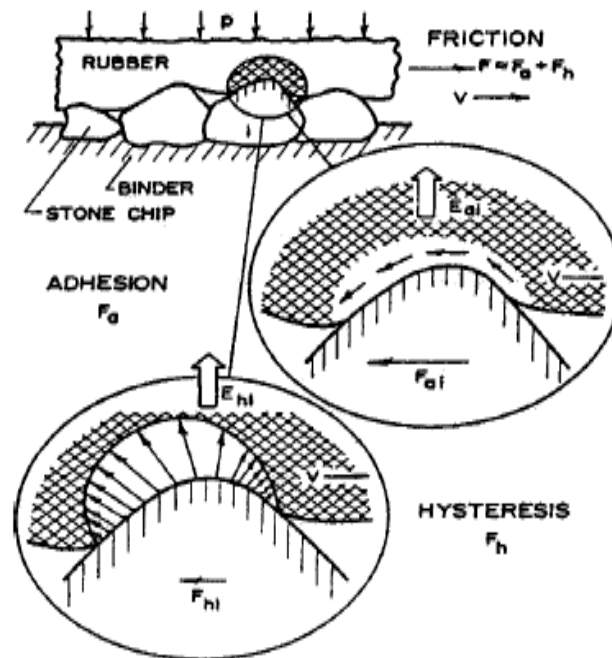


Figure 2.3. Schematic of Hysteresis and Adhesive Forces Acting on Tire-Pavement Interface (Bazlamit and Reza 2005)

The hysteresis component of skid resistance is due to the energy lost as the tire compresses and expands while traveling over the irregular pavement surface. This deformation occurs even if the surface of the pavement is perfectly lubricated, and it is therefore the main component of wet weather skid resistance (Bazlamit and Reza 2005). The magnitude of the hysteresis component of skid resistance is controlled by the asphalt macrotexture. The height, width, and density of the macro-projections from the pavement surface dictate the amount of energy lost due to deformation of the tire and therefore the hysteresis component (Jayawickrama and Graham 1995). Temperature also plays a major role in the magnitude of the hysteresis component. At higher

temperatures, the tire rubber becomes more flexible, and therefore leads to lower hysteresis loss (Jayawickrama and Thomas 1998).

The adhesive force is a result of the contact between the roadway and the tire. This force is defined as the frictional component due to tangential shearing forces at the actual contact surface between the tire and the aggregate. The magnitude of the adhesive force is largely dependent upon the microtexture of the pavement since the microtexture cuts through the water layer and allows contact with the tire (Bazlamit and Reza 2005, Jayawickrama and Graham 1995).

FACTORS AFFECTING SKID RESISTANCE

Many factors affect the skid resistance of pavements. Bazlamit and Reza (2005) grouped the factors into four specific categories: pavement variables, traffic variables, weather variables, and other factors. Of these, pavement variables are considered to be the most important and are the only variables that can be controlled at construction, but all four will be discussed at length within this section.

Pavement Variables

Pavement variables refer to the mix design and surface texture components. Both mix design and micro- and macro-texture are highly dependent upon the size, gradation, angularity, and shape of aggregate particles as well as the mineralogy and petrography of the particles. Aggregates compose more than 90 percent of an asphalt mix by weight and therefore play a very important role in the development of pavement

skid resistance. Most commonly, the coarse aggregate particles come into contact with tires at the pavement surface, and are therefore the focus of this discussion (Dahir 1979).

Many studies have shown that angular, more cubical aggregate particles provide better pavement performance in both rutting and texture (McGahan 2005, Henry and Dahir 1979). Flat and elongated aggregate particles are not desired, as they are believed to have deleterious effects on performance (Prowell et al. 2005), although this has not been proven through studies.

The coarse aggregates come into contact with tires more often than the fines do, and are therefore believed to be the most important part of the mix. To resist weathering and crushing, an aggregate must be hard, tough, well bonded, and chemically sound (Dahir 1979). These characteristics enable the coarse aggregate to hold up under repeated heavy loads as well as environmental conditions and maintain the pavement structure. Poor quality aggregates break down after certain loading and are pressed into the pavement surface, offering little in terms of macrotexture, and therefore become dangerous at high speeds (Kamel and Musgrove 1981).

The mineralogy of an aggregate particle is extremely important when predicting long-term abrasion resistance. Studies have found that aggregates with higher percentages of silica are more resistant to abrasion (Stephens and Goetz 1960). Also, aggregates composed of many different mineral types show more favorable wear patterns than those composed of a single mineral type. The size of the mineral grains also plays a major role in the abrasion resistance of aggregate particles. Particles with well dispersed, fine grains have been found to be more resistant to abrasion and impact

than those with larger grains. Aggregate mineralogy plays a major role in determining surface texture as well, and therefore greatly influences the microtexture of the pavement (Akesson et al. 2001).

Several studies have shown that mix type plays little role in the determination of skid resistance, while others have argued that mix type is important. Stroup-Gardner et al. (2004) found that changing from Marshall to Superpave mixes did not generate measurable changes in the measured texture. This may be true for the change between Marshall and Superpave, but newer generation mixes such as open graded friction courses (OGFC) or stone matrix asphalt (SMA) have shown to have considerably higher skid resistance and texture values due to the coarser mixes (Kamel and Musgrove 1981, Stroup-Gardner et al. 2004).

Traffic Variables

Higher speeds and heavier loads have caused the need for increased quality aggregates to be used in pavements to provide higher levels of skid resistance as well as resistance to breakage under heavier loads. The higher the traffic volume of the road, the faster the pavement will polish, and therefore the rate that aggregates polish and lose texture needs to be accounted for (Dahir et al. 1976).

Weather Variables

Many different aspects of weather affect the skid resistance of a pavement. Precipitation causes a short-term decrease in the skid resistance of a pavement due to the

accumulation of water on the pavement surface, but if the precipitation continues for an extended period, the skid resistance of the pavement will most likely increase as contaminants wash away (Murad 2004). Many studies have identified seasonal variation in skid resistance, with the summer having the lowest skid resistance and the winter having the highest (Bazlamit and Reza 2005, Dahir et al. 1976, Jayawickrama et al. 1996). Jayawickrama et al. (1996) actually quantified this seasonal variation to be between 5 and 15 skid numbers, due, they thought, to temperature and precipitation patterns that occur throughout the year.

Other Variables

Other variables that affect skid resistance that Bazlamit and Reza (2005) listed were contaminants and geometric design. As contaminants build up on the surface of the pavement, they act as lubricants or they can mask the texture present on the pavement and reduce the skid resistance of the pavement. This occurs often during dry spells and in many areas can happen cyclically due to normal weather patterns. When designing a pavement, the geometric design such as grade and curvature need to be considered as well to anticipate differing wear patterns for these areas than what would be expected on a normal roadway.

AGGREGATE POLISHING

Aggregates in an asphalt mix polish differently based upon their mineralogy. Figure 2.4, from Dahir (1979), shows four different methods by which aggregates

provide texture to a pavement surface. The first method is a very hard, angular aggregate composed of a single mineral type. This aggregate resists polishing, but will eventually become less textured and more rounded. The second aggregate type results in nearly the same type of wear pattern as the first, unless the crystals forming the particle are not well cemented. If this occurs, the worn particles will break off, exposing a fresh surface and therefore maintaining high skid resistance. The third and fourth aggregate types wear similarly. Both of these aggregates are composed of a hard mineral and a weak mineral. For the fourth wear method, the air voids act as the weak mineral type. As the particles weather, the weak mineral breaks down and releases the worn hard minerals, exposing fresh, unweathered surfaces that retain their texture for extended periods of time.

The friction of the pavement is initially provided by macrotexture. This high level of texture initially provided will decrease over time to a steady-state terminal value (Skerritt 1993). This terminal value usually takes approximately 2 to 3 years to reach, regardless of traffic levels. This process is illustrated in Figure 2.5, from Skerritt (1993). This terminal skid resistance is highly dependent upon the microtexture of the pavement.

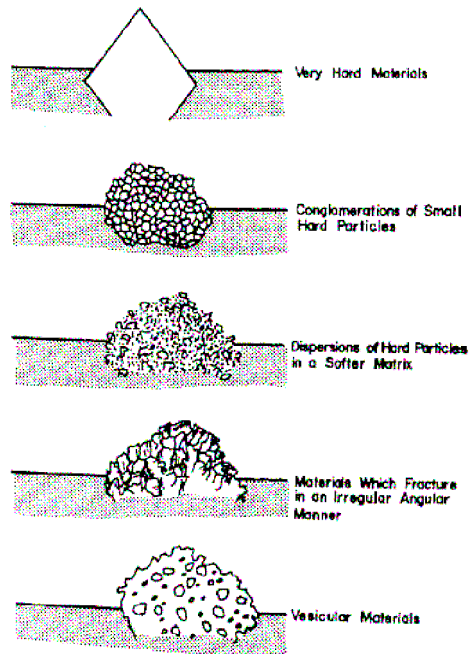


Figure 2.4. Aggregate Methods for Providing Pavement Texture (Dahir 1979).

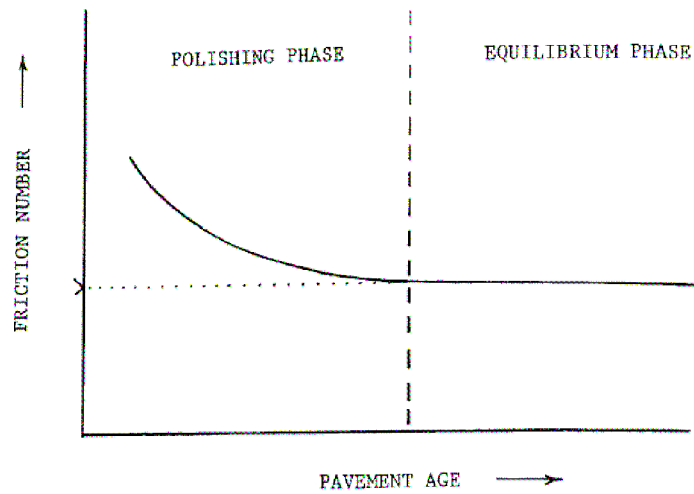


Figure 2.5. Decrease in Pavement Skid Resistance Due to Polishing of Traffic (Skeritt 1993).

PREDICTIVE MODELS FOR SKID RESISTANCE

Throughout the past several decades, many models and experimental methods have been developed to predict the skid resistance of pavements based upon different laboratory tests. These models are used to ensure that the pavement provides adequate skid resistance throughout its design life without building several test sections to evaluate the aggregates. The laboratory tests that these models are based upon are relatively easy and not very time consuming to run and are therefore favorable methods.

Many of the methods that have been developed are based upon using the British Polish Value (BPV). It is widely thought that this test measures only the microtexture of the pavement, or the terminal polish value once the pavement reaches its equilibrium skid resistance, but studies by Liu (2004) found that the BPV is dependent upon macrotexture as well. Other studies have found that the operator, pattern of aggregates on the polishing coupons, number of times the skid pad has been used, and curvature of the coupon all affect the final polish value (Mahmoud 2005). Therefore, any model that uses BPV as a measure of skid resistance has a high inherent variability.

Crouch et al. (1996) used a modified American Association of State Highway Transportation Officials (AASHTO) TP33 device to measure the uncompacted voids in coarse aggregates that were subjected to various times in the Los Angeles (LA) Abrasion test. By running the LA Abrasion for various times, the change in the aggregates could be assessed by measuring the amounts of abrasion and breakage. The uncompacted voids measurement provides an indirect assessment of how the angularity of aggregates has changed. Figure 2.6 shows the results of three of the aggregates tested by Crouch

and his colleagues. The figure shows that the longer the aggregates were in the LA abrasion test, the lower the uncompact voids. This indicates that the aggregates were becoming more rounded and thus wearing and breaking. An R^2 value of approximately 0.8 was found between the performance of test sections and the performance measure developed by Crouch et al. (1996). Although this method does evaluate how the aggregates change over time, it is still considered an indirect method and it uses the the LA test, which primarily breaks aggregates rather than abrading them.

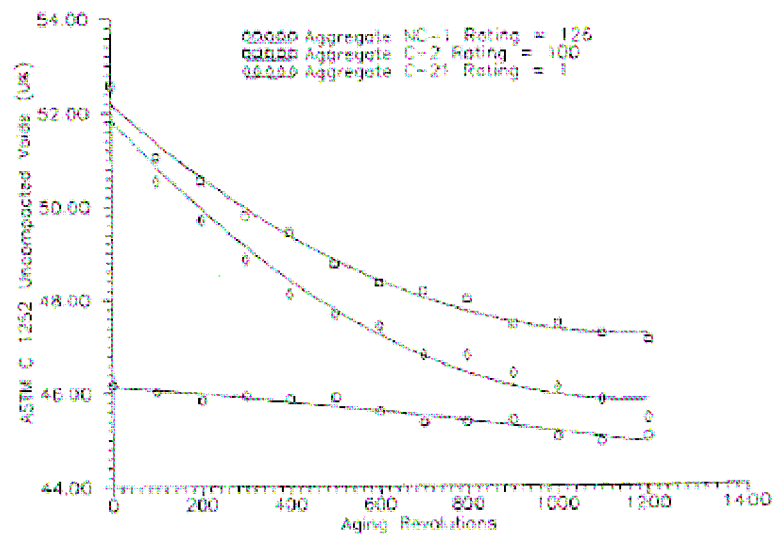


Figure 2.6. Decrease in Uncompact Voids after Increased Time in LA Abrasion Test (Crouch et al. 1996).

Do et al. (2000) used lasers to determine a surface profile of pavement sections. This profile was used to determine the microtexture and macrotexture of the pavement. These microtexture and macrotexture components were then used to predict the skid

resistance of the pavement. This predicted value was compared to skid measurements and resulted in an R^2 value of approximately 0.80. This method would be useful for collecting skid data in the field at high speed and may be possible to use for design purposes by looking at the surface profiles of compacted specimens.

Dahir et al. (1976) attempted to relate the acid insoluble mineral percentage to field skid performance. They found a correlation, but it was not high enough to support a regression equation. Dahir et al. (1976) did note that the minimum skid number collected from the field did correlate well with laboratory polishing results, indicating that the minimum polish value collected in the laboratory is somewhat indicative of the terminal texture reached in the field. Also, they discussed that the change between initial and terminal polish value in the laboratory offered an estimation of how well the aggregate resisted abrasion.

Stroup-Gardner et al. (2004) measured the mean profile depth, indicative of macrotexture, and related it to measured skid number. This measurement resulted in an ability to estimate the skid number to a relatively close degree. This method is good for evaluating a pavement once built, but offers little help in the design side.

Mullen et al. (1974) studied the mineralogy of aggregates in relation to skid resistance. They discovered an optimum percentage of hard minerals distributed within a softer matrix. This allows for selection of materials that should perform well in the field (Figure 2.7). It is easy to see that the optimum percentage of hard minerals falls between 40 and 70 percent.

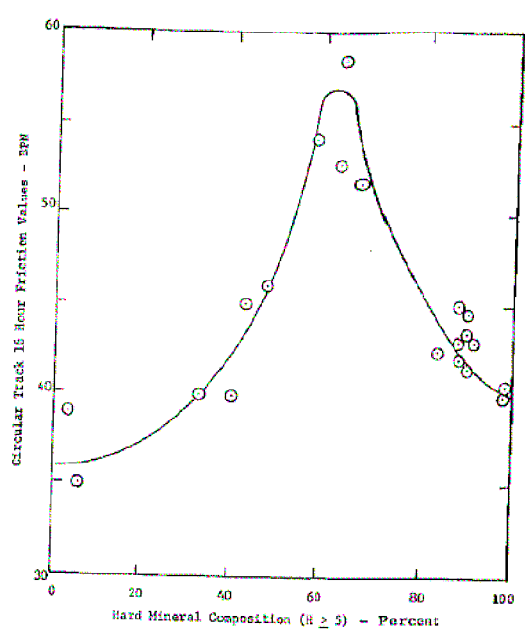


Figure 2.7. Mineral Composition Related to Skid Resistance (Mullen et al. 1974).

Many models have been developed to predict the skid resistance of a pavement surface. Henry and Dahir (1979) and Kamel and Musgrove (1981) both use the BPV of an aggregate sample as a parameter for the prediction of a pavement skid resistance. Henry and Dahir (1979) further state that the BPV is a function of the microtexture of an aggregate and attempt to use the percent normalized gradient, a function of macrotexture, to incorporate both aspects into the prediction of pavement skid resistance. As stated previously, the BPV is highly variable and would therefore be difficult to use as a predictor for skid resistance.

Stephens and Goetz (1960) used the fineness modulus to determine the skid resistance of an asphalt pavement. They stated in their results that the time that a mix maintains a high resistance to skid needs to be considered. They found that sharp edges

of highly angular particles abraded quickly and the skid resistance of the pavement therefore reduced quickly. This study showed that not only does a pavement need to start off with a high skid resistance, it needs to maintain it throughout its life span as well.

Liu (2004) specifically investigated the gaps between the aggregates as the main factor for texture. By varying the width between aggregates and using the British Pendulum to measure the BPV, he determined an optimum gap. Skid resistance was found to decrease as the gap width increased.

Prowell et al. (2005) suggested that Micro-Deval may be more suitable to determining an aggregate's resistance to weathering and abrasion than the sulfate soundness test. They also stated that Micro-Deval abrasion loss is related to the change in macrotexture over time. This agrees with Mahmoud (2005) in stating that the Micro-Deval is a better test in general to determine the polishing resistance of aggregates.

SUMMARY

Although many factors affect the skid resistance of a pavement, the only properties that can be controlled at the time of construction are the pavement properties. These properties include aggregate angularity, shape, texture, and gradation as well as mix design. The quality of the aggregates needs to be tested to ensure that it will provide adequate skid resistance throughout the life cycle of the pavement.

Many methods are available to indirectly measure aggregate properties. However, these methods do not offer a direct measure of the change in aggregate properties due to abrasion and polishing.

CHAPTER III

DEVELOPMENT AND ANALYSIS OF TXDOT AGGREGATE DATABASE

OVERVIEW

Throughout the implementation process of AIMS, 106 aggregate samples were tested at the Texas Transportation Institute laboratory. Table A.1 in Appendix A summarizes the aggregate mineralogy, TxDOT classification, and TxDOT laboratory sample number of these aggregates. These aggregates were scanned using AIMS before Micro-Deval (BMD), tested in the Micro-Deval, and scanned again using AIMS after Micro-Deval (AMD). The data from these tests were cataloged and compared to results obtained by testing similar samples at the TxDOT laboratory. Table 3.1 shows a summary of the number of samples tested, where the “BOTH” column denotes that the same aggregate sample was tested at both the TxDOT and TTI laboratories.

The aggregate database was analyzed to determine the correlation between the TTI and TxDOT measurements and explore relationships between the aggregate properties included in the database. Statistical clustering analysis was conducted on the AIMS data to determine new bounds for classification of aggregates in either low, medium, or high categories for texture, angularity, and sphericity. The method for calculating the angularity of particles and the texture scale were modified in order to enhance the accurate portrayal of aggregate shape properties.

Table 3.1. Summary of Tests Run between the Two Laboratories.

	TTI	TxDOT	BOTH
Angularity BMD	106	108	104
Angularity AMD	110	97	96
Texture BMD	75	108	72
Texture AMD	83	99	72
Sphericity BMD	75	106	74
Sphericity AMD	83	100	72
Micro-Deval	105	134	98

This research proposes a new method to better classify aggregates as part of the wet weather accident reduction program. This proposed method uses the texture results obtained from AIMS and the magnesium sulfate soundness test to classify aggregates for pavement skid performance.

AGGREGATE TESTS AND PROCEDURES

In the National Cooperative Highway Research Program (NCHRP) 539 study, Prowell et al. (2005) noted several consensus aggregate properties and source properties that played a major role in the performance of HMA pavements. Superpave defined the four important consensus aggregate properties to be coarse aggregate angularity, flat and elongated particles, uncompacted voids in fine aggregates, and sand equivalents. Aggregate durability and deleterious material content are two additional source properties that were discussed by Prowell et al. (2005). These properties are related to the transport, compaction, and continuous wear of aggregates throughout the life of the pavement. Although specifications for the consensus aggregate properties have been

uniformly adopted through different agencies, the source properties vary due to regional differences in geology.

In order to assess the quality of aggregates used within the state of Texas, TxDOT initiated the Aggregate Quality Monitoring Program (AQMP). The AQMP sets forth a method to ensure the quality and consistency of aggregates produced within the state. It also allows expedited use of aggregates for a project if quality tests have been run on them at regular intervals. TxDOT standard Tex-499-A states which tests and the frequency of testing that are required. The specific tests required for asphalt pavements are LA abrasion, magnesium sulfate soundness, and polish stone value. The database developed in this study includes a number of consensus aggregate properties, durability properties, and AIMS measurements. The following sections discuss these aggregate properties and associated test methods.

Aggregate Consensus Properties

Crushed Face Count

The crushed face count test was run according to TxDOT procedure Tex-460-A. This test assesses the percentage of the aggregate that has at least two crushed faces. This index is usually used as a measure of the angularity of a particle since it is assumed that a particle having at least two crushed faces has an acceptable level of angularity. This test is done by manual inspection in order to determine unweathered faces that constitute at least one-quarter of the projected area of the rock. Table A.6 of Appendix A summarizes the results from this test.

Flat and Elongated Particles

High proportions of flat and elongated particles are believed to be detrimental to asphalt pavement performance. Flat and elongated particles are specified by their length to thickness ratio and are determined using TxDOT procedure Tex-280-F. For this test, length is defined as the maximum dimension of the particle, width is the maximum dimension perpendicular to the length, and thickness is the maximum dimension perpendicular to the length and width.

An aggregate sample is obtained using a sampling technique according to TxDOT procedure Tex-221-F. Approximately 100 particles of each of sieve sizes 5/8 inch (16.0 mm), 1/2 inch (12.6 mm), and 3/8 inch (9.5 mm) are obtained using sieve analysis. The particles retained on the 7/8 inch (22.4 mm) and those passing the 3/8 inch sieve are not considered for this test. The number of particles with length to thickness ratios above a certain value are then determined (typically ratios of 3:1 or 5:1 are used for specifications). The percent of particles in each sieve size classified into each group is reported to the nearest 0.1 percent. The percent of flat and elongated particles within each sieve group are multiplied by its weight percent to determine the total flat and elongated percent of the aggregate blend. Figure 3.1 shows a calculation example from the TxDOT Bituminous Test Manual to compute the percent flat and elongated particles for one sieve size. The total percent flat and elongated is the summation of the percentage for each sieve size. The results from this test are summarized in Appendix A Table A.6.

Calculation Example					
Sieve	%	%	%	%	adjusted %
7/8 in.	4.8				
5/8 in.	17.8 →	17.8	17.8 ÷	88.5 =	20.1
1/2 in.	42.1 →	42.1	42.1 ÷	88.5 =	47.6
3/8 in.	28.6 →	28.6	28.6 ÷	88.5 =	32.3
No. 4	6.7 →	0.0	0.0 ÷	88.5 =	0.0
		88.5			100.0

Suppose the 5/8 in. sieve has a flat and elongated % of 5.2 for the ratio 5:1, then:

$$\frac{\text{Adjusted \%} \times \text{flat and elongated \%}}{100} = \text{weighted percentage}$$

$$\frac{20.1\% \times 5.2\%}{100} = 1.05\%$$

Figure 3.1. Calculation Example to Compute Percent Flat and Elongated Particles (TxDOT 2006).

Sand Equivalent Test

There is a TxDOT procedure for the sand equivalent test (Tex-203-F), but it was not conducted in this study. Clay-like fines in an aggregate blend used in an asphalt pavement cause the mix to be susceptible to moisture damage. The portion of the aggregate blend that passes the #4 sieve is mixed together to make a sample of 500 g. This sample is placed into a graduated cylinder and mixed with water to form a solution that has an exact height of 15 inches. This solution is agitated and then left to rest, allowing the sand to settle and the clay to remain in solution. The height of the clay and sand levels are then measured and used to calculate the sand equivalent using Equation 3.1.

$$\text{Sand Equivalent Value} = 100 \times \frac{\text{Sand Height Reading}}{\text{Clay Height Reading}} \quad (3.1)$$

Flakiness Index

The flakiness index is a measure of the percentage of particles in a coarse aggregate mix that has a shortest dimension less than one-half of the nominal size. The test is conducted according to TxDOT procedure Tex-224-F. In this test, aggregates are sieved into sizes 7/8 inch (22.4 mm), 5/8 inch (16.0 mm), 3/8 inch (9.5 mm), and 1/4 inch (6.3 mm). Those aggregates retained on the 7/8 inch and passing the 1/4 inch sieve are discarded and not included in the flakiness index determination. The total number of particles remaining needs to be more than 200. The aggregate retained on the 5/8 inch sieve that also pass through the 3/8 inch sieve and particles from those retained on 3/8 inch sieve that pass through the 1/4 inch sieve are used to determine the number of aggregates with a shortest dimension less than one-half of the nominal size. These particles are combined and are considered the passing sample. The flakiness index is calculated using Equation 3.2 and is reported to the nearest whole number. Table A.6 in Appendix A summarizes the results for the flakiness index for the aggregates tested in this study.

$$\text{Flakiness Index} = \frac{\text{Passing Sample Particle Count}}{\text{Total Number of Particles}} \quad (3.2)$$

Durability and Deleterious Materials Tests

Micro-Deval

The Micro-Deval test assesses aggregate resistance to abrasion and weathering. This test was run according to TxDOT specification Tex-461-A. The aggregate blend with a total weight of 1500 ± 5 g, summarized in Table 3.2, is soaked in 2000 ± 500 mL of water for a minimum of one hour. This mixture is then placed in a steel cylinder with 5000 ± 5 g of steel ball bearings. This mixture of water, aggregate, and ball bearings is rotated for 105 minutes at 100 ± 5 rpm. After abrasion, the aggregates are washed, and the weight loss is considered to be that passing the #16 sieve. Equation 3.3 calculates the percent of weight loss, and Appendix A Table A.5 summarizes the results for all aggregates.

Table 3.2. Weight Specifications for Micro-Deval Test.

Passing	Retained On	Weight (g)
1/2 inch	3/8 inch	750 ± 5
3/8 inch	1/4 inch	375 ± 5
1/4 inch	#4	375 ± 5

$$PercentLoss = \frac{(\text{Weight Before} - \text{Weight After})}{\text{Weight Before}} \quad (3.3)$$

Los Angeles Abrasion

The LA Abrasion Test assesses aggregate resistance to degradation during transport, mixing, and compaction. This test was run according to TxDOT procedure Tex-410-A. In this test, 5000 ± 5 g of an aggregate mix is placed into a steel cylinder with six to twelve 46.8 mm steel spheres, depending on the gradation used for the mix. The aggregates and steel spheres are then rotated at 30 to 33 rpm until the total number of rotations reaches 500. Weight loss is measured as aggregate passing the #12 sieve, and percent weight loss is calculated using Equation 3.4. The LA Abrasion Test differs from the Micro-Deval because the steel spheres used are much larger and it is a dry method. The LA Abrasion is therefore more of an assessment of an aggregate's resistance to breakage than abrasion due to wear. Table A.5 of Appendix A summarizes the results from this test.

$$\text{Percent Loss} = \frac{(\text{Weight Before} - \text{Weight After})}{\text{Weight Before}} \quad (3.4)$$

Magnesium Sulfate Soundness

The magnesium sulfate soundness test, run according to TxDOT procedure Tex-411-A, assesses an aggregate's resistance to freeze-thaw cycles, and therefore examines the durability of the aggregates.

The gradation of the aggregate blend used for this test depends upon the type of pavement mix that the aggregate is to be used in. According to the test procedure, the aggregate mix is placed in a specified concentration of a magnesium sulfate solution.

The aggregates are left in the solution for 16 to 18 hours, and then removed and dried in an oven. This cycle is repeated five times, and then the samples are washed thoroughly. Weight loss is determined based on the size of aggregate before and after the test. For example, a particle initially retained on a 2 inch sieve must pass a 1.5 inch sieve to be considered weight loss after testing, while a #4 particle must pass a #5 sieve to be considered weight loss. The percent loss is calculated for each size and then multiplied by its gradation percent and summed to determine the total percent loss of the aggregate blend. The results from the magnesium sulfate soundness test are summarized in Table A.5 of Appendix A.

British Polish Value

The British Polish Value (BPV) or Polished Stone Value provides an indication of the aggregate's resistance to polishing, which is an important property in controlling asphalt pavement skid resistance. To determine the terminal value of the BPV, accelerated polishing tests are conducted using TxDOT procedure Tex-438-A. In this test, aggregates are arranged into resin coupons with an arched shape, as shown in Figure 3.2. Once the resin has fully cured, the coupons are placed on a rotating wheel and polished for nine hours. The polished coupons are then skidded with a rubber pad while wet to determine the terminal British Polish Number (BPN). The reported BPN is the average of five consecutive skid measurements. The results from the accelerated polishing tests run at the TxDOT laboratory are summarized in Table A.6 of Appendix A.

Aggregate Imaging System Data

Many of the current methods used for aggregate classification are based on indirect methods of measuring aggregate properties. Analyzing aggregates using AIMS offers direct measurement of an aggregate particle's angularity, texture, and shape. Capabilities of AIMS are extensively discussed in the NCHRP 4-30 study as well as TxDOT Implementation Report 5-1707-01-1. A brief discussion of the AIMS analysis methods follows.



Figure 3.2. Coupon Before and After Polishing.

Aggregate Angularity

To measure the angularity of a particle, a black particle projection is captured by using a backlit table where aggregate particles are placed. The particle projection is then used to determine the angularity index. The angularity index is the average of the change in the angles of the gradient vectors around the particle circumference (Masad et

al. 2005). Basically, the circumference is divided into segments, and the gradients are calculated for these segments. As shown later, the segment length is important in determining the accuracy and variability of the analysis method. The angularity index is calculated using Equation 3.5. The previous analysis using this method calculated the gradient orientation (θ) using adjacent pixels (segment = 2 pixels), and then calculated the difference in the gradients separated by 3 pixels (Δ in Equation 3.5 is equal to 3). The maximum value of the gradient angularity index was set at 10,000 by Al-Rousan (2004) and was used during the course of this study. Examples of gradient vectors for smooth and angular particles are shown in Figure 3.3.

$$\text{Gradient Angularity Index} = \frac{1}{\frac{N}{\Delta} - 1} \sum_{i=1}^{N-\Delta} |\theta_i - \theta_{i+\Delta}| \quad (3.5)$$

where:

i is the i^{th} pixel on the perimeter of the particle,

N is the total number of pixels in the perimeter, and

θ is the orientation of the gradient at a given pixel.

Δ is number of pixels between gradients used in the calculations.

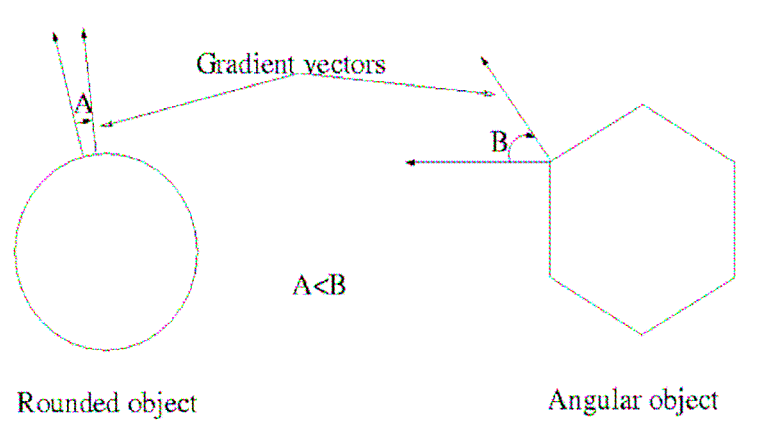


Figure 3.3. Illustration of Angle Differences between Gradients for Smooth and Angular Particles.

Texture

AIMS offers a method to analyze the surface texture of aggregate particles as well as the polishing coupons. The texture index is determined by taking a grayscale image of the surface of the aggregate particle. This image is then analyzed using the wavelet method to determine the texture of the particle. The wavelet method is discussed in depth in the NCHRP 4-30 study (Masad et al. 2005). Six different scales of texture on a particle surface can be analyzed by this method. Level 1 corresponds to the smallest scale texture, while level 6 corresponds to the largest texture scale. The current method used to compare the texture of aggregates uses texture level 6 (Al-Rousan 2004). As shown later in this study, different texture levels are recommended based on the results obtained from analyzing the comprehensive database of aggregates.

Sphericity

Sphericity is a measure of how close the lengths the three dimensions of an aggregate particle are. A sphericity index of 1.0 denotes that a particle is a perfect sphere or cube, while sphericity decreases as a particle becomes more flat and/or elongated. The AIMS software uses Equation 3.6 to calculate the sphericity index. The three dimensions of a particle are determined using only two scans by one camera. Two of the dimensions for this calculation are obtained using the image projection used in angularity analysis, while the third dimension is obtained by determining the distance that the camera has to move vertically from a reference point in order for the image to be in focus.

$$Sphericity = \sqrt[3]{\frac{d_s * d_i}{d_l^2}} \quad (3.6)$$

where:

d_s is the shortest dimension,

d_i is the intermediate dimension, and

d_l is the longest dimension.

COMPARISON BETWEEN TXDOT AND TTI AIMS RESULTS

The data collected for the database were used in the comparison between the two AIMS units since aggregate samples from the same sources were scanned at TxDOT and TTI. The comparison included the shape characteristics (angularity, texture, and

sphericity) of individual aggregate particles and the texture of aggregates glued to the polishing coupons.

Coarse Aggregate Angularity

Aggregate particles from three size groups (retained on 3/8 inch, 1/4 inch, and #4 sieves) were scanned both before and after abrasion in the Micro-Deval test. In order to simplify the analysis, the average angularity of the three sizes combined was used as the basis for comparison between the two systems. Table A.2 of Appendix A contains all data for the gradient angularity.

The average angularity results from the two systems are shown in Figure 3.4. Linear regression was conducted in order to determine the R^2 value for the comparison between the two systems. The results indicate some positive correlation between the angularity measured using the two devices. However, this correlation is not sufficient, and it was decided that the analysis method should be modified to improve the correlation.

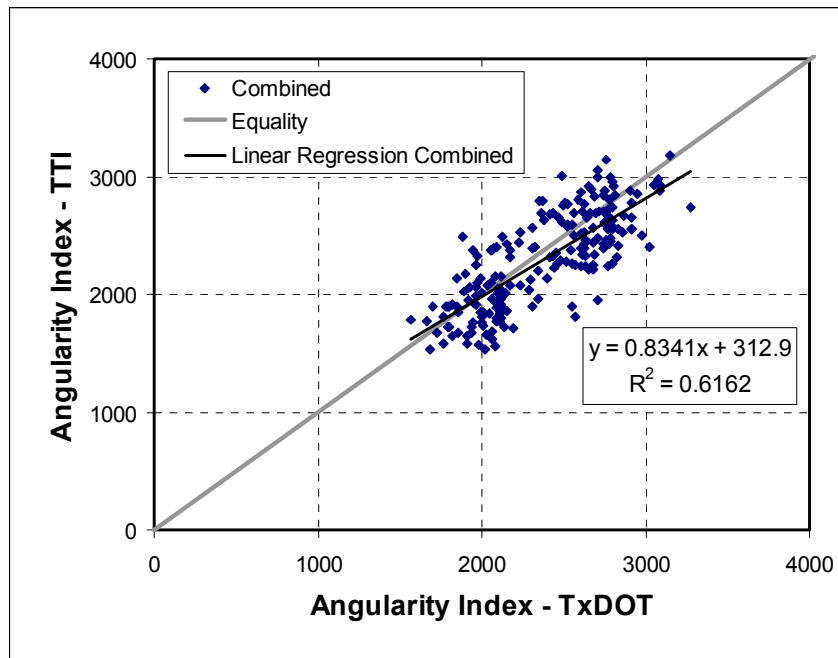


Figure 3.4. Combined BMD and AMD Average Gradient Angularity Index Comparison.

Modification of Coarse Aggregate Angularity

As discussed earlier, the angularity analysis (Equation 3.5) was conducted using adjacent pixels (segment = 2 pixels) in order to determine the gradient orientation (θ), and the difference between gradients was taken to be 3 pixels (Δ in Equation 3.5 is equal to 3). Analysis has revealed the parameters used in the angularity method to be sensitive to slight changes in the surface angularity. However, the method was highly influenced by noise at the surface boundary, which was thought to be the primary reason for the reduced correlation between the AIMS units. As such, the researchers decided to examine the angularity analysis results using different numbers of segments at the circumference. In doing so, the number of segments and Δ in Equation 3.5 are taken to

be the same. The analysis focused on comparing the sensitivity and variability of the angularity results of the 10 aggregates listed in Table 3.2. Fifty-six particles from each of the aggregates were analyzed using the current method and by dividing the circumference of each particle into 30, 35, 40, 45, and 50 segments. Table 3.3 summarizes the average, standard deviation, and coefficient of variation (COV) for each aggregate using the different analysis methods.

The results in Table 3.3 and Figure 3.5 show that using 30 segments resulted in the minimum COV for all 10 aggregates. Plotting the results of the current method versus the method with 30 segments (Figure 3.6) showed a good correlation, with $R^2 = 0.83$, with the results very close to the equality line. Therefore, using 30 segments is as sensitive as the current method in distinguishing between aggregates, but it has much less variability within the same aggregate source. Based on these favorable results, 30 was chosen as the number of segments to be used in determining the gradient angularity index. This new method will be referred to as the modified angularity method as opposed to the current method employed in AIMS.

Table 3.3. Summary of Varying the Number of Steps Used to Calculate the Gradient Angularity Index.

Aggregate		Current Method	Number of Segments in Proposed Method				
			30	35	40	45	50
1	Average	3592.47	3292.28	3474.75	3682.51	3809.04	4374.16
	Standard Deviation	1307.72	617.01	719.96	789.30	942.90	1019.02
	COV	36.40%	18.74%	20.72%	21.43%	24.75%	23.30%
2	Average	2602.91	2540.38	2438.71	2371.94	2126.29	2181.82
	Standard Deviation	1200.68	773.18	895.48	930.30	892.48	924.85
	COV	46.13%	30.44%	36.72%	39.22%	41.97%	42.39%
3	Average	2792.79	2829.80	2792.00	2712.64	2756.26	2759.74
	Standard Deviation	1060.30	763.08	833.93	863.67	923.00	969.80
	COV	37.97%	26.97%	29.87%	31.84%	33.49%	35.14%
4	Average	2219.15	2460.80	2249.07	2096.33	1985.97	1911.80
	Standard Deviation	975.16	719.35	744.04	728.63	778.55	714.90
	COV	43.94%	29.23%	33.08%	34.76%	39.20%	37.39%
5	Average	2826.94	3062.20	3032.74	2942.41	2953.89	3019.68
	Standard Deviation	1414.78	613.26	672.12	620.42	785.40	941.13
	COV	50.05%	20.03%	22.16%	21.09%	26.59%	31.17%
6	Average	3098.19	2912.00	2968.55	3130.62	3211.91	3285.79
	Standard Deviation	1295.32	601.10	902.24	831.61	1022.47	997.80
	COV	41.81%	20.64%	30.39%	26.56%	31.83%	30.37%
7	Average	2632.05	2558.25	2518.84	2484.33	2469.78	2479.70
	Standard Deviation	1055.36	902.15	1133.02	1217.45	1142.68	1308.58
	COV	40.10%	35.26%	44.98%	49.01%	46.27%	52.77%
8	Average	1811.29	1734.50	1436.17	1192.33	1061.85	1027.76
	Standard Deviation	1072.38	465.96	553.38	575.10	535.23	604.32
	COV	59.21%	26.86%	38.53%	48.23%	50.40%	58.80%
9	Average	1892.66	2155.42	1873.35	1667.55	1512.83	1421.17
	Standard Deviation	952.44	704.09	737.64	685.42	714.89	662.32
	COV	50.32%	32.67%	39.38%	41.10%	47.25%	46.60%
10	Average	2441.17	2828.37	2692.90	2658.03	2639.98	2499.97
	Standard Deviation	1366.33	756.68	842.27	892.24	890.41	1006.38
	COV	55.97%	26.75%	31.28%	33.57%	33.73%	40.26%

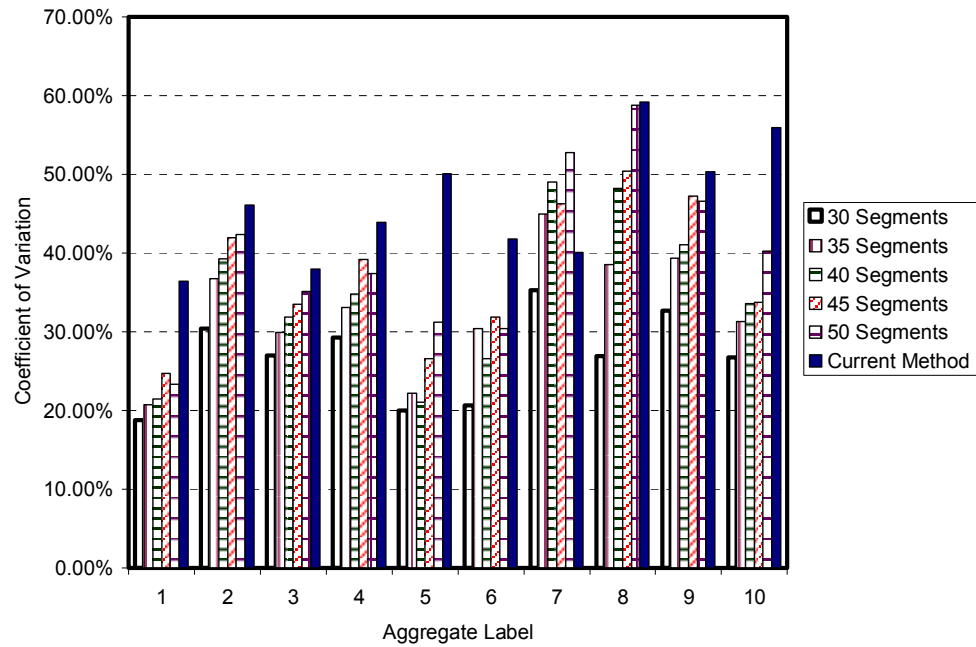


Figure 3.5. Comparison of COV versus Number of Steps in Angularity Analysis for 10 Test Aggregates.

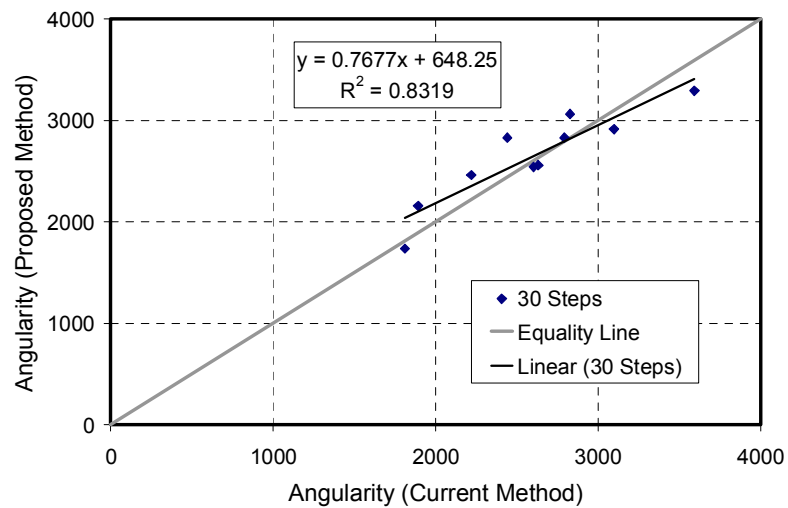


Figure 3.6. Comparison of Current and Proposed Angularity Methods.

Comparison of Modified and Original Angularity Methods for Database

Aggregates

All of the database aggregates were analyzed using the modified angularity method. Using the TTI results, the modified angularity was compared to the original angularity index. Figure 3.7 shows the comparison for aggregates before and after Micro-Deval.

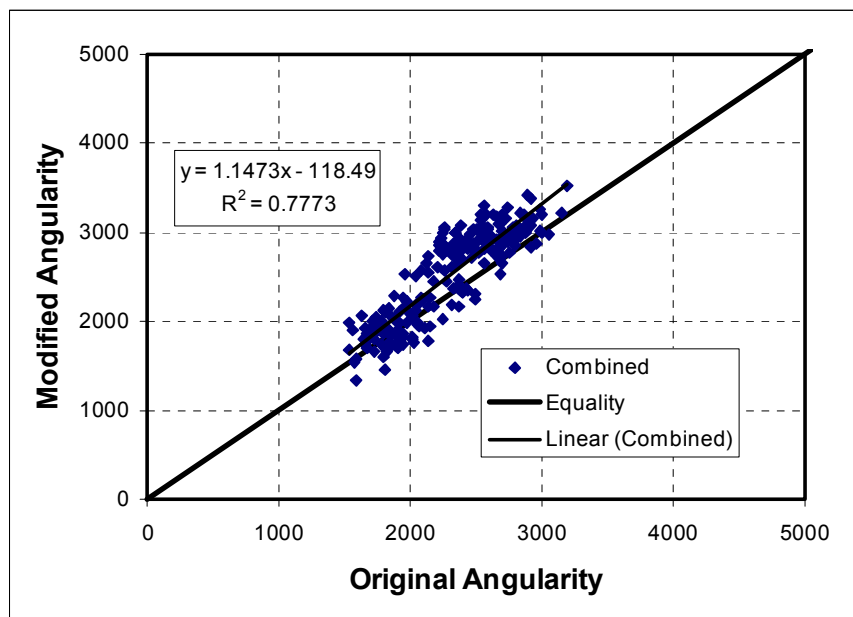


Figure 3.7. Combination of BMD and AMD Comparison between Modified and Original Angularity.

The results support that the two methods yield similar overall results. As discussed above, the method with 30 segments was chosen because it had the lowest coefficient of variation among the methods using different numbers of segments. In

order to validate this point, the COV was calculated for all aggregates in the database. Figures 3.8 and 3.9 show the results of plotting the COV of the modified angularity versus the original angularity. The modified angularity gives a considerably lower COV in nearly all cases.

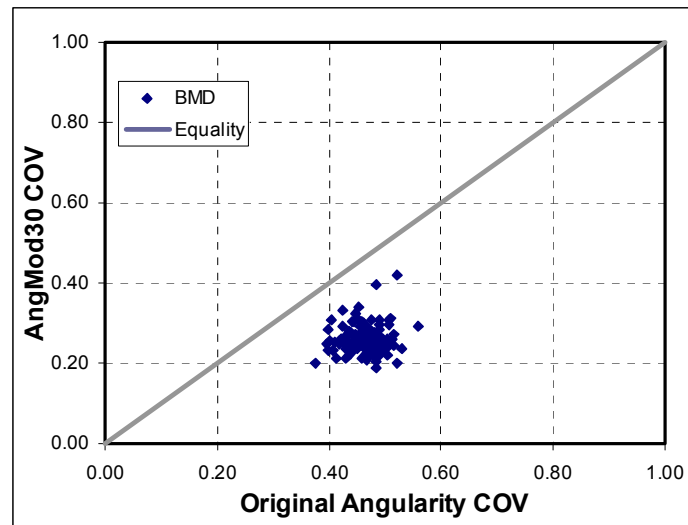


Figure 3.8. BMD Comparison between Modified and Original Angularity COV.

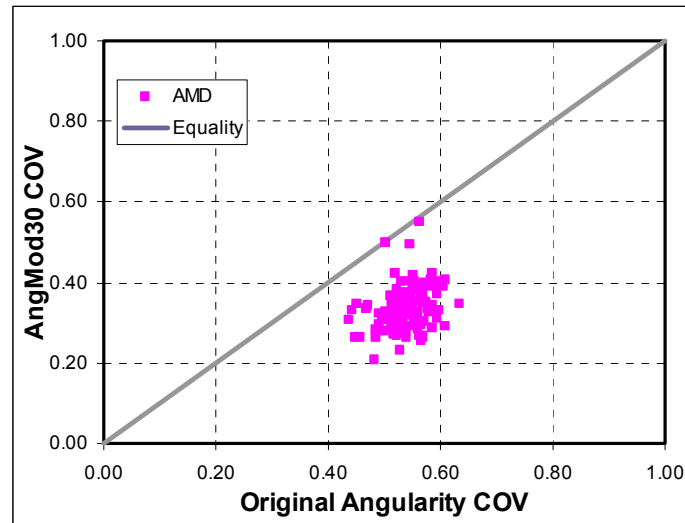


Figure 3.9. AMD Comparison between Modified and Original Angularity COV.

Comparison of AIMS Units Using Modified Angularity

Graphs of the comparison between the TTI and TxDOT AIMS units are given in Figures 3.10, 3.11, and 3.12 for aggregates BMD, AMD, and combined, respectively. The regression equations are given in Table 3.4. The modified angularity values are all given in Table A.7 of Appendix A.

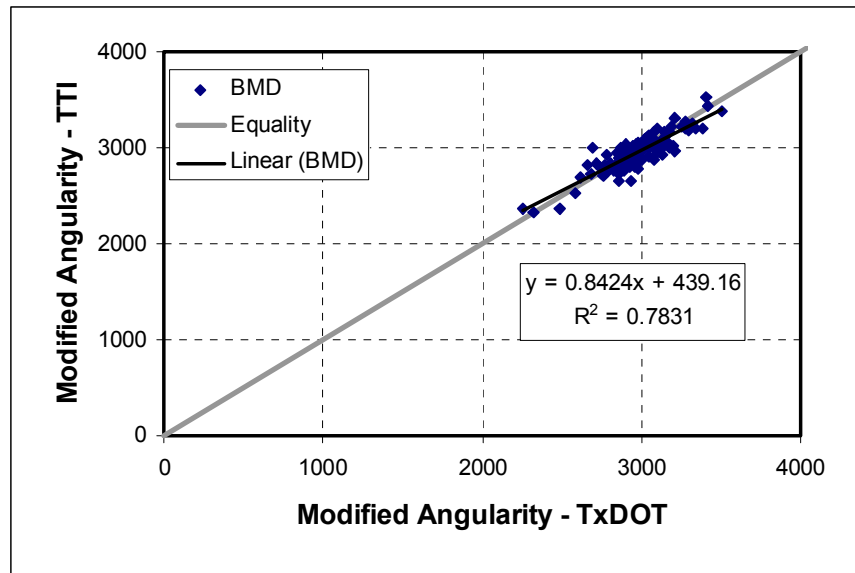


Figure 3.10. Modified Angularity Comparison BMD.

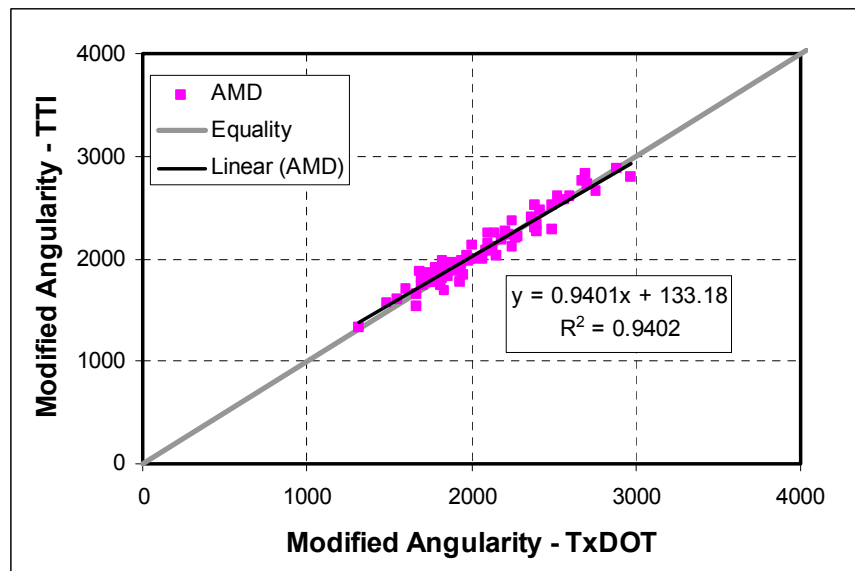


Figure 3.11. Modified Angularity Comparison AMD.

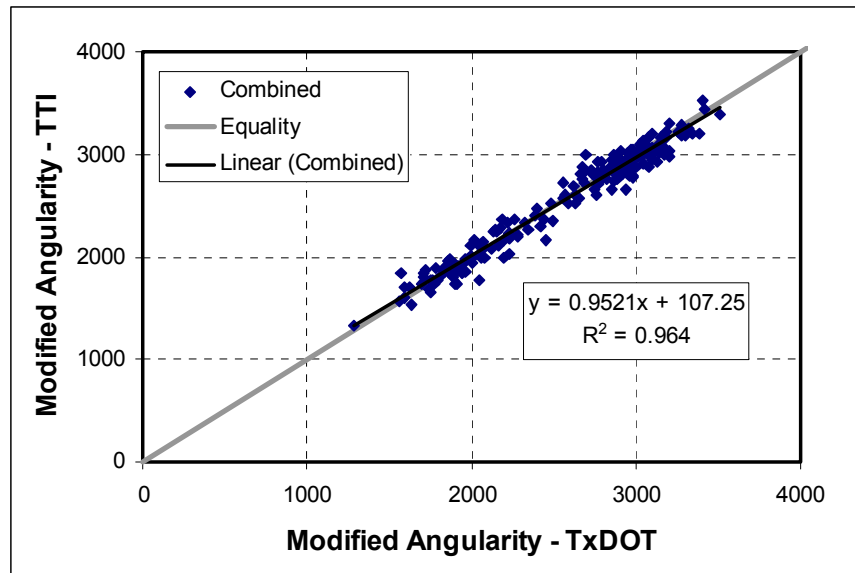


Figure 3.12. Modified Angularity Comparison Combined BMD and AMD.

Table 3.4. Modified Angularity Regression Summary.

	Equation	R ² value
BMD	$TTI = 0.8424 * TxDOT + 439.16$	0.7831
AMD	$TTI = 0.9401 * TxDOT + 133.18$	0.9402
Combined	$TTI = 0.9521 * TxDOT - 107.25$	0.9640

The modified angularity index shows a much better correlation between the two AIMS units. The combination of BMD and AMD results gives an R² value of 0.96 with very small bias, indicating that the two units give nearly the same results. This is a much more favorable comparison than the original angularity method that had an R² value of 0.62. Also, the modified method offers a lower coefficient of variation than the original method.

Aggregate Particle Texture Comparison

As discussed earlier, the wavelet method is capable of analyzing the different texture scales on a particle surface. The AIMS analysis software provides six levels of texture; however, only level 6, representing the largest scale of texture in the analysis, has been used thus far in classifying aggregates. Comparison of the texture indices given by the two AIMS units is shown in Figures 3.13, 3.14, and 3.15 for aggregates BMD, AMD, and combined, respectively. Table 3.5 summarizes the regression analysis results for these comparisons. All texture data are summarized in Table A.3 of Appendix A. The two systems are highly correlated, with R^2 values greater than 0.88.

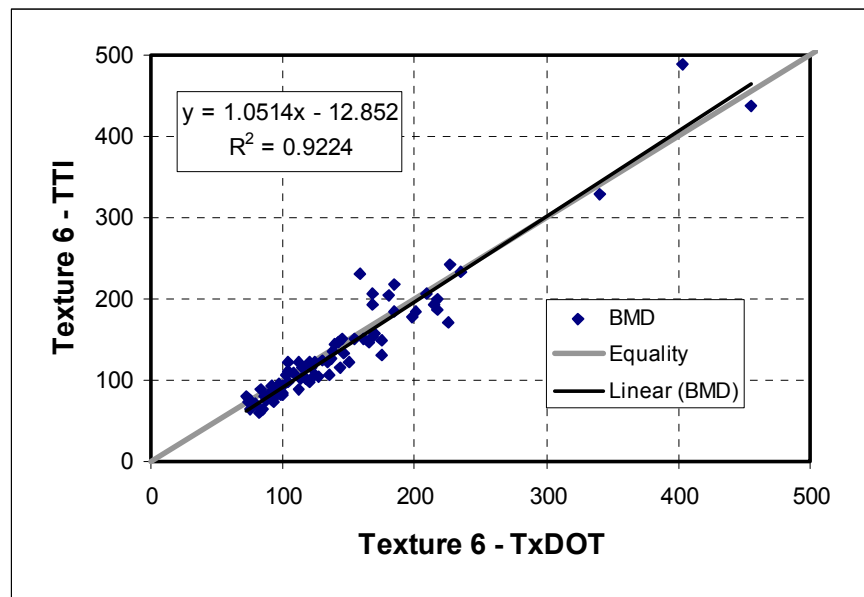


Figure 3.13. Texture Level 6 Comparison of BMD Aggregates.

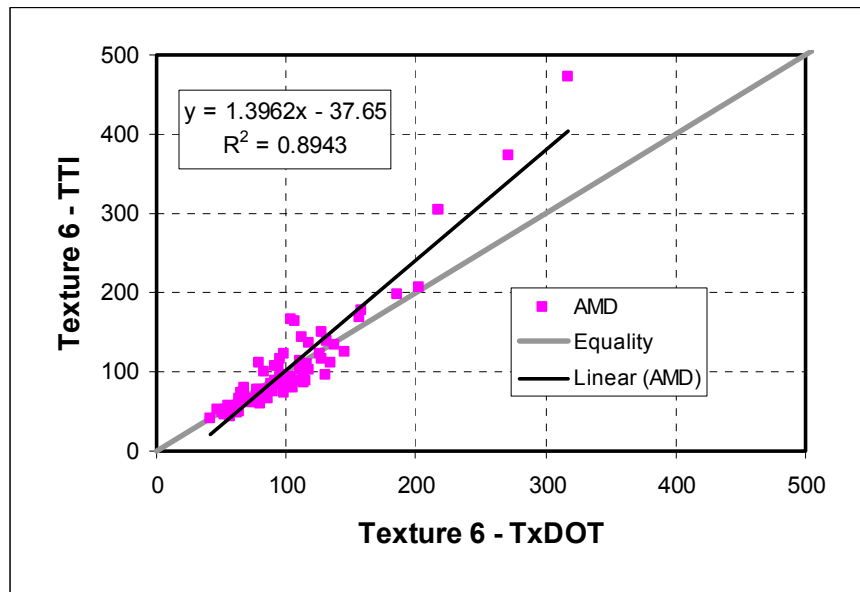


Figure 3.14. Texture Level 6 Comparison of AMD Aggregates.

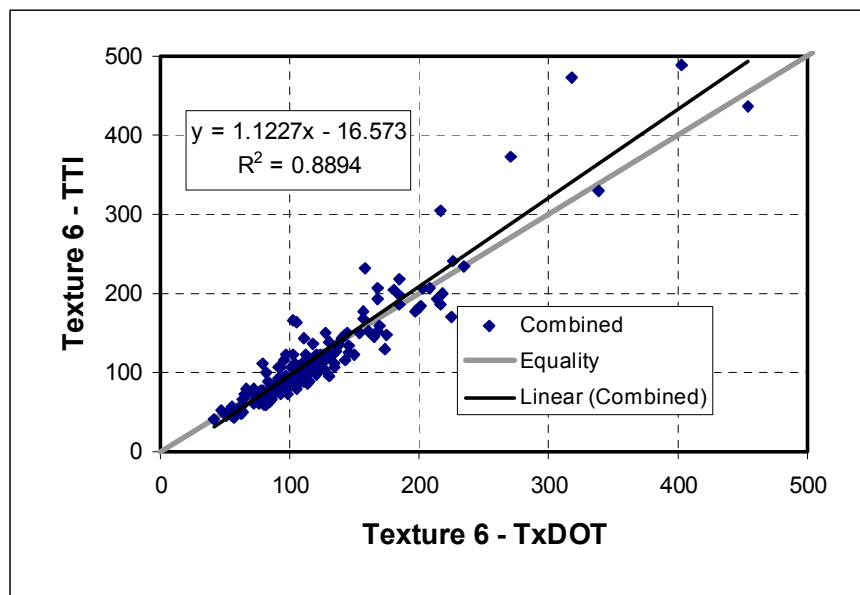


Figure 3.15. Texture Level 6 Comparison of Combined BMD and AMD Aggregates.

Table 3.5. Texture Level 6 Regression Results.

	Equation	R² value
BMD	$TTI = 1.0514 * TxDOT - 12.85$	0.9224
AMD	$TTI = 1.3962 * TxDOT - 37.65$	0.8943
Combined	$TTI = 1.1227 * TxDOT - 16.57$	0.8894

Modification of Texture Method

During the course of the construction of the database and comparison of its results, the texture values for aggregates with fine texture such as some sandstones were thought to be low compared to aggregates that have coarse surface texture. Also, some of these sandstones had a history of good performance in terms of texture and the retention of texture under traffic loading. Based on this observation, it was decided to conduct further analysis to examine the influence of the texture level on ranking of aggregates.

The texture analysis was conducted on six sandstone aggregates, a granite, a quartzite, and two limestone aggregates. Table 3.6 lists the aggregate names used for this portion of the study as well as their corresponding TxDOT lab number in the database. The aggregates passed the 3/4 inch sieve and were retained on sieve #4.

The different texture levels were captured using three different magnifications (9x, 12x, and 16x), using two different objective lenses (0.25 and 0.5 objective lenses), and the assessment of three texture levels (levels 4, 5, and 6). In the AIMS procedure, the 0.25 objective lens is used to analyze the coarse aggregates, while the 0.5 objective

lens is used to analyze the fine aggregates. However, they were both used in this experiment to analyze coarse aggregates to examine the influence of magnification on the analyzed texture scale. The 56 particles from each of the aggregates listed in Table 3.6 were analyzed. The results from levels 1 and 2 were not able to discriminate among the different aggregate sources; the results were within a small range of the same six sandstones. Level 3 correlated highly to level 4.

Table 3.6. Summary of Sample Names and TxDOT Lab Numbers.

Sample	Study Name	TxDOT Lab Number
Sandstone 1	SS-1	05-0771
Sandstone 2	SS-2	05-0828
Sandstone 3	SS-3	05-1190
Sandstone 4	SS-4	05-1210
Sandstone 5	SS-5	05-1221
Sandstone 6	SS-6	05-1222
Granite	Granite	N/A*
Limestone 1	LS-1	N/A*
Quartzite	Qtz	05-0946
Limestone 2	LS-2	05-0251

**These materials were not used to construct the database and therefore do not have TxDOT Lab numbers.*

Figure 3.16 shows the results of analyzing the six sandstone aggregates using level 6 texture, three magnifications, and coarse (0.25 objective) and fine (0.5 objective) lenses. Table 3.7 shows a summary of the variables used in this analysis. For the sandstones tested, the average texture index generally increased with the use of the fine

lens compared with the coarse lens due to capturing smaller scale of texture. Changing the magnification level for the same lens did not have considerable effect on texture. However, in general the highest texture index was either for the 12x or the 16x magnification. These findings support the assumption that sandstones have a finer texture than what is typically measured using the current AIMS procedure.

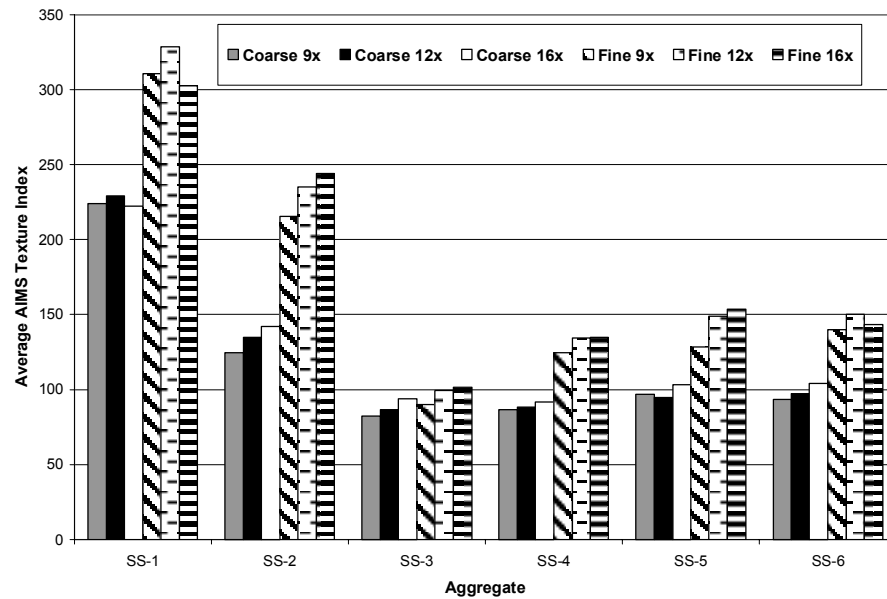


Figure 3.16. Average Level 6 Texture Indices of Six Sandstones with Varying Magnification and Objective Lens.

Table 3.7. Summary of Texture Scale versus Magnification Level.

Relative Texture Scale	Lens	Magnification	Texture Level
Fine	0.50 objective	16	4
Medium	--	12	5
Coarse	0.25 Objective	9	6

Using texture levels 4, 5, and 6, the effect of texture scale was compared among the different aggregates as well. As shown in Figure 3.17, the granite and limestone aggregates exhibited an increase in texture index as the texture level increased. The sandstones and quartzite each had a lower texture index for level 6 than the other two levels. This again shows that most of the texture in the tested sandstones was of a small scale (fine texture), while the texture in the tested granite and limestone was more pronounced in the large scale (coarse texture).

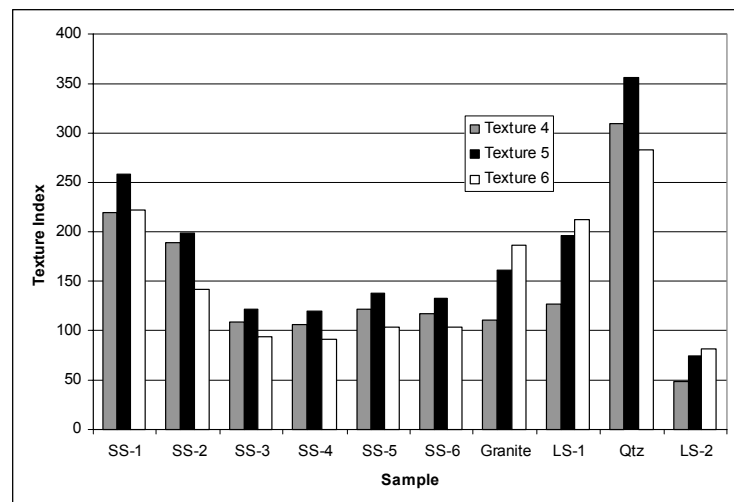


Figure 3.17. Comparison of Texture Levels of Six Sandstones, One Granite, One Highly Textured Limestone, One Quartzite, and One Low Textured Limestone.

As the data suggest, the sandstone and quartzite aggregates both have a much finer texture than what is typically considered in the AIMS procedure. It was therefore decided to use the average of levels 4 and 5 in analyzing aggregate texture. The results from averaging these two levels were also found to be consistent with the experience of

skid resistance of these aggregates in asphalt pavement surfaces. The change to the new texture levels requires minimal software modification and no changes to the system hardware. Using texture levels 4 and 5 with the same coarse lens (0.25 objective lens) gave very good correlation with using the fine lens (0.5 objective) and level 6. However, the first alternative is more favorable than using the fine lens, as this makes it difficult to achieve automated focusing and control of top lighting intensity on aggregate surface. The average of texture levels 4 and 5 was used as a basis of comparison between the two AIMS units. The level 6 texture was plotted against the average texture for levels 4 and 5 for all aggregates in the database. These plots are shown in Figure 3.18 for BMD samples and in Figure 3.19 for AMD samples.

The values for the average of texture levels 4 and 5 is higher than level 6 for the sandstones, as shown in Figures 3.18 and 3.19. The majority of the limestone and gravel samples exhibited a higher level 6 texture than the averages of levels 4 and 5. The COV was also studied to determine the variability of the texture within the aggregate samples, and the results are shown in Figure 3.20 for BMD samples and Figure 3.21 for AMD samples. It can be seen by looking at Figures 3.20 and 3.21 that the sandstones generally had the lowest COV. These results lead to the conclusion that sandstone aggregates have a more uniform texture compared with the gravels and limestones.

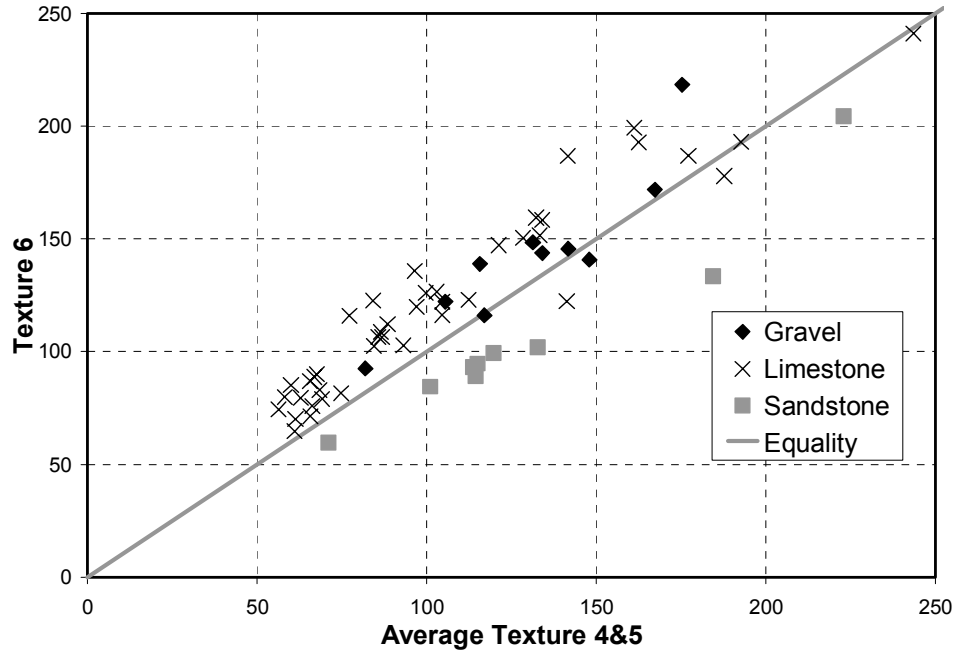


Figure 3.18. Texture Level Comparison for BMD Samples.

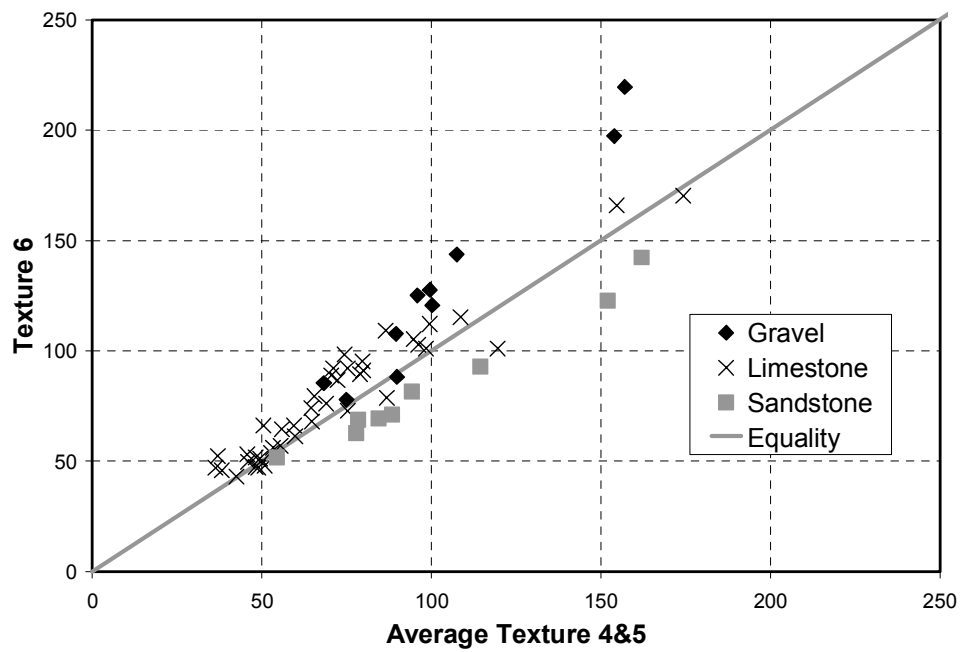


Figure 3.19. Texture Level Comparison for AMD Samples.

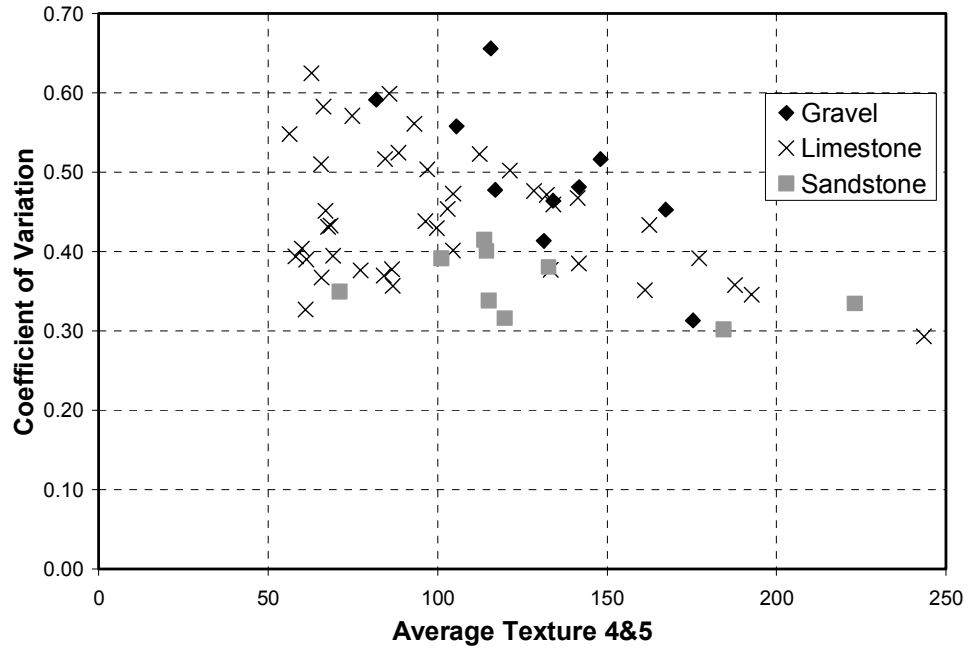


Figure 3.20. Coefficient of Variation Comparison for BMD Samples.

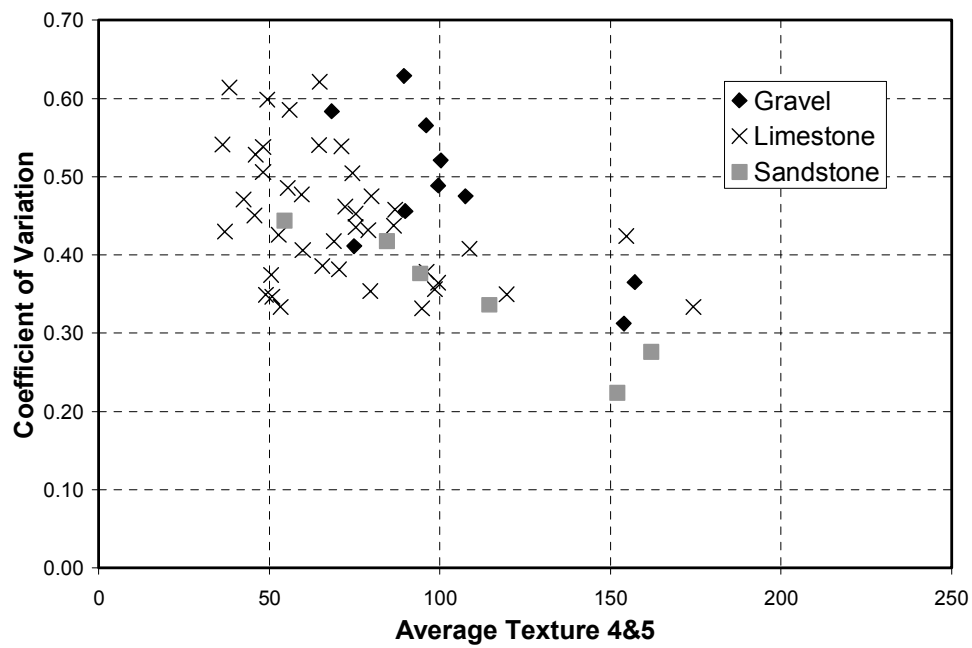


Figure 3.21. Coefficient of Variation Comparison for AMD Samples.

Comparison of AIMS Units Using Average Texture Levels 4 and 5

The correlation between the two AIMS units was assessed using the average of texture levels 4 and 5. The graphs for this comparison are shown in Figure 3.22 for the BMD samples, in Figure 3.23 for the AMD samples, and in Figure 3.24 for the combination of BMD and AMD samples. Table 3.8 shows the linear regression results for the comparison. The regression results show that there is a high correlation between the systems, with an R^2 value of 0.92 for the combined samples. All of the average of texture levels 4 and 5 are available in Table A.8 of Appendix A.

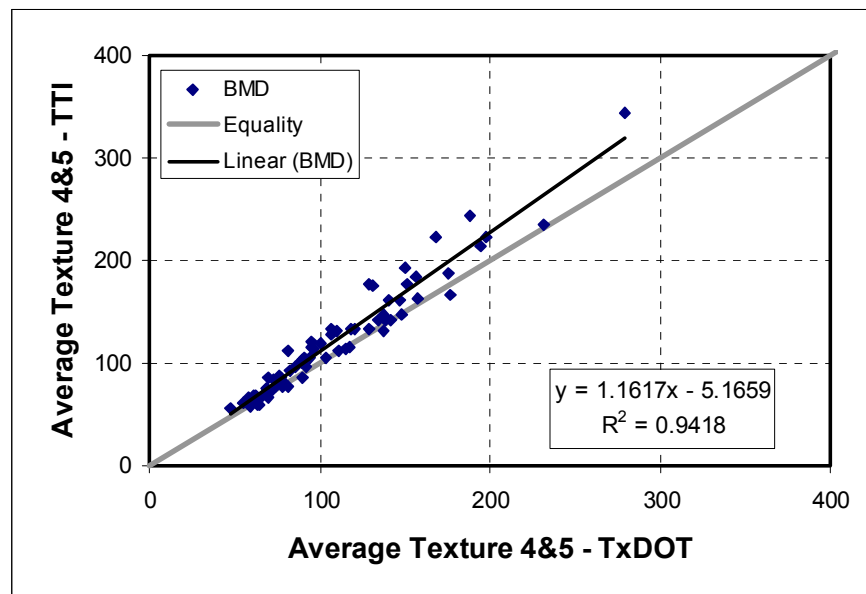


Figure 3.22. Average of Texture Levels 4 and 5 Comparison of BMD Samples.

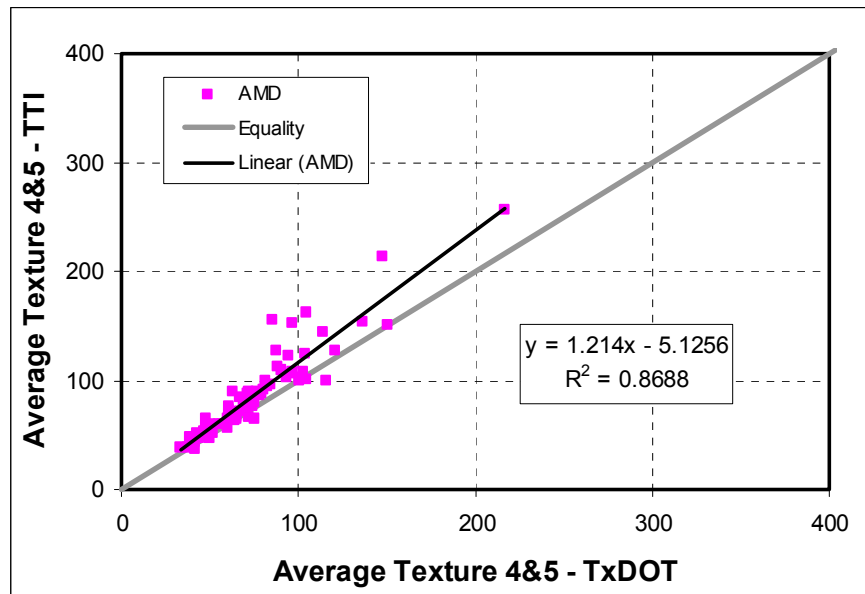


Figure 3.23. Average of Texture Levels 4 and 5 Comparison of AMD Samples.

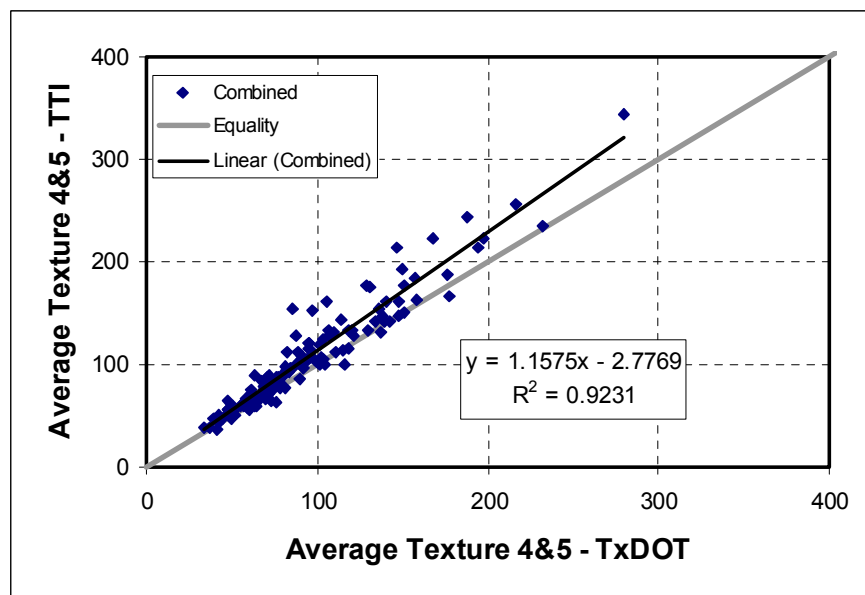


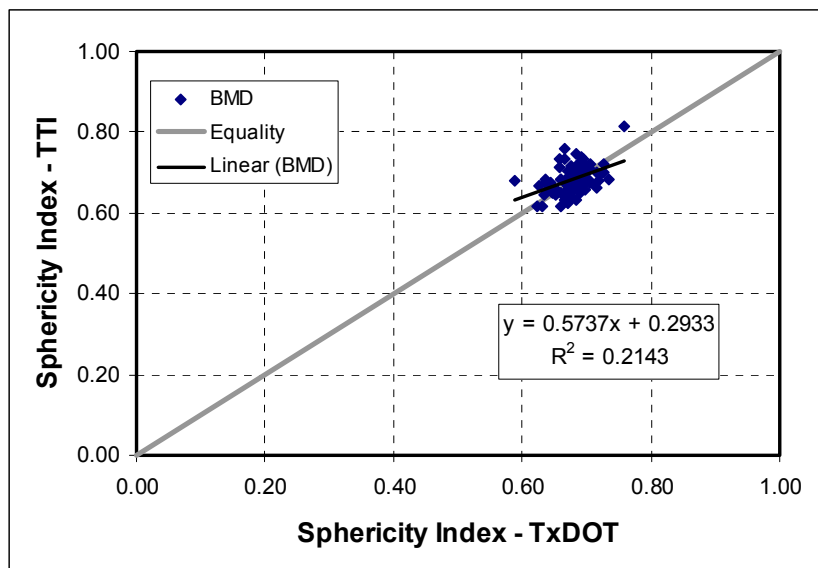
Figure 3.24. Average of Texture Levels 4 and 5 Comparison of Combined BMD and AMD Samples.

Table 3.8. Average of Texture Levels 4 and 5 Regression Results.

	Equation	R ² value
BMD	$TTI = 1.1617 * TxDOT - 5.1659$	0.9418
AMD	$TTI = 1.2140 * TxDOT - 5.1256$	0.8688
Combined	$TTI = 1.1575 * TxDOT - 2.7769$	0.9231

Sphericity Comparison

The sphericity indices from the two AIMS units were cataloged in the database and used for comparison of the units. The comparison of the two systems is shown in Figure 3.25 for BMD samples, Figure 3.26 for AMD samples, and Figure 3.27 for the combination of BMD and AMD samples. The regression results are also summarized in Table 3.9. Table A.4 in Appendix A contains all data for the sphericity.

**Figure 3.25. Sphericity Comparison for BMD Samples.**

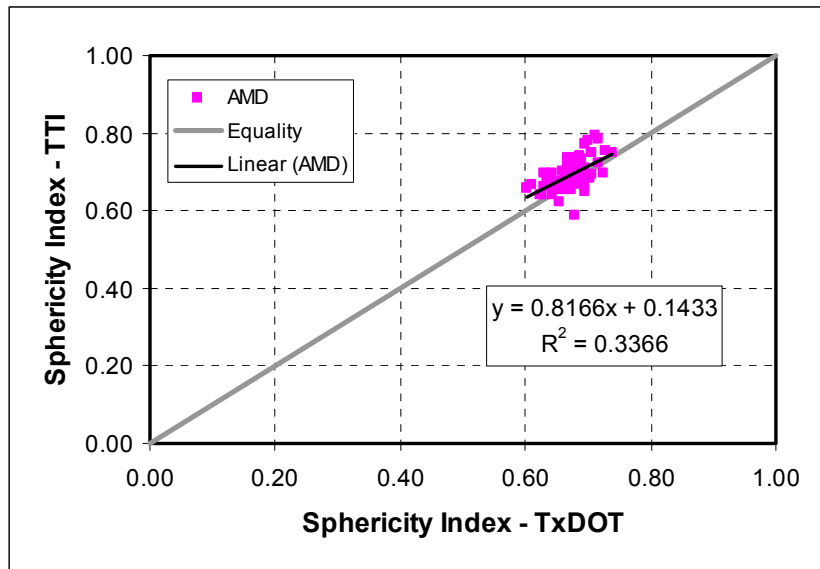


Figure 3.26. Sphericity Comparison for AMD Samples.

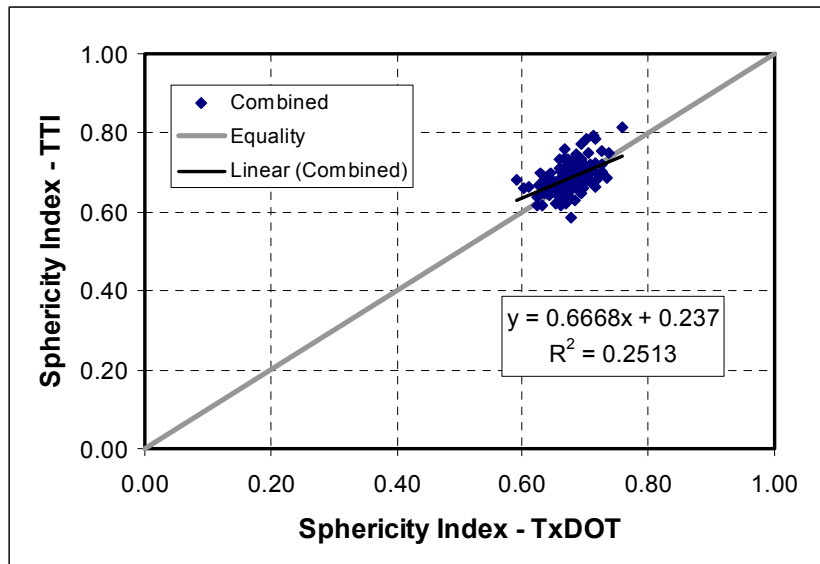


Figure 3.27. Sphericity Comparison for Combined BMD and AMD Samples.

Table 3.9. Sphericity Regression Results.

	Equation	R² value
BMD	$TTI = 0.5737 * TxDOT + 0.2933$	0.2143
AMD	$TTI = 0.8166 * TxDOT + 0.1433$	0.3366
Combined	$TTI = 0.6668 * TxDOT + 0.2370$	0.2513

Most of the sphericity values are between 0.6 and 0.7. The low spread in the data contributed to the low correlation between the TxDOT and TTI sphericity values. In general, most of the data are close together, and the variation between the two units would not cause the average to fall into another category. The distribution of the sphericity values within a sample is a better way to compare the TxDOT and TTI measurements.

Comparison of the Texture of Polishing Coupons

Aggregate coupons were polished using the British polishing wheel at the TxDOT laboratory. These coupons were then scanned using the AIMS at both of laboratories. The coupon texture measurements consist of placing four coupons on the lighting table, then performing texture analysis at magnification 12x with a moving interval of 12 mm in the x-direction and 8 mm in the y-direction. A total 120 images of the surface of aggregates in four coupons were captured in this analysis method. Images were analyzed using the same wavelet method used for aggregate particles. Seventy-five

coupons of various aggregates were used in this analysis. Table 3.10 summarizes the aggregate types used in these coupons.

Table 3.10. Aggregate Types Used in Coupons.

Aggregate Type	Number of Coupons
Limestone	50
Gravel	14
Lightweight Aggregate	1
Igneous Rock	1
Sandstone	7
Miscellaneous	2

The average texture results are compared in Figure 3.28. An excellent correlation exists between the coupon measurements using the two AIMS units. The R^2 is equal to 0.9137, and the equation of linear fit is $TTI = 1.1051 \times TxDOT - 9.8133$. The deviation from the equality line is accepted due to variation in the samples and orientation on the scanning table.

The confidence interval (C.I.) for the difference between the means was calculated using Equation 3.8. Based on these results, it was found that only 11 C.I.'s out of 75 do not contain zero. The C.I. containing zero indicates that the TTI and TxDOT texture measurements have the same mean value. It must be kept in mind that for the statistical analysis with 95 percent confidence level, there is always a chance for 5 percent of the data analyzed to be rejected (C.I. do not contain zero), while in reality it should not be rejected (C.I. contain zero). The categorical analysis indicated that only six cases have a p-value < 0.05 .

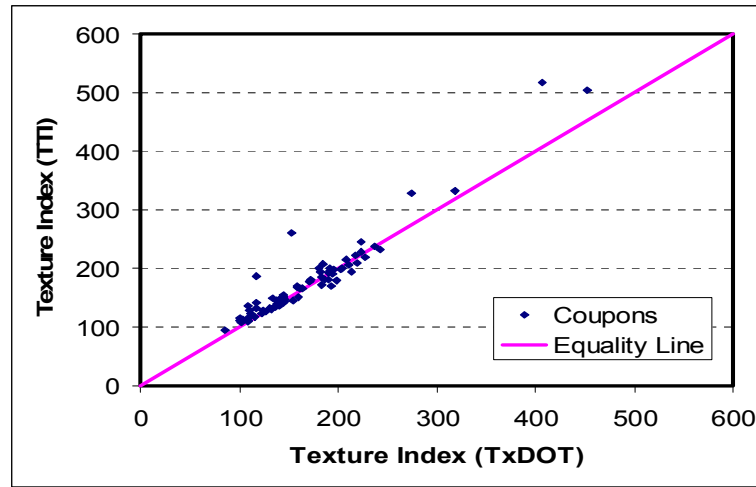


Figure 3.28. Aggregate Polished Coupon Texture Results.

$$(\bar{X}_{TTI_{i,j}} - \bar{X}_{TxDOT_{i,j}}) \pm 1.96 \times \sqrt{(\sigma_{TTI_{i,j}}^2 + \sigma_{TxDOT_{i,j}}^2)} \quad (3.8)$$

where:

$\bar{X}_{TTI_{i,j}}$ = estimated value of the mean for aggregate property scanned at TTI,

$\bar{X}_{TxDOT_{i,j}}$ = estimated value of the mean for aggregate property scanned at
TxDOT,

$\sigma_{TTI_{i,j}}$ = standard error in estimation of the mean for aggregate property at
TTI,

$\sigma_{TxDOT_{i,j}}$ = standard error in estimation of the mean for aggregate property at
TxDOT,

i = aggregate number with values of 1, 2, ..., 10, and

j = aggregate size with values of 1, 2, 3, 4, where 4 indicates the combined sizes.

Comparison of Micro-Deval Results

Aggregates were tested in the Micro-Deval at both the TTI and TxDOT laboratories. In the Micro-Deval test, aggregates are subjected to abrasion, polishing, and breakage. Consequently, the same exact sample cannot be tested in both machines. One hundred aggregate samples were included in the comparison. Aggregate types and weight loss results are listed in Table A.5 of Appendix A.

The data plotted in Figure 3.29 show that the two Micro-Deval machines produce almost the same results, except for a few cases. The statistical analysis involves fitting a linear model to the data and then determining the confidence intervals for the slope and the intercept of this model. The linear regression model is summarized in Table 3.11.

Figure 3.29 shows that there are two points that do not follow the general trend. These two points were investigated, and it was found that the TTI measurements of these two aggregates were not accurate, as the number of revolutions at the end of the Micro-Deval test was below the lower acceptable limit. According to the Micro-Deval test specification, those two results must be discarded. Therefore, the statistical analysis was repeated after removing the two points with results as shown in Figure 3.30. The new linear regression model is summarized in Table 3.12. The R^2 increased from 0.923 to 0.970, while the intercept decreased from 0.812 to 0.234. This intercept

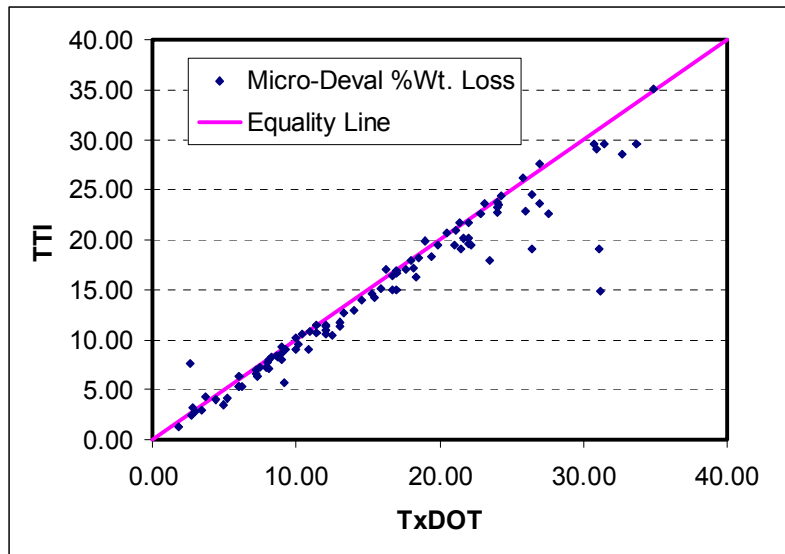


Figure 3.29. Micro-Deval Analysis of Variability: Weight Loss Results (All Data Points).

Table 3.11. Micro-Deval Analysis of Variability: Weight Loss Linear Model Results (All Data Points).

		Confidence Interval	
		Lower Limit	Upper Limit
Slope	0.872	0.822	0.922
Intercept	0.812	-0.08	1.705
R²	0.923		

became closer to zero, which is the intercept of the equality line. Although the confidence intervals for the intercept contained zero for the two cases, the second case is closer to equally spread around zero. The slope value increased from 0.872 to 0.924, indicating that data became closer to the equality line. Neither confidence intervals for the slope in the two cases contained one, but the confidence interval is closer to one in the second case.

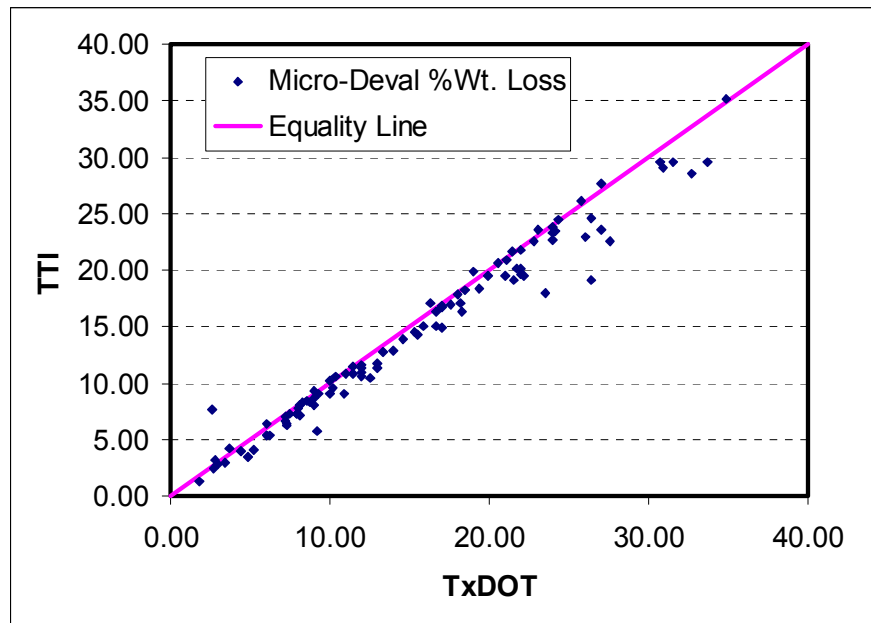


Figure 3.30. Micro-Deval Analysis of Variability: Weight Loss Results (Excluding Outliers).

Table 3.12. Micro-Deval Analysis of Variability: Weight Loss Linear Model Results (Excluding Outliers).

		Confidence Interval	
		Lower Limit	Upper Limit
Slope	0.924	0.891	0.957
Intercept	0.234	-0.335	0.804
R²	0.970		

Residual analysis is important as it provides the proof for the goodness of fit using the linear model. Residual analysis for the two fitted models showed that the second one is much better, as the residual is more spread out and closer to the normal distribution than the first model.

Correlation of Micro-Deval and Magnesium Sulfate Soundness

Many literature sources indicate that there is often a relationship between the percent loss between the Micro-Deval test and the sulfate soundness test (Wu et al. 1998, Rogers 1998, Prowel et al. 2005). This relationship was tested using the measurements conducted in this study. The magnesium sulfate soundness test was conducted according to TxDOT standard Tex-411-A, and the Micro-Deval test was conducted according to TxDOT standard Tex-461-A. The percent loss from each test was plotted against each other and a linear regression analysis was conducted to assess the correlation between the two properties. The relationship between the two test results is shown in Figure 3.31.

A reasonable correlation exists between the two aggregate properties, as both tests measure an aggregate's resistance to wear and weathering. The R^2 coefficient of 0.61 is very near that of Rogers (1998) and Prowel et al. (2005), who noted R^2 values of 0.66 and 0.76, respectively. The relationship found by Cooley and James (2003) was considerably lower than this, with an R^2 value of 0.10, but this value seemed to be influenced by two outlying points. Without these values, the correlation would most

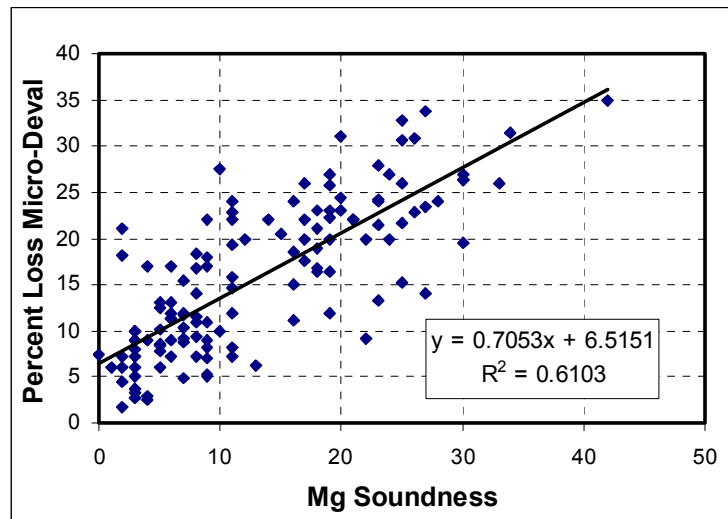


Figure 3.31. Correlation of Percent Loss of Sulfate Soundness and Micro-Deval.

likely be much closer to the value obtained in other studies. Although the Micro-Deval is typically considered a measure of mechanical degradation and magnesium sulfate soundness is considered a measure of an aggregate's susceptibility to weathering, this and other studies clearly indicate a relationship between the results from these tests for an aggregate source.

Analysis of Accelerated Polish Test

The accelerated polish test results using Tex-438-A were analyzed and grouped into different ranges as shown in Table 3.13. As given in Table 3.13 and Figure 3.32, the results were within a very small range, where 61 percent of the data were between a PSV of 28 and 32, a range of only 4 PSV. Kandhal et al. (1993) reported similar results; they reported that 59 percent of limestone aggregates are between the values of 28 and 32, while 75 percent of gravel aggregate's results are in the same range. With such a large

percentage of aggregates falling within a small range, distinguishing between similar aggregates becomes difficult. The other drawback of this test, which is presented in the literature review, is that this test result (PSV) is a function of many factors other than texture. The AIMS texture measurements of aggregates are therefore preferred to the PSV method due to the shorter testing time and more sensitive results.

Table 3.13. PSV Frequency Percentage Distribution.

Range	Frequency	Percentage (Percent)
$24 < \text{PSV} \leq 28$	7	21
$28 < \text{PSV} \leq 32$	20	61
$32 < \text{PSV} \leq 36$	1	3
$36 < \text{PSV} \leq 40$	4	12
$40 < \text{PSV} \leq 44$	0	0
$44 < \text{PSV} \leq 48$	0	0
$48 < \text{PSV} \leq 52$	1	3
Total	33	100

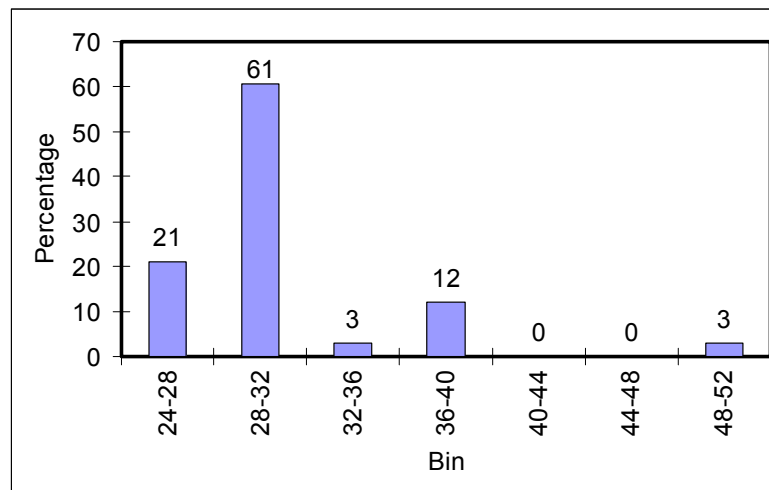


Figure 3.32. PSV Percentages Histogram.

SUMMARY

This chapter presents the data produced and cataloged in the database as part of this study. These data were used to compare the AIMS units that are in use at the TTI and TxDOT laboratories. The comparison of the two AIMS units confirmed the findings of Mahmoud (2005) that the two AIMS units provide very similar results.

The angularity analysis method was improved in order to reduce the variability in the measurements within the same aggregate source. The texture analysis method was also enhanced in order to increase the sensitivity of the method to fine texture (smaller scale texture).

The difference in Micro-Deval measurements conducted using two machines was also analyzed in this chapter. Excellent correlation was found between the measurements of the two machines. Correlation between the two properties of percent loss due to Micro-Deval and magnesium sulfate soundness was also assessed. This resulted in a moderate correlation.

Finally, the results from the accelerated polishing test of the database aggregates were analyzed. The majority of the residual PSV measurement fell within a very small range. This makes distinguishing between like aggregates difficult, and the AIMS texture method is therefore preferred due to its increased sensitivity and decreased time requirements.

CHAPTER IV

CLASSIFICATION OF AGGREGATES

OVERVIEW

The current AIMS software classifies each aggregate particle into one of four or five levels, depending upon the property being studied. Table 4.1 summarizes the classifications used for each of the AIMS measured properties. These classifications were originally developed as part of the NCHRP 4-30 study (Masad et al. 2005). The original classification was based on testing 13 aggregate sources with a wide range of characteristics. The Ward's Linkage clustering method in SPSS was used in classifying these aggregates.

Table 4.1. Summary of Aggregate Properties and Classifications.

		Aggregate Property		
		Angularity	Texture	Sphericity
Classification Groups	Rounded	Polished	Flat/Elongated	
	Sub-Rounded	Smooth	Low Sphericity	
	Sub-Angular	Low Roughness	Moderate Sphericity	
	Angular	Moderate Roughness	High Sphericity	
	---	High Roughness	---	

During the course of this study, the researchers decided that the classification system should be simplified into only three categories for each aggregate property: low,

medium, and high. Also, a larger number of aggregate samples has been tested than was originally tested in the NCHRP 4-30 study. This chapter presents the method used to determine the bounds for each of the aggregate properties.

The chapter also revisits the aggregate classification method used by TxDOT as part of the wet weather accident reduction program. A new method that relies on AIMS texture measurements and magnesium sulfate soundness is recommended. The threshold values used in this proposed classification method are not supported by performance data, and future research should focus on accurate determination of these threshold values.

CLASSIFICATION USING CLUSTERING ANALYSIS

To determine the original clusters, the Ward's Linkage clustering method within SPSS was used. The Ward's Linkage clustering method is based upon minimizing the distance between each individual measurement and its cluster. For the NCHRP study, the Euclidean distance was set as the distance that was to be minimized for clustering the cases. This distance is calculated using Equation 4.1.

$$Dist = \frac{\sum_{i=1}^n (x_i - \bar{x})(y_i - \bar{y})}{\sqrt{\sum_{i=1}^n (x_i - \bar{x})^2 \sum_{i=1}^n (y_i - \bar{y})^2}} \quad (4.1)$$

where:

x and y represent two p -dimensional observations (items),

$x = [x_1, x_2, \dots, x_p]$, and

$y = [y_1, y_2, \dots, y_p]$.

Ward's Linkage method tries to make the similarity or distance measures sum of squares within groups as small as possible (Al-Rousan 2004).

For this study, the K-mean clustering method in SPSS was used. K-mean clustering is a non-hierarchical clustering method. A specified number of clusters is chosen, three in this case. Each of the data points is randomly assigned to one of the clusters until each of the clusters has approximately the same number of data points. The distance between each data point and each cluster is then calculated. A data point is in the correct cluster if it is closest to its own cluster; otherwise, the point is moved to the cluster it is closest to. This process is repeated until no data points change clusters after calculating the distance from the clusters. This method is very helpful in quickly analyzing a large number of data points but final clustering results depend upon the initial clusters chosen (Lingras and Huang 2005).

Clustering was conducted for the modified angularity method, the average of texture levels 4 and 5, and sphericity. The analysis was done for all particles from the three sieve sizes (3/8 inch, 1/4 inch, and #4) analyzed BMD, AMD, and combined for the TTI data. The clustering results for the angularity index are summarized in Table 4.2, while the results for the average of texture levels 4 and 5 are summarized in Table 4.3 and the sphericity results are summarized in Table 4.4. The percentages of particles that fell within each of the categories are summarized in Tables 4.5 through 4.7.

Table 4.2. Bounds for Modified Gradient Angularity.

	Low	Medium	High
Angularity – BMD only	< 2590.26	2590.26 – 3615.90	> 3615.90
Angularity – AMD only	< 1738.04	1738.04 – 2717.17	> 2717.17
Angularity – Combined	< 2056.82	2056.82 – 3193.55	> 3193.55

Table 4.3. Bounds for Average of Texture Levels 4 and 5.

	Low	Medium	High
Texture – BMD only	< 118.5	118.5 – 238.5	> 238.5
Texture – AMD only	< 106.5	106.5 – 274.5	> 274.5
Texture – Combined	< 111.5	111.5 – 243.5	> 243.5

Table 4.4. Bounds for Sphericity.

	Low	Medium	High
Sphericity – BMD only	< 0.549	0.549 – 0.717	> 0.717
Sphericity – AMD only	< 0.592	0.592 – 0.739	> 0.739
Sphericity – Combined	< 0.573	0.573 – 0.729	> 0.729

Table 4.5. Percentage of Particles Falling Within Each Category for Angularity.

	Low	Medium	High
Angularity – BMD only	33.51 %	48.33 %	18.16 %
Angularity – AMD only	35.16 %	47.64 %	17.20 %
Angularity – Combined	31.62 %	47.75 %	20.63 %

Table 4.6. Percentage of Particles Falling Within Each Category for Texture.

	Low	Medium	High
Texture – BMD only	57.95 %	32.50 %	9.55 %
Texture – AMD only	70.63 %	26.86 %	2.51 %
Texture – Combined	63.73 %	30.04 %	6.23 %

Table 4.7. Percentage of Particles Falling Within Each Category for Sphericity.

	Low	Medium	High
Sphericity – BMD only	11.01 %	48.52 %	40.46 %
Sphericity – AMD only	16.53 %	48.13 %	35.34 %
Sphericity – Combined	13.93 %	48.59 %	37.48 %

As shown in Tables 4.2 and 4.3, the AMD samples have lower cluster bounds than the BMD samples for both texture and angularity. This difference is expected since the particles have been abraded and therefore have less texture and more rounded edges. Because the AMD particles are more rounded, it is reasonable that the sphericity clusters are higher, which is the case for these results, as evident in Table 4.4. As expected, in each aggregate property the bounds of the combined sample fall between those of the individual AMD or BMD bounds.

CLASSIFICATION USING QUARTILE ANALYSIS

The clustering analysis used in the previous section gave bounds for the three categories of aggregates. However, a small percentage of aggregates (less than 10 percent) fall under the high texture category. For the angularity analysis, the percentages

of aggregates classified as high angularity were less than 25 percent. It is believed that this classification would penalize aggregates with relatively high texture and angularity. The aggregates used in this study represented a wide range of mineralogy. Visual inspection of these aggregates revealed that they included materials with the highest angularity and texture that can be encountered. Therefore, classification was proposed to be based on quartiles. In this approach, the bounds are selected such that 25 percent of all aggregate particles are low, 50 percent are in the medium range, and 25 percent are in the high range. These bounds, based upon individual particle measurements, are shown in Tables 4.8, 4.9, and 4.10 for angularity, texture, and sphericity, respectively.

It is sometimes desirable to classify an aggregate sample based on average properties. Therefore, the bounds for the average properties were determined based on the quartile analysis (25 percent of aggregates within the low range, 50 percent in the medium range, and 25 percent in the high range). The bounds based on average aggregate properties are presented in Tables 4.11, 4.12, and 4.13 for angularity, texture, and sphericity, respectively. In the case of sphericity, aggregates have a very small range for average angularity. It may therefore be desirable to classify sphericity based upon distribution, such as percent flat and elongated or some other measure such as percent less than 0.6.

Table 4.8. Individual Particle Angularity Quartiles.

	First Quartile	Median	Third Quartile
BMD Only	2420.46	2885.91	3417.84
AMD Only	1528.24	2017.96	2508.22
Combined	1880.73	2463.79	3060.59

Table 4.9. Individual Particle Texture Quartiles.

	First Quartile	Median	Third Quartile
BMD Only	65.0	103.5	161.5
AMD Only	46.5	74.0	115.5
Combined	54.5	87.0	138.5

Table 4.10. Individual Particle Sphericity Quartiles.

	First Quartile	Median	Third Quartile
BMD Only	0.615	0.691	0.763
AMD Only	0.624	0.698	0.772
Combined	0.620	0.694	0.767

Table 4.11. Average Angularity Quartiles.

	First Quartile	Median	Third Quartile
BMD Only	2838.18	2939.01	3056.53
AMD Only	1832.14	1981.01	2239.57
Combined	1981.33	2656.14	2938.13

Table 4.12. Average Texture Quartiles.

	First Quartile	Median	Third Quartile
BMD Only	77.71	113.14	147.42
AMD Only	56.24	79.00	103.36
Combined	67.77	92.08	132.09

Table 4.13. Average Sphericity Quartiles.

	First Quartile	Median	Third Quartile
BMD Only	0.661	0.681	0.705
AMD Only	0.667	0.687	0.713
Combined	0.664	0.682	0.709

Figure 4.1 shows angularity versus texture for the BMD samples, AMD samples are plotted in Figure 4.2, and the combination of BMD and AMD are shown in Figure 4.3. Igneous aggregates generally have the highest angularity, as seen in Figures 4.1, 4.2, and 4.3. Limestones have a wide spread in texture, and gravels have a narrower spread than the limestones in texture, but have both moderate levels of angularity and texture. The previous chapter discussed the low variability in the sandstone samples, which is considered an important factor contributing to the abrasion resistance of these aggregates.

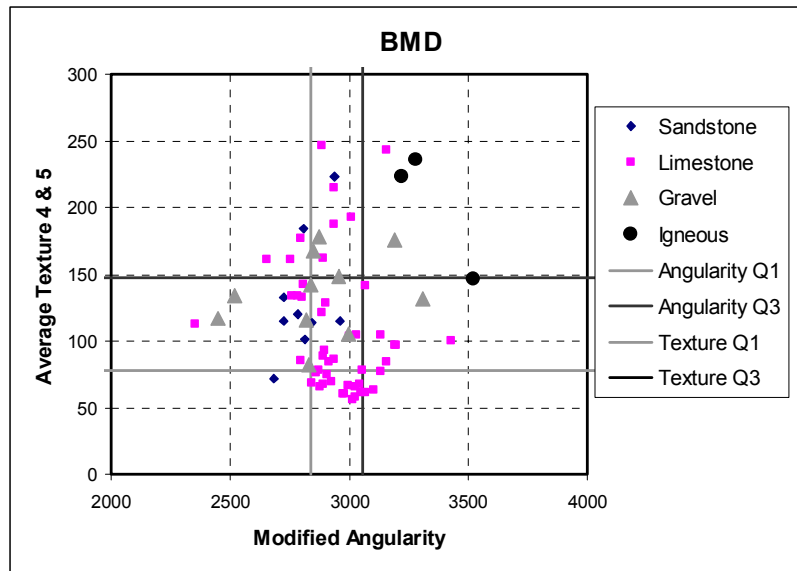


Figure 4.1. Clustering Comparison Based on Mineralogy for BMD Samples.

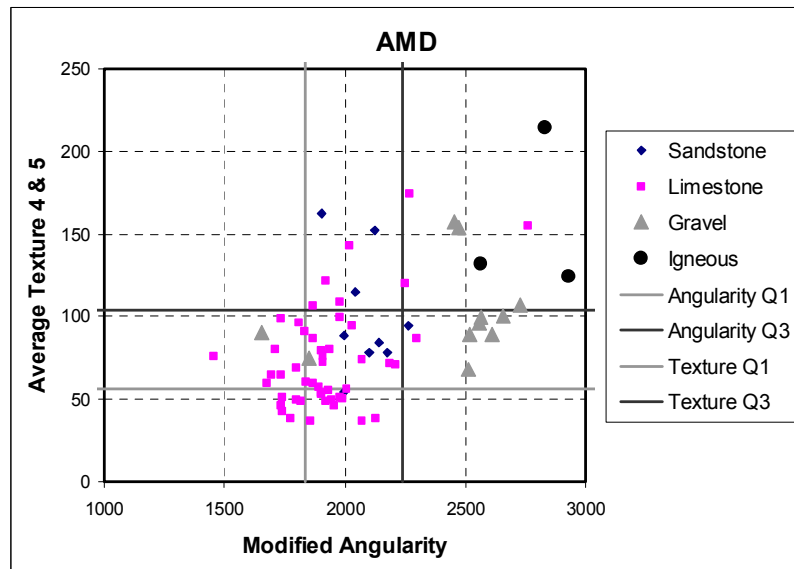


Figure 4.2. Clustering Comparison Based on Mineralogy for AMD Samples.

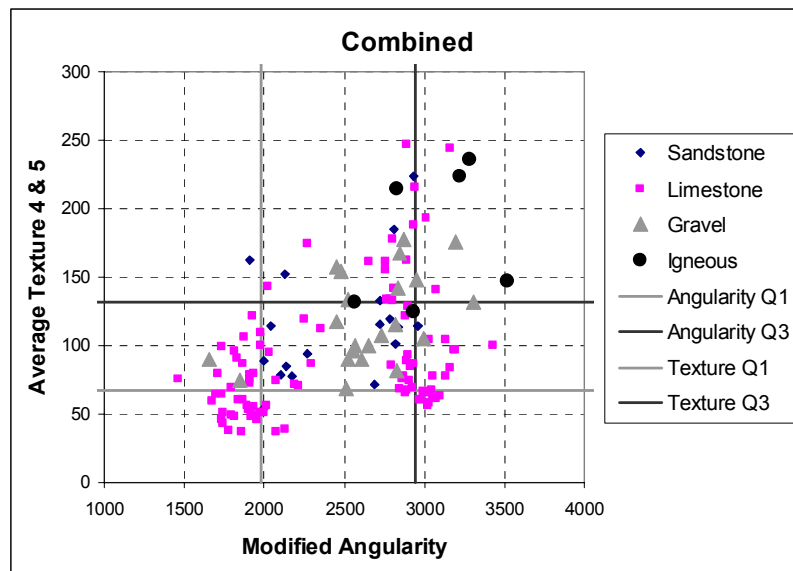


Figure 4.3. Clustering Comparison Based on Mineralogy for Combined Samples.

CLASSIFICATION OF AGGREGATES USED IN ASPHALT PAVEMENT SURFACES

TxDOT has implemented the WWARP, which is aimed at reducing the number of accidents due to inadequate surface friction of pavement in wet weather situations. To determine the surface friction demand, several inputs are studied. These inputs include, but are not limited to, precipitation, traffic volume and speed, accident history, and skid performance. Once these and several other inputs are evaluated, an aggregate is chosen based upon its classification to fit the surface friction needs of the roadway. The aggregates are classified as A, B, C, and D, with A as the best and D as the worst. The method of classification is based upon the magnesium sulfate soundness test and the residual polished stone value. The chart used for classification purposes is shown in Figure 4.4.

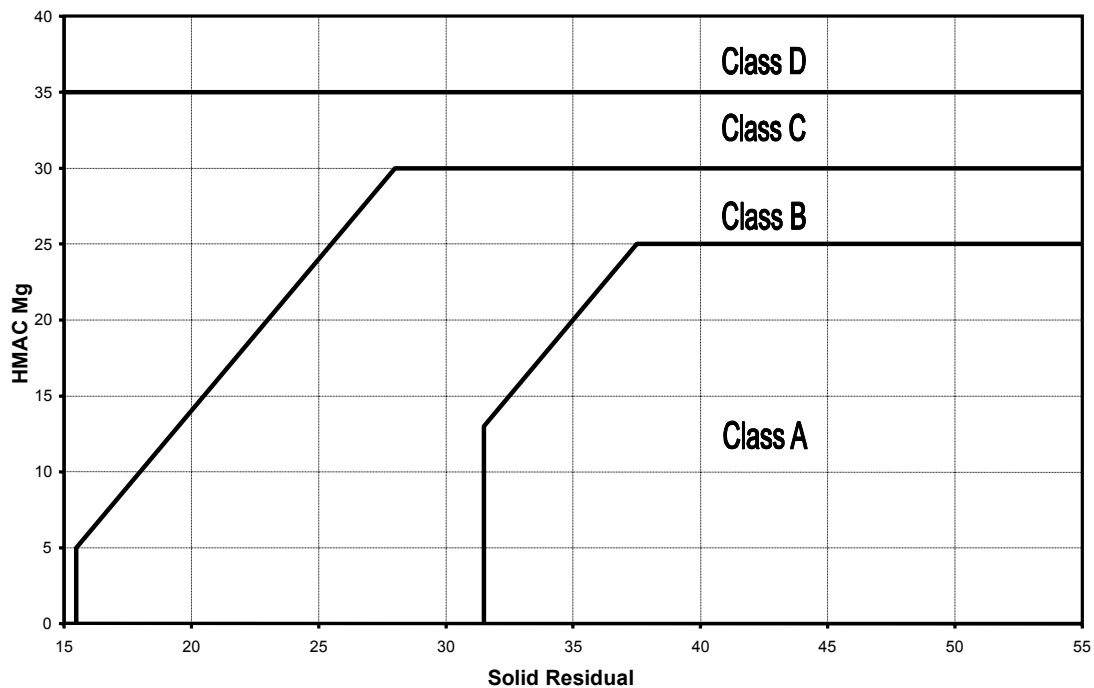


Figure 4.4. Surface Aggregate Classification for WWARP.

As shown earlier in this report, as well as in other studies, a great percentage of the values for the residual PSV fall within a small range (see Table 3.13 and Figure 3.32). The classification method currently used places the vast majority of aggregates in classification B or worse. Therefore, a new method needs to be developed using a measure of texture with more sensitivity than the PSV as well as a measure of weather resistance.

The proposed method is based on the average of AIMS texture levels 4 and 5 of the AMD aggregates, the COV of the texture measurements, and a measure of aggregate's resistance to weathering. Since the current method used in the WWARP is

the magnesium sulfate soundness rather than the Micro-Deval, the magnesium sulfate soundness test was used. However, it is believed that classification can be done using the Micro-Deval when more data become available on the relationship between Micro-Deval results and resistance to weathering. Texture measurements replace the PSV because the PSV is not sensitive enough to distinguish between aggregates, whereas the AIMS results offer a more sensitive assessment of aggregate texture. The time required to obtain AIMS results is also significantly less than that required to obtain the residual PSV.

Aggregates were classified using the original method to determine a baseline for comparison. Of all aggregates tested, only 36 had all the data necessary to classify them using the original method and the proposed method. These data include the terminal PSV, magnesium sulfate soundness, percent loss due to Micro-Deval, average texture, and texture COV. These properties as well as the original and proposed surface classification are included in Table 4.14. Figure 4.5 shows the new classification chart. The changes in the number of aggregates classified within each category are summarized in Table 4.15.

The aggregates within the shaded area in Figure 4.5 are classified as A or B based on texture COV. A COV of less than 0.4 classifies an aggregate as A, while a COV greater than 0.4 classifies an aggregate as B. The aggregates within the A section have texture in the top 25 percent among all aggregates, while aggregates in the shaded region have texture values in the third quartile among all aggregates. The maximum magnesium sulfate level for an aggregate to be classified as A was set at 18 percent,

which Kandhal and Parker (1998) denoted as the dividing line between good and poor performing aggregates. The dividing line between B and C as well as between C and D were set according to the current TxDOT method.

Table 4.14. Aggregate Surface Classification Properties.

Sample Number	Class	PSV Final	Sulfate Soundness	% Loss MD	Ave. Txtr.	COV	Prop. Class
05-0041	A	48	10	27.6	88.18	0.225	A
05-1002	A	37	19	22.2	81.74	0.339	B
05-1260	A	32	2	18.2	80.14	0.644	B
05-0129	B	25	8	11.0	100.95	0.369	A
05-0149	B	24	11	15.9	68.95	0.428	B
05-0178	B	27	25	21.7	41.42	0.552	C
05-0213	B	21	8	16.7	61.30	0.483	B
05-0235	B	26	3	2.7	105.00	0.507	A
05-0245	B	25	3	2.8	116.15	0.482	A
05-0247	B	26	3	3.7	102.64	0.491	B
05-0251	B	21	6	11.4	96.34	0.345	A
05-0350	B	33	25	15.3	78.57	0.42	B
05-0368	B	27	25	32.7	39.18	0.483	C
05-0397	B	24	11	19.4	56.73	0.497	B
05-0399	B	26	20	23.1	43.37	0.486	C
05-0519	B	23	16	18.5	75.30	0.49	B
05-0532	B	28	22	19.9	72.46	0.373	B
05-0535	B	35	26	22.8	216.34	0.315	B
05-0545	B	27	27	33.7	41.88	0.354	C
05-0768	B	23	3	10.0	67.08	0.379	B
05-0828	B	30	5	6.0	96.63	0.197	A
05-0832	B	27	11	12.0	90.98	0.415	B
05-0922	B	25	23	24.0	59.69	0.629	C
05-0938	B	26	2	4.4	147.21	0.196	A

Table 4.14. (cont.)

Sample Number	Class	PSV Final	Sulfate Soundness	% Loss MD	Ave. Txtr.	COV	Prop. Class
05-0941	B	30	3	3.4	63.25	0.603	B
05-0992	B	24	6	17.0	60.83	0.475	B
05-1183	B	25	23	24.1	42.14	0.52	C
05-1201	B	31	7	8.7	75.53	0.435	B
05-1207	B	32	23	13.3	71.14	0.559	B
05-1223	B	25	19	25.8	47.56	0.531	C
05-1235	B	25	2	21.1	47.67	0.554	B
05-0347	C	26	34	31.5	59.82	0.622	C
05-0365	C	25	30	26.4	65.3	0.535	C
05-1205	C	26	30	27	44.03	0.357	C
05-0496	D	35	57	31.2	50.62	0.439	D

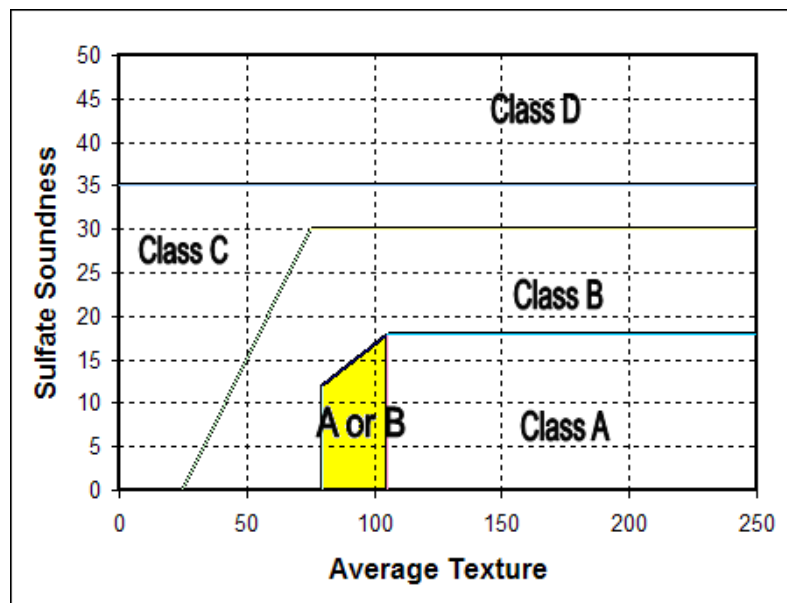


Figure 4.5. Proposed Surface Aggregate Classification Method.

Many of the aggregates tested fell into the B aggregate surface classification based on the current method. This result was expected due to the limited range observed in the terminal PSV value used for classification purposes. Likely, many of these aggregates would change classification using the new method, especially since this method is more sensitive to differences in aggregate properties than the current method.

The summary results in Table 4.15 show that many aggregates changed classification using the new method. Although many aggregates change classification, none change more than one level. Therefore, no aggregates initially classified as A are now classified as C, or vice versa. The majority of the changes came in those aggregates classified as B. The end result of the new classification is a more sensitive classification that allows for the aggregates to be more spread out over the groups instead of having the majority classified as B.

Table 4.15. Changes in Aggregate Classification.

Current Classification		Proposed Classification Count			
	Count	A	B	C	D
A	3	1	2		
B	29	6	16	7	
C	3			3	
D	1				1
Total	36	7	18	10	1

It should be noted that no performance testing or field evaluation was done to assess the results of this new classification. Future research will be necessary to validate the method and refine the cutoff values for classification. Classification methods using the percent loss due to Micro-Deval instead of or along with magnesium sulfate soundness should be investigated as well.

SUMMARY

This chapter documented the refinements of the aggregate shape classification method used in AIMS. The bounds for the new categorization of low, medium, and high were determined using the Ward's Linkage clustering analysis. The clustering results were found to penalize the aggregates with high texture, as only 10 percent of aggregates were classified as having a high texture. Consequently, quartiles analysis was conducted to classify aggregates in groups that belong to low (lowest 25 percent of the data), medium (middle 50 percent of the data), and high (top 25 percent of the data) categories. The aggregate surface classification for the wet weather accident reduction program was also revised to incorporate AIMS results in the classification of aggregates.

CHAPTER V

RELATIONSHIP OF AGGREGATE TEXTURE TO PAVEMENT SKID RESISTANCE

OVERVIEW

A skid resistant pavement is a necessity for driver safety. The skid resistance of a pavement is composed of both macrotexture, or surface projections, and microtexture, or roughness. The many different variables that influence the skid resistance of a pavement include, but are not limited to, aggregate gradation, texture, shape, porosity, toughness, abrasion resistance, mineralogy, and petrography.

This chapter sets forth a method to relate aggregate shape properties to pavement skid resistance. This method includes measuring the shape, angularity, and texture of aggregates using the aggregate imaging system (AIMS) before and after polishing particles with the Micro-Deval process. The shape characteristics and their changes due to polishing are related to field skid measurements through statistical analysis.

BACKGROUND

A pavement's skid resistance is an important property to consider when designing an asphalt mix due to correlation between low skid resistance and accident rates (Stephens and Goetz 1960). Wet weather accident reduction programs have been initiated in several states with a focus on the skid resistance of pavements. Kamel and Musgrove (1981) noted a 54 percent reduction in wet and 29 percent reduction in overall

accidents on pavements with a higher skid resistance. The aggregate properties that influence pavement skid resistance are gradation, size of particle, texture, shape, porosity, toughness, abrasion resistance, mineralogy, and petrography (Mahmoud 2005). The skid resistance of a pavement surface has two main components, microtexture and macrotexture. These components of skid resistance are discussed thoroughly in the literature review.

The combination of microtexture and macrotexture give a pavement its skid resistance. The microtexture of a pavement correlates to the skid number at lower speeds, while the macrotexture is most important at higher speeds. Therefore, aggregates used in high speed applications need to be highly textured, angular, and abrasion resistant. Henry and Dahir (1979) assert that pavement surfaces need to maintain a high level of surface texture after wear to ensure safety.

As stated by Mahmoud (2005), current methods to measure polishing resistance of aggregates are not adequate. This causes a problem in relating any of these methods to skid resistance of pavements due to the minimal correlation between them. Another method to relate aggregate properties to pavement skid resistance needs to be developed.

For many of the models discussed in the literature review, only a few of the influencing variables are included in the model. For skid resistance to be truly predicted, all of the aspects need to be considered, i.e., gradation, polishing resistance, texture, shape, and angularity. The methodology that follows considers all of these as inputs into the predictive equation.

EXPERIMENTAL METHODOLOGY

Since many methods have low correlation to skid resistance of pavement, a new method is proposed to relate the measurable aggregate properties to skid resistance. This method uses the AIMS in conjunction with the Micro-Deval abrasion test to evaluate initial aggregate characteristics and their changes after different levels of polishing. Data for this study were obtained using the research facilities at Texas Transportation Institute and nine test sections built in the Atlanta District of Texas.

PAVEMENT TEST SECTIONS

The nine test sections were built by TxDOT in late 2000. According to Chowdury et al. (2003), these sections were part of a project to reconstruct and rehabilitate IH-20 in Harrison County. The specific location of these sections is from 0.5 miles west of FM 3251 to 0.5 mile east of SH 43. Data collection for these sections during construction went beyond typical collection for quality control/quality assurance (QA/QC), to ensure collection of properties for future evaluation.

The nine test sections consist of three different aggregate types: quartzite, sandstone, and siliceous gravel, combined in three different mix types: CMHB-C, Superpave, and Type C. Table 5.1 denotes which sections correspond to what aggregate and what mix type and their corresponding gradation. These sections therefore offer a wide variety in texture, angularity, abrasion resistance, and gradation. The pavement structure consisted of damaged continuously reinforced concrete pavement fabric interface between them, and then finally the surface course with average thickness

of 2 inches. The source of the aggregates are as follows: quartzite from Martin Marietta, Jones Mill quarry; sandstone from Meridian, Sawyer, Oklahoma; and siliceous river gravel from Hanson suppliers in Prescott, Arkansas. All of the mixes used the same asphalt, a PG 76-22 from Wright Asphalt in Houston, Texas. All of the mix design results are documented in Chowdury et al. (2003).

Mix Design

The Type B mix consisted of approximately 90 percent limestone from Hanson suppliers in Perch Hill and 10 percent field sand from Marshall, Texas. It was found that the optimum asphalt content of this mixture was 3.8 percent.

The Superpave mixes were designed following the current Superpave procedures. The Superpave mixture used in this study is a ½-inch Superpave mixture gradation passing below the restricted zone. The mixes were designed to carry 30 million equivalent single axle loads (ESALs). The number of gyrations used for N_{ini} , N_{des} , and N_{max} were 9, 125, and 205, respectively. Section 1 consisted of approximately 67 percent siliceous river gravel, 32 percent limestone screenings, and 1 percent hydrated lime. Section 2 was composed of 91 percent sandstone, 8 percent igneous screening, and 1 percent hydrated lime. The section 3 mix contained 89 percent quartzite, 10 percent igneous screenings, and 1 percent hydrated lime. All mixes passed below the restricted zone.

The dense graded CMHB-C mixtures were designed using the current TxDOT procedure. These mixture types are designed to have a relatively high binder content

and large amount of coarse aggregates. Section 4 contains approximately 79 percent siliceous gravel, 20 percent igneous screenings, and 1 percent hydrated lime. The section 5 mix contains 87 percent sandstone, 12 percent igneous screenings, and 1 percent hydrated lime. Lastly, section 6 is composed of 87 percent quartzite, 12 percent igneous screenings, and 1 percent hydrated lime. The newly designed Type C mixture was also used in these test sections. Type C is also a dense graded mixture relatively finer than the CMHB-C mixture. The section 7 mixture contained 61 percent siliceous gravel, 30 percent limestone screenings, 8 percent igneous screenings, and 1 percent hydrated lime. The section 8 mix consisted of 99 percent sandstone and 1 percent hydrated lime. Section 9 was composed of 91 percent quartzite, 8 percent igneous screenings, and 1 percent hydrated lime.

SKID MEASUREMENTS

The skid resistance of these sections has been measured twice since construction. Although the skid resistance has only been measured twice, three different conditions can be considered from these measurements. The first set of skid measurements was taken during the summer of 2004. The second set of skid measurements was taken in late November of 2005. During this set of skid measurements, the outside lane and the shoulder were both tested. By testing the outside lane, the change in skid resistance from previous measurements could be determined. The reason for taking skid resistance measurements of the shoulder was to simulate the initial skid resistance of the newly built pavement. Since the initial skid resistance of the pavement was never measured,

the shoulder should give a reasonable assessment of this value due to the minimal traffic that it receives.

The skid resistance measurements were taken using a skid trailer following American Society of Testing and Materials (ASTM) method E274-97. Using this method, a trailer of known weight is pulled along the roadway. As the trailer is pulled, one of the tires, typically the left, is locked. Water is applied to the roadway shortly before the tire is locked to allow measurement under wet conditions. The force required to pull the trailer is then measured. The skid resistance of the pavement is measured as the skid number, in Equation 5.1. This gives a measure of the steady-state friction force. For the measurements in this study, the test was conducted at 55 mph.

$$SN = (F/W) \times 100 \quad (5.1)$$

where:

F is the force required to pull the trailer and

W is the weight of the trailer.

EVALUATION OF AGGREGATE POLISHING

To evaluate the aggregate's resistance to abrasion and degradation, the method developed by Mahmoud (2005) was used. This method involves using the Micro-Deval test and the AIMS. The aggregates were run at 15, 30, 45, 60, 75, 90, 105, and 180

minutes in the Micro-Deval machine and then scanned using AIMS to determine the change in aggregate shape properties.

AIMS

The aggregate imaging system, or AIMS, numerically determines the angularity, shape, and texture of coarse aggregates as well as the form and angularity of fine aggregates. The scans are automated and require little operator input. Bathina (2005) determined that there is no operator bias in this method, and there is little training required to use the system.

For the coarse aggregate scans, 56 particles are aligned on a 7 x 8 grid. Two scans are run, resulting in the determination of three dimensions of the particle. The first scan takes a backlit, black and white silhouette of the particles to determine the angularity of the particle and two of its dimensions. The second scan takes grayscale images of the aggregates. These images are analyzed using the wavelet method to determine the surface texture of the particles. The third dimension of the particle is determined by the distance that the camera pans out to focus on the surface of the particle.

For the coarse aggregates, AIMS produces six different texture levels. Each level is a measure of texture of a different size. Level 1 is the smallest, while level 6 is the largest scale texture measured using the wavelet analysis. For this study, levels 4, 5, and 6 were compared due to the different texture scales present in the material used.

A few grams of the fine aggregate are spread evenly across the surface of the machine. The system takes 400 images along a 20 x 20 grid and captures any particles that are fully within the image taken. These backlit, silhouetted images are then analyzed to determine the angularity and two-dimensional form of the aggregates.

MICRO-DEVAL TEST

The Micro-Deval test measures the abrasion, or polishing, resistance of an aggregate. In this test, aggregate samples are placed in a metal canister with steel ball and water. The TxDOT standard procedure, Tex-461-A, was followed when preparing samples.

The samples were run for various times for this study. Typically, the test is run for one time only of 105 minutes. For this test, a separate aggregate sample was run for each 15, 30, 60, 75, 90, 105, and 180 minutes, while all other specifications were followed. After each time, the aggregate was scanned on the AIMS to determine the shape properties. By running the Micro-Deval for the specified times, the change in shape properties over time can be determined as well as a terminal condition that the aggregate will reach, assumed to be the results at the 180 minute mark.

STATISTICAL MODEL

The results from AIMS can be used to build a model relating the aggregate properties to time in the Micro-Deval. Mahmoud (2005) proposed a model to relate texture to time in Micro-Deval in the form of Equation 5.2. In this equation, a, b, and c

are regression constants, while t is the time in the Micro-Deval. Mahmoud did not propose any other models to relate either form or angularity to time in the Micro-Deval. These would both need to be determined in order to relate the aggregate properties to in field skid measurements

$$AIMSTexture = a + b * \exp(-c * t) \quad (5.2)$$

RESULTS

The multiple time Micro-Deval testing was completed on all the aggregate used in the test sections. The texture values were fit using the previously defined equation as suggested by Mahmoud (2005). The statistical analysis was run using the SPSS version 11.5 software package. The results of this statistical analysis are shown in Table 5.2, while the AIMS texture results are shown in Figure 5.1 with the regression model superimposed.

Table 5.2. Regression Coefficient Summary.

Aggregate	Texture Level	a	b	c
Siliceous Gravel	Level 4	66.19	21.04	0.06738
	Level 5	91.70	12.45	0.06687
	Level 6	49.38	49.54	0.00000
Sandstone	Level 4	123.70	33.69	0.04641
	Level 5	58.66	91.60	0.00130
	Level 6	0.21	112.77	0.00041
Quartzite	Level 4	133.54	81.17	0.03632
	Level 5	137.90	75.32	0.02875
	Level 6	103.67	53.18	0.01219

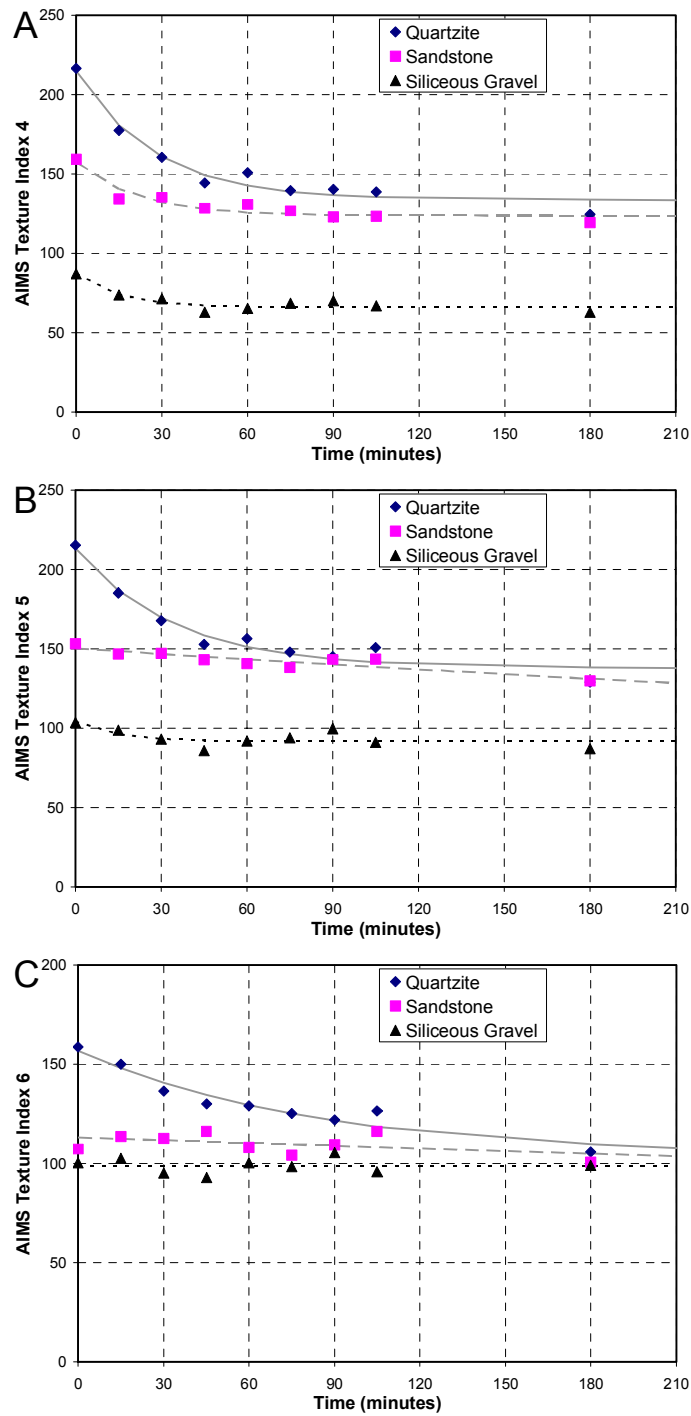


Figure 5.1. AIMS Texture Index versus Time in the Micro-Deval Test with Regression Results for A) Texture Level 4, B) Texture Level 5, and C) Texture Level 6.

As a general trend, the texture and angularity of the aggregates decrease as the time in the Micro-Deval increases. This is what was expected as more polishing occurred. Also, the siliceous gravel has the lowest texture at all three levels, as expected. Each of the aggregates had the same general amount of angularity as well.

The equation fit the texture results well. Problems arose when the curve was rather flat and, in the case of the level 6 gravel, varied up and down. Few aggregates showed a general trend of constant texture, but in this case the sandstone retained its texture throughout the process and the gravel had little to begin with, so it changed very little.

Skid resistance measurements have been made on the three test sections over the course of the past five years. The initial conditions were not sampled, as the test sections were originally used for a project outside of the Texas Transportation Institute's control, but recently the shoulder was tested to simulate the initial construction values of the mixes assuming that the shoulder has been subjected to minimal wear. The skid resistance measurement results are shown in Figure 5.2 with standard errors ranging from 0 to 4.72 skid numbers. The results for skid resistance are also tabulated by aggregate and mix type in Table 5.3.

The skid number reduced over time, as expected. In some cases the summer 2004 measurement had the lowest skid number. This is in part due to the number of the skid reading being much lower than the number during the other tests and in part because the pavement has a seasonal variability in skid resistance (Burchett and Rizenbergs 1979), and was normally lowest near the end of the summer. This could lead

to lower readings than those taken during the winter months when the other samples were taken.

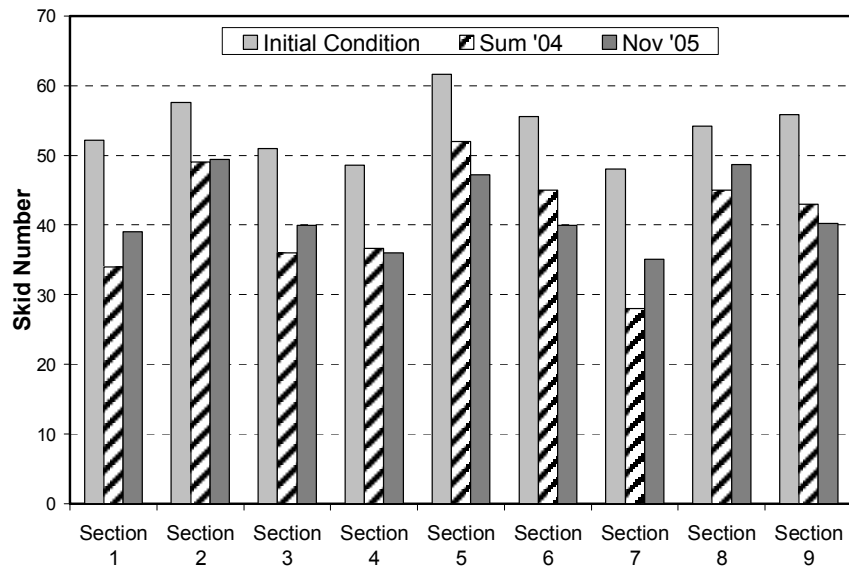


Figure 5.2. Skid Results of IH-20 Test Sections.

Table 5.3. Skid Measurement of Test Sections.

Measurement Time	Mix Type	Aggregate Type			Average
		Siliceous Gravel	Sandstone	Quartzite	
Initial Conditions	Superpave	52.20	57.57	51.00	53.59
	CMHB-C	48.57	61.63	55.56	55.25
	Type C	48.00	54.13	55.80	52.64
	Average	49.59	57.77	54.12	
Summer 2004	Superpave	34.00	49.00	36.00	39.67
	CMHB-C	36.67	52.00	45.00	44.56
	Type C	28.00	45.00	43.00	38.67
	Average	32.89	48.67	41.33	
November 2005	Superpave	39.00	49.38	39.90	42.76
	CMHB-C	36.00	47.17	39.90	41.02
	Type C	35.11	48.70	40.20	41.34
	Average	36.70	48.41	40.00	

When looking at the data in Table 5.3, a trend can be noticed between aggregate type, mix type, and skid resistance. The sandstone clearly had the highest skid resistance at each time sampled, with quartzite second and gravel last. In most cases, all mixes had nearly the same skid resistance, except for the summer 2004 when the gravel Type-C mix measurement was considerably lower than that of the others. CMHB-C type mixes seem to have the best skid resistance initially and in the summer, while the Superpave mixes seem best over time, as they have the highest measurements at the last collection time.

Analysis of variance (ANOVA) at a significance level of 0.05 was used to test the significance of both the aggregate type and mix type on the value of skid number using SPSS version 11.5. The results showed that aggregate type is a statistically significant factor (p -value < 0.05), while a p -value of 0.089 for mix type indicates that the mix type is not statistically significant. Also, multiple comparisons among the aggregate types show that the three aggregates are different pairwise. Of course, mix type is an important factor in influencing skid resistance. However, it seems that the mixes used in this study were not different enough in gradation to influence the measured skid number.

The texture results at all levels did not show good distinction between the sandstone and quartzite at the terminal texture levels. However, the pavement skid resistance of the sandstone sections was better than that of the quartzite sections. It is noted that there were only slight differences in aggregate gradation within each mix type (Table 5.1). Therefore, aggregate gradation does not explain this difference among the

mixtures. The coefficient of variation was evaluated for each set of AIMS measurements after each time intervals in the Micro-Deval. Figure 5.3 shows the comparison between texture and coefficient of variation for each of the three aggregates tested and different texture levels studied. Each of the time steps (0 to 180 minutes) is used as a point for comparison. Sandstone had the lowest variation (most uniform texture) of the three aggregates tested. Therefore, the uniformity of sandstone texture contributed to the high skid resistance of the sandstone sections compared with the quartzite sections. In other words, both the average texture value and texture variation are important in influencing skid resistance.

SUMMARY

A method was developed for measuring the influence of coarse aggregate texture on asphalt pavement skid resistance. This method has the advantages of 1) polishing aggregates within a time period much shorter than that used in the British pendulum/wheel method (ASTM E303/ASTM D3319), 2) identifying the texture levels that influence skid resistance, and 3) accounting for the variation of texture within an aggregate sample. The method was capable of explaining the differences in skid resistance of pavement sections that were constructed using three different aggregate sources and three different gradations. ANOVA showed that aggregate type is statistically significant in affecting skid resistance. The developed method can be used by engineers to select the acceptable aggregate texture levels to improve asphalt pavement skid resistance and thereby

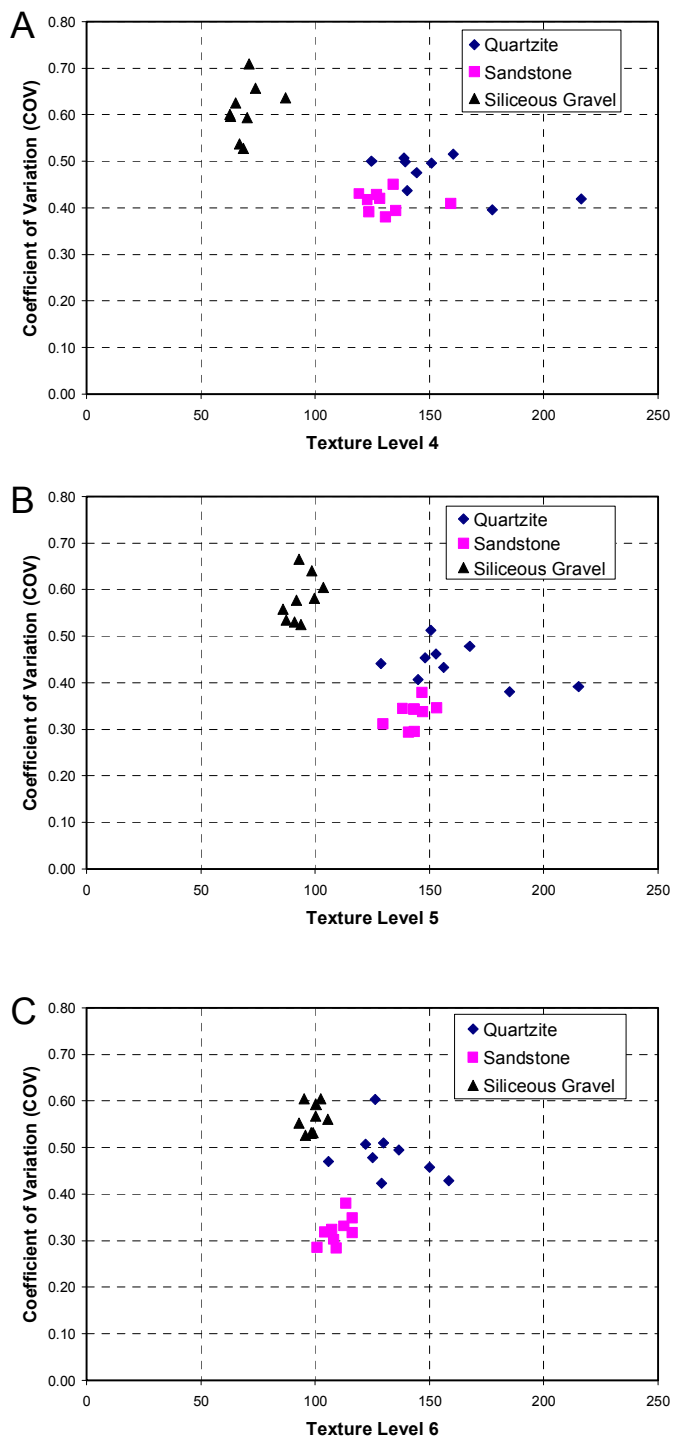


Figure 5.3. COV versus AIMS Texture Index for A) Texture Level 4, B) Texture Level 5, and C) Texture Level 6.

enhance the safety of motorists, especially in wet weather conditions. Also, it provides information about the change in aggregate texture as a function of time in the Micro-Deval test as shown in Equation 5.2. As such, this information can be used in the future to develop a model to predict skid resistance as a function of time, aggregate properties, mix properties, traffic, and environmental conditions.

CHAPTER VI

CONCLUSIONS AND RECOMMENDATIONS

CONCLUSIONS

This study focused on providing support for the implementation of the aggregate imaging system in TxDOT operations. The following points summarize the main efforts undertaken in this study and the primary conclusions:

- Detailed statistical analyses compared AIMS measurements collected at the TxDOT and TTI laboratories. All statistical analysis methods supported the main finding that measurements from the two AIMS units were not statistically different. Texture measurements on polishing coupons were also compared. The two AIMS units scanned the same exact coupons. More than 80 percent of samples were not statistically different when measured using the two AIMS units.
- There was excellent correlation between the measurements of the two Micro-Deval machines at TTI and TxDOT. The results from the two machines are not different statistically.
- A database of aggregate properties was developed based on the measurements conducted at TxDOT and TTI. The database includes the following test results:

- AIMS measurements of texture, angularity, and shape (sphericity). Tests were conducted according to procedures published in TxDOT implementation report 5-1707-01-1;
 - Crushed face count of coarse aggregates (Tex-460-A);
 - Flat and elongated particles (Tex-280-F);
 - Flakiness index (Tex-224-F);
 - Micro-Deval weight loss (Tex-461-A);
 - Los Angeles Abrasion (Tex-410-A);
 - Magnesium sulfate soundness (Tex-411-A); and
 - British polish value (Tex-438-A).
- The database was further used to compare the AIMS units that are in use at the TTI and DOT laboratories. The comparison between the two AIMS units confirmed the findings in Chapter III that the two AIMS units provide very similar results.
 - The correlation between percent loss due to Micro-Deval and magnesium sulfate soundness was assessed. Moderate correlation was found between these tests.
 - Results from the accelerated polishing test were analyzed and it was found that the majority of the residual PSV measurement fell within a very small range. The small range of PSV measurements makes it difficult to distinguish between aggregates.

- The AIMS angularity analysis method was improved in order to reduce the variability in the measurements within the same aggregate source. The new method had a much smaller coefficient of variation than the previous method.
- The texture analysis method was also enhanced in order to increase the sensitivity of the method to fine texture (smaller scale texture). The texture levels used in the new AIMS analysis are more in agreement with the previous experience of aggregate performances in pavement surfaces.
- The AIMS aggregate classification method was revised based on the data collected on the TxDOT aggregates. The new limits were used to determine the percentage of particles in an aggregate sample that fall into the low, medium, and high categories for each of the shape characteristics (texture, angularity, and sphericity). Also, new limits were calculated in order to classify an aggregate sample based on the average measured properties. The limits were selected based on quartile analysis of the data such that 25 percent of the aggregates belong to the low category, 50 percent of the aggregates belong to the medium category, and the remaining 25 percent belong to the high category.
- A new method for aggregate classification was developed for use as part of the Wet Weather Accident Reduction Program. This method relies on AIMS texture measurements and magnesium sulfate soundness. This method allows direct measurement of aggregate wear resistance and

terminal texture. This method is also more sensitive than the current method and relies on the average aggregate texture as well as the variation of texture in an aggregate sample. The new method changed the classifications of some the aggregates compared with the current method. However, none of the aggregates changed from A to C, B to D, or vice versa. All changes shifted an aggregate sample from one category to either one of its adjacent categories. The classification limits used in this proposed method are not supported by performance data, and future research should focus on accurate determination of these limits.

- A method was developed for measuring the influence of coarse aggregate texture on asphalt pavement skid resistance. This method has the advantages of 1) polishing aggregates within a time period much shorter than that used in the British pendulum/wheel method (ASTM E303/ASTM D3319), 2) identifying the texture levels that influence skid resistance, and 3) accounting for the variation of texture within an aggregate sample. The method was capable of explaining the differences in skid resistance of pavement sections that were constructed using three different aggregate sources and three different gradations.
- ANOVA conducted on skid measurements showed that aggregate type was statistically significant in affecting skid resistance.

RECOMMENDATIONS

- The reproducibility of AIMS measurements using more than two units should be studied.
- The limits used in the new method for classification of aggregates as part of the WWARP should be further examined based on the performance of aggregates in asphalt pavement in terms of skid resistance.
- More aggregates should be tested using the methodology described in Chapter V to develop a predictive model for pavement skid resistance.

REFERENCES

- Akesson, U., Lindqvist, J.E., and Stigh, J. (2001). "Relationship between texture and mechanical properties of granites." *Bull. Eng. Geol. Env.*, 60, 277-284.
- Al-Rousan, T. M. (2004). "Characterization of aggregate shape properties using a computer automated system." PhD Dissertation, Texas A&M University, College Station, Tex.
- Bathina, M. (2005). "Quality analysis of the aggregate imaging system (AIMS) measurements." M.S. Thesis, Texas A&M University, College Station, TX.
- Bazlamit, S.M., and Reza, F. (2005). "Changes in asphalt pavement friction components and adjustment of skid number for temperature." *Journal of Transportation Engineering*, 131, 470-476.
- Burchett, J.L., and Rizenbergs, R.L. (1979). "Seasonal variations in the skid resistance pavements in Kentucky." *Research Report 532*, Kentucky Department of Transportation.
- Chowdhury, A., Bhasin, A. and Button, J.W. (2003). "As built properties of test pavements on IH-20 in Atlanta District." *FHWA Report 4203-2*, Texas Transportation Institute, College Station, TX.
- Cooley, L., Jr., and James, R. (2003). "Micro-Deval testing of aggregates in the southeast." *Transportation Research Record 1837*, Transportation Research Board, National Research Council, Washington, D.C., 73-79.

- Crouch, L., Shirley, G., Head, G., and Goodwin, W. (1996). "Aggregate polishing resistance pre-evaluation." *Transportation Research Record* 1530, Transportation Research Board, National Research Council, Washington, D.C., 103-110.
- Dahir, S.H. (1979). "A review of aggregate selection criteria for improved wear resistance and skid resistance of bituminous surfaces." *Journal of Testing and Evaluation*, 7, 245-253.
- Dahir, S.H., Meyer, W.E., and Hegmon, R.R. (1976). "Laboratory and field investigation of bituminous pavement and aggregate polishing." *Transportation Research Record* 584, Transportation Research Board, National Research Council, Washington, D.C., 1-14.
- Diringer, K.T., and Barros, R.T. (1990). "Predicting the skid resistance of bituminous pavements through accelerated laboratory testing of aggregates." *Surface Characterization of Roadways: International Research and Technologies, ASTM 1301*, American Society for Testing and Materials, Philadelphia, Pennsylvania, 61-76.
- Do, M.-T., Zahouani, H., and Vargiolu, R. (2000). "Angular parameter for characterizing road surface microtexture." *Transportation Research Record* 1723, Transportation Research Board, National Research Council, Washington, D.C., 66-72.

- Forster, S. (1989). "Pavement microtexture and its relation to skid resistance." *Transportation Research Record* 1215, Transportation Research Board, National Research Council, Washington, D.C., 151-164.
- Henry, J., and Dahir, S. (1979). "Effects of textures and the aggregates that produce them on the performance of bituminous surfaces." *Transportation Research Record* 712, Transportation Research Board, National Research Council, Washington, D.C., 44-50.
- Jayawickrama, P.W., and Graham, G.L. (1995). "Use of skid performance history as basis for aggregate qualification for seal coats and hot-mix asphalt concrete surface courses." *Transportation Research Record* 1501, Transportation Research Board, National Research Council, Washington, D.C., 31-38.
- Jayawickrama, P.W., Prassana, R., and Senadheera, S.P. (1996). "Survey of state practices to control skid resistance on hot-mix asphalt concrete pavements." *Transportation Research Record* 1536, Transportation Research Board, National Research Council, Washington, D.C., 52-58.
- Jayawickrama, P.W., and Thomas, B. (1998). "Correction of field skid measurements for seasonal variations in Texas." *Transportation Research Record* 1639, Transportation Research Board, National Research Council, Washington, D.C., 147-154.
- Kamel, N., and Musgrove, G.R. (1981). "Design and performance of bituminous mixes in Ontario." *Regional Transportation Advisory Committee (RTAC) Forum*, 5 (3), 53-64.

- Kamel, N., Musgrove, G.R. and Rutka, A. (1982). "Design and Performance of Bituminous Friction Course Mixes." *Transportation Research Record* 843, 40-50.
- Kandhal, P., Parker, F., Jr., and Bishara, E. (1993). "Evaluation of Alabama limestone aggregates for asphalt wearing courses." *Transportation Research Record* 1418, Transportation Research Board, National Research Council, Washington, D.C., 12-21.
- Kandhal, P., and Parker, F. Jr. (1998). "Aggregate tests related to asphalt concrete performance in pavements." *National Cooperative Highway Research Program Report* 405, Transportation Research Board, National Research Council, Washington, D.C.
- Lingras and Huang (2005). "Statistical, evolutionary, and neurocomputing clustering techniques: cluster-based and object-based approaches." *Artificial Intelligence Review*, 23, 3-29.
- Liu, Y. (2004). "Effect of surface macrotecture on skid resistance measurements by the British Pendulum Test." *Journal of Testing and Evaluation*, 32, 304-309.
- Mahmoud, E.M. (2005). "Development of experimental method for the evaluation of aggregate resistance to polish, abrasion, and breakage." M.S. Thesis, Texas A&M University, College Station, TX.
- Masad, E., Al-Rousan, T., Button, J., Little, D., and Tutumluer, E. (2005). "Test methods for characterizing aggregate shape, texture, and angularity." *National*

Cooperative Highway Research Program NCHRP Project 4-30A Final Report,
National Research Council, Washington, D.C.

- McGahan, J. (2005). "The development of correlations between HMA pavement performance and aggregate shape properties." M.S. Thesis, Texas A&M University, College Station, TX.
- Mullen, W.G., Dahir, S.H.M., and El Madani, N.F. (1974). "Laboratory evaluation of aggregates, aggregate blends, and bituminous mixes for polish resistance." *Transportation Research Record 523*, Transportation Research Board, National Research Council, Washington, D.C., 56-64.
- Murad, M.M. (2004). "A review of asphalt pavement friction testing, safety requirements, and their application in design and maintenance." *International Journal of Pavements: Maintenance and Rehabilitation of Pavement and Technological Control*, 3, 63-75.
- Prowell, B.D., Zhang, J., and Brown, E.R. (2005). "Aggregate properties and the performance of Superpave-designed hot mix asphalt." *National Cooperative Highway Research Program Report 539*, Transportation Research Board, National Research Council, Washington, D.C.
- Rogers, C. (1998). "Canadian experience with the Micro-Deval test for aggregates." *Advances in Aggregates and Armourstone Evaluation*, 13, 139-147.
- Roque, R., Dominguez, G., and Romero, P. (1995). "Effect of asphalt mixture characteristics and design on frictional resistance of bituminous wearing course

- mixtures.” *Transportation Research Record* 1507, Transportation Research Board, National Research Council, Washington, D.C., 39-50.
- Skertitt, W.H. (1993). “Aggregate type and traffic volume as controlling factors in bituminous pavement friction.” *Performance-related Testing and Evaluation of Characteristics of Aggregates and New Geomaterials*, 1418, 22-29.
- Stephens, J.E., and Goetz, W.H. (1960). “Designing fine bituminous mixtures for high skid resistance.” *Highway Research Board Proceedings*, 39, 173-190.
- Stroup-Gardiner, M., Studdard, J., and Wagner, C. (2004). “Evaluation of hot mix asphalt macro- and microtexture.” *Journal of Testing and Evaluation*, 32 (1), 1-10.
- Texas Department of Transportation (TxDOT) (2006). “200-F, Bituminous test procedures.” Austin, Texas, June 2006.
- Wu, Y., Parker, F., and Kandhal P. (1998). “Aggregate toughness/abrasion resistance and durability/soundness tests related to asphalt concrete performance in pavements.” *Transportation Research Record* 1638, Transportation Research Board, National Research Council, Washington, D.C., 85-93.

APPENDIX A

DATABASE SUMMARY

Table A.1. Aggregate Mineralogy and Classification.

Sample Number	Material Code	Material Type
04-1205	O18	Crushed Limestone
04-1220	O18	Crushed Limestone
04-1277	O18	Crushed Limestone
04-1283	O18	Crushed Limestone
04-1285	O18	Crushed Limestone
04-1300	O18	Crushed Limestone
04-1307	O18	Crushed Limestone
05-0005	O19	Crushed Dolomite
05-0007	O18	Crushed Limestone
05-0009	O18	Crushed Limestone
05-0011	O32	Crushed Rhyolite
05-0014	O15	Partly Crushed Sil. & LS Gravel
05-0017	O14	Crushed Sil. & LS Gravel
05-0020	O11	Crushed Sil. Gravel
05-0029	O33	Crushed Rhyolite Gravel
05-0041	O48	Lightweight Aggregate
05-0048	O25	Partly Crushed LS & Sil. Gravel
05-0077	O14	Crushed Sil. & LS Gravel
05-0081	O19	Crushed Dolomite
05-0083	O19	Crushed Dolomite
05-0086	O29	Crushed Sandstone
05-0089	O18	Crushed Limestone
05-0093	O18	Crushed Limestone
05-0109	O18	Crushed Limestone
05-0129	O18	Crushed Limestone
05-0143	O18	Crushed Limestone
05-0149	O18	Crushed Limestone
05-0151	O18	Crushed Limestone
05-0161	O14	Crushed Sil. & LS Gravel
05-0178	O18	Crushed Limestone
05-0213	O18	Crushed Limestone
05-0216	O18	Crushed Limestone
05-0231	O24	Crushed LS & Sil. Gravel

Table A.1. Continued.

Sample Number	Material Code	Material Type
05-0235	O11	Crushed Sil. Gravel
05-0238	O14	Crushed Sil. & LS Gravel
05-0239	O14	Crushed Sil. & LS Gravel
05-0245	O17	Crushed Sil. & Calcareous Gravel
05-0247	O17	Crushed Sil. & Calcareous Gravel
05-0251	O18	Crushed Limestone
05-0266	O49	Crushed LS Rock Asphalt
05-0317	O50	Crushed Traprock
05-0320	O32	Crushed Rhyolite
05-0321	O18	Crushed Limestone
05-0337	O14	Crushed Sil. & LS Gravel
05-0338	O14	Crushed Sil. & LS Gravel
05-0347	O18	Crushed Limestone
05-0350	O18	Crushed Limestone
05-0365	O18	Crushed Limestone
05-0368	O18	Crushed Limestone
05-0397	O18	Crushed Limestone
05-0399	O18	Crushed Limestone
05-0493	O18	Crushed Limestone
05-0494	O18	Crushed Limestone
05-0496	O29	Crushed Sandstone
05-0519	O18	Crushed Limestone
05-0521	O49	Crushed LS Rock Asphalt
05-0532	O18	Crushed Limestone
05-0534	O18	Crushed Limestone
05-0535	O49	Crushed LS Rock Asphalt
05-0543	O14	Crushed Sil. & LS Gravel
05-0545	O18	Crushed Limestone
05-0630	O29	Crushed Sandstone
05-0643	O18	Crushed Limestone
05-0649	O18	Crushed Limestone
05-0693	O33	Crushed Rhyolite Gravel
05-0708	O29	Crushed Sandstone

Table A.1. Continued.

Sample Number	Material Code	Material Type
05-0715	O18	Crushed Limestone
05-0716	O18	Crushed Limestone
05-0719	O18	Crushed Limestone
05-0768	O19	Crushed Dolomite
05-0770	O19	Crushed Dolomite
05-0771	O29	Crushed Sandstone
05-0774	O18	Crushed Limestone
05-0800	O18	Crushed Limestone
05-0806	O18	Crushed Limestone
05-0822	O19	Crushed Dolomite
05-0824	O19	Crushed Dolomite
05-0826	O51	Crushed Granite
05-0828	O29	Crushed Sandstone
05-0832	O18	Crushed Limestone
05-0921	O18	Crushed Limestone
05-0922	O18	Crushed Limestone
05-0938	O51	Crushed Granite
05-0941	O11	Crushed Sil. Gravel
05-0943	O12	Partly Crushed Sil. Gravel
05-0946	O40	Quartzite
05-0992	O18	Crushed Limestone
05-0995	O18	Crushed Limestone
05-1002	O18	Crushed Limestone
05-1009	O21	Crushed Limestone Gravel
05-1183	O18	Crushed Limestone
05-1184	O18	Crushed Limestone
05-1190	O29	Crushed Sandstone
05-1194	O18	Crushed Limestone
05-1201	O18	Crushed Limestone
05-1205	O18	Crushed Limestone
05-1207	O18	Crushed Limestone
05-1210	O29	Crushed Sandstone
05-1213	O18	Crushed Limestone

Table A.1. Continued.

Sample Number	Material Code	Material Type
05-1221	O29	Crushed Sandstone
05-1222	O29	Crushed Sandstone
05-1223	O18	Crushed Limestone
05-1235	O18	Crushed Limestone
05-1236	O18	Crushed Limestone
05-1260	O18	Crushed Limestone
05-1262	O18	Crushed Limestone
05-1269	O18	Crushed Limestone
05-1274	O33	Crushed Rhyolite Gravel
05-1314	O18	Crushed Limestone
05-1319	O18	Crushed Limestone
05-1341	O49	Crushed LS Rock Asphalt
05-1354	O18	Crushed Limestone
05-1357	O18	Crushed Limestone
05-1358	O18	Crushed Limestone
05-1359	O18	Crushed Limestone
05-1360	O18	Crushed Limestone
05-1361	O18	Crushed Limestone
05-1383	O29	Crushed Sandstone
05-1389	O18	Crushed Limestone
05-1397	O18	Crushed Limestone
05-1412	O14	Crushed Sil. & LS Gravel
05-1419	O14	Crushed Sil. & LS Gravel
05-1422	O19	Crushed Dolomite
05-1423	O55	Crushed Slag
05-1425	O18	Crushed Limestone
05-1438	O18	Crushed Limestone
05-1452	O14	Crushed Sil. & LS Gravel
05-1458	O14	Crushed Sil. & LS Gravel
05-1468	O19	Crushed Dolomite
05-1475	O48	Lightweight Aggregate
05-1476	O18	Crushed Limestone
06-0004	O18	Crushed Limestone

Table A.1. Continued.

Sample Number	Material Code	Material Type
06-0009	O18	Crushed Limestone
06-0025	O14	Crushed Sil. & LS Gravel
06-0028	O18	Crushed Limestone
06-0031	O51	Crushed Granite
06-0041	O18	Crushed Limestone
06-0078	O50	Crushed Traprock
06-0082	O49	Crushed LS Rock Asphalt
06-0086	O18	Crushed Limestone
06-0087	O18	Crushed Limestone
06-0107	O18	Crushed Limestone
06-0116	O19	Crushed Dolomite
06-0121	O19	Crushed Dolomite
06-0136	O11	Crushed Sil. Gravel
06-0143	O11	Crushed Sil. Gravel
06-0162	O18	Crushed Limestone
06-0175	O14	Crushed Sil. & LS Gravel
06-0182	O18	Crushed Limestone
06-0196	O21	Crushed Limestone Gravel
06-0199	O19	Crushed Dolomite
06-0257	O18	Crushed Limestone

Table A.2. Gradient Angularity.

Sample Number	TxDOT			TTI		
	Average Angularity		Percent Loss Ang.	Average Angularity		Percent Loss Ang.
	BMD	AMD		BMD	AMD	
04-1205	2326.20	2059.90	11.45	2391.28	1852.14	22.55
04-1220	2609.40	1863.00	28.60	2240.59	1668.30	25.54
04-1277	2548.20	1974.50	22.51	2619.33	1924.13	26.54
04-1283	2626.80	1948.60	25.82	2261.70	2025.59	10.44
04-1285	3213.10	2051.40	36.16	2920.38	1809.61	38.04
04-1300	2991.90	1581.50	47.14	2555.70	1791.52	29.90
04-1307	3156.20	1872.60	40.67	2979.65	1899.69	36.24

Table A.2. Continued.

Sample Number	TxDOT			TTI		
	Average Angularity		Percent Loss Ang.	Average Angularity		Percent Loss Ang.
	BMD	AMD		BMD	AMD	
05-0005	2821.70	1916.80	32.07	2810.87	2488.04	11.48
05-0007	2778.70	2140.50	22.97	2341.73	2013.54	14.01
05-0009	2565.50	1950.70	23.96	2782.41	2179.63	21.66
05-0011	2956.60	2517.30	14.86	2860.44	2316.60	19.01
05-0014	2947.20	2016.70	31.57	2882.88	2372.51	17.70
05-0017	2597.40	2071.50	20.25	2499.45	2141.13	14.34
05-0020	2699.40	2225.20	17.57	2687.65	1874.24	30.26
05-0029	2588.60	2081.00	19.61	2619.93	2076.84	20.73
05-0041	2204.90	1820.60	17.43	2403.33	1583.58	34.11
05-0048	2164.40	2101.10	2.92	2425.10	1914.09	21.07
05-0077	2753.90	2517.10	8.60	2688.99	2276.43	15.34
05-0081	2736.60	1996.60	27.04	2533.27	2331.66	7.96
05-0083	2642.40	2184.20	17.34	2861.77	2313.58	19.16
05-0086	2513.30	2229.20	11.30	2696.34	1941.21	28.01
05-0089	3072.30	2108.90	31.36	2653.82	2391.61	9.88
05-0093	2723.00	1693.30	37.81	2560.39	1778.80	30.53
05-0109	2746.60	2166.90	21.11	2607.94	2157.20	17.28
05-0129	2624.80	2085.60	20.54	2383.92	1538.37	35.47
05-0143	2489.70	1953.20	21.55	3000.07	1949.25	35.03
05-0149	2254.10	1897.40	15.82	2527.23	1701.11	32.69
05-0151	2849.60	1781.40	37.49	2827.28	1905.71	32.60
05-0161	2843.60	2392.30	15.87	2953.53	2791.45	5.49
05-0178	2935.20	1754.60	40.22	2667.21	1894.66	28.96
05-0213	2680.80	1949.90	27.26	2340.39	1765.07	24.58
05-0216	2798.80			2476.35	1844.10	25.53
05-0231	2364.80	1983.90	16.11	2274.41	1827.69	19.64
05-0235	2616.00	2354.80	9.98	2688.98	2119.71	21.17
05-0238	2493.40	2174.70	12.78	2680.61	1800.57	32.83
05-0239	2799.80	2351.30	16.02			-
05-0245	2343.80	2249.80	4.01	2692.67	2030.63	24.59
05-0247	2882.50	2443.90	15.22	2842.35	2134.11	24.92
05-0251	2764.90	2372.60	14.19	2698.69	1898.01	29.67

Table A.2. Continued.

Sample Number	TxDOT			TTI		
	Average Angularity		Percent Loss Ang.	Average Angularity		Percent Loss Ang.
	BMD	AMD		BMD	AMD	
05-0266	2737.50	2096.40	23.42	3051.98	2008.19	34.20
05-0317	2866.40	2106.40	26.51	3146.42	1972.02	37.32
05-0320	2805.60	2129.20	24.11	2996.06	2376.54	20.68
05-0321	2873.40	2064.20	28.16	2923.72	1992.44	31.85
05-0337	2953.80	2748.10	6.96			-
05-0338	2402.00	1970.00	17.99	2791.78	2371.86	15.04
05-0347	2801.90	2185.00	22.02	2876.84	1790.19	37.77
05-0350	2305.80	2036.60	11.67	2567.76	1665.28	35.15
05-0365	3212.00	2166.40	32.55	2885.56	1623.43	43.74
05-0368	2829.20	2134.00	24.57	2989.02	1549.76	48.15
05-0397	2260.10	1664.40	26.36	2397.32	1532.34	36.08
05-0399	2926.20	1833.40	37.35	2779.06	1691.40	39.14
05-0493	2946.50			2513.85	1778.13	29.27
05-0494	2849.60			2433.82	2046.02	15.93
05-0496	3048.50	2304.40	24.41	2403.70	1715.20	28.64
05-0519	2468.20	2094.40	15.14	2621.33	1735.61	33.79
05-0532	2797.60	1966.00	29.73	2250.64	1584.58	29.59
05-0535	3097.40	1999.90	35.43	2507.48	1767.41	29.51
05-0543	2722.20			2464.62	2141.47	13.11
05-0545	2520.30	1998.47	20.71	2594.54	1758.04	32.24
05-0630	2810.60			2554.70	1947.57	23.77
05-0643	2624.10	1797.89	31.49	2589.19	1720.87	33.54
05-0649	2805.90	2173.27	22.55	2423.10	1663.60	31.34
05-0693	2862.90			2558.39	2174.95	14.99
05-0708	2391.00			2332.68	1745.32	25.18
05-0768	2765.67	1921.35	30.53	2721.47	2124.05	21.95
05-0770	2976.40	1964.65	33.99	2533.94	2250.29	11.19
05-0771	2760.30	2109.98	23.56	2706.39	1834.72	32.21
05-0774	2744.24	2131.08	22.34	2390.28	2488.38	-4.10
05-0822	2614.00	2456.58	6.02	2773.04	2357.79	14.97
05-0824	3083.10	2083.20	32.43	2930.76	2148.49	26.69
05-0826	3252.40	2522.88	22.43	3187.28	2578.47	19.10

Table A.2. Continued.

Sample Number	TxDOT			TTI		
	Average Angularity		Percent Loss Ang.	Average Angularity		Percent Loss Ang.
	BMD	AMD		BMD	AMD	
05-0828	2914.30	2102.62	27.85	2308.91	2047.36	11.33
05-0832	2454.50	1800.57	26.64	2220.50	1897.34	14.55
05-0921	2687.60	1850.54	31.15	2705.40	2134.76	21.09
05-0922	2693.80	1791.19	33.51	2510.16	1894.66	24.52
05-0938	3352.10	2640.77	21.22	2739.89	2916.01	-6.43
05-0941	2608.00	2347.75	9.98	2764.32	1957.29	29.19
05-0943	2813.40	2289.48	18.62	2664.54	2041.35	23.39
05-0946	2821.40	2462.60	12.72	2836.66	2264.02	20.19
05-0992	2791.80	2555.68	8.46	2580.15	1903.37	26.23
05-0995	2726.00	2067.79	24.15	2895.59	1966.66	32.08
05-1002	2603.40	2710.39	-4.11	2748.92	1951.26	29.02
05-1009	2226.19	2571.75	-15.52	2439.83	1806.59	25.95
05-1183	2913.30	1959.96	32.72	2550.01	2059.75	19.23
05-1184	2544.90	2103.28	17.35	2283.12	2007.18	12.09
05-1190	2611.70	2041.00	21.85	2431.58	1833.39	24.60
05-1201	2678.60	1859.50	30.58	2805.18	1852.81	33.95
05-1205	2842.80	2054.06	27.75	2562.06	2098.26	18.10
05-1207	2818.90	1845.63	34.53	2476.34	1901.03	23.23
05-1210	2746.10	2117.02	22.91	2424.44	1962.98	19.03
05-1213	2846.30	2155.86	24.26	2743.56	1864.86	32.03
05-1221	2755.62	1966.66	28.63	2613.30	1911.07	26.87
05-1222	2645.77	2094.24	20.85	2658.51	1773.11	33.30
05-1223	2768.67	1975.70	28.64	2577.14	2103.62	18.37
05-1235	2542.98	1936.52	23.85	2381.24	1674.32	29.69
05-1236	2681.28	1923.13	28.28	2217.49	2063.77	6.93
05-1260	2604.93	1817.65	30.22	2387.94	1646.53	31.05
05-1262	2835.32	1729.24	39.01	2421.09	1679.01	30.65
05-1269	2738.54	2106.63	23.07			-
05-1274	2738.88	2171.94	20.70	2703.72	2374.20	12.19
05-1319	2795.80	2012.20	28.03	2259.68	1852.81	18.01
05-1360	2653.82	2108.98	20.53	2219.50	2050.71	7.60
05-1389	2571.44	2135.43	16.96	2249.64	1726.90	23.24

Table A.2. Continued.

Sample Number	TxDOT			TTI		
	Average Angularity		Percent Loss Ang.	Average Angularity		Percent Loss Ang.
	BMD	AMD		BMD	AMD	
05-1419	2637.41	2339.38	11.30	2240.60	2200.08	1.81
05-1422	2680.27	1910.74	28.71	2435.16	1652.88	32.12
05-1468	2773.70	2086.21	24.79	2235.58	1881.61	15.83
06-0009	2632.39	2064.44	21.58	2331.01	1681.69	27.86
06-0082	2763.65	1789.51	35.25	2466.29	1720.53	30.24
06-0086	2784.25	2086.21	25.07	2446.87	1793.20	26.71

Table A.3. Aggregate Surface Texture.

Sample Number	TxDOT			TTI		
	Average Texture		Percent Loss Txtr.	Average Texture		Percent Loss Txtr.
	BMD	AMD		BMD	AMD	
04-1205	246.80	135.40	45.14			
04-1220	222.90	130.10	41.63			
04-1277	387.20	204.90	47.08			
04-1283	198.80	120.70	39.29			
04-1285	323.50	194.70	39.81			
04-1300	283.90	52.10	81.65			
04-1307	109.10	88.30	19.07			
05-0005	153.40	72.90	52.48			
05-0007	83.70	55.00	34.29			
05-0009	154.20	96.00	37.74			
05-0011	99.50	87.50	12.06			
05-0014	130.10	119.90	7.84			
05-0017	115.70	105.20	9.08			
05-0020	103.60	108.70	-4.92			
05-0029	107.30	106.20	1.03			
05-0041	73.40	67.30	8.31	73.61	79.24	-7.65
05-0048	112.30	103.30	8.01			
05-0077	104.60	65.10	37.76			
05-0081	73.60	79.50	-8.02			

Table A.3. Continued.

Sample Number	TxDOT			TTI		
	Average Texture		Percent Loss Txtr.	Average Texture		Percent Loss Txtr.
	BMD	AMD		BMD	AMD	
05-0083	73.60	80.70	-9.65			
05-0086	124.00	94.00	24.19			
05-0089	50.30	51.00	-1.39			
05-0093	53.80	30.20	43.87			
05-0109	51.10	61.10	-19.57			
05-0129	201.20	134.80	33.00	183.96	110.45	39.96
05-0143	83.30	100.90	-21.13			
05-0149	169.20	91.20	46.10	158.40	88.82	43.93
05-0151	115.70	92.60	19.97			
05-0161	110.40	97.00	12.14			
05-0178	72.30	42.10	41.77	79.47	41.70	47.53
05-0213	136.00	88.00	35.29	126.58	85.10	32.78
05-0216	92.20			79.67	50.32	36.84
05-0231	143.30	113.60		115.52	86.18	25.40
05-0235	165.30	128.00	22.57	145.68	115.39	20.79
05-0238	139.90	89.50	36.03	143.79	75.91	47.21
05-0239	173.00	137.10	20.75			
05-0245	225.40	146.00	35.23	171.11	124.71	27.11
05-0247	174.20	131.20	24.68	130.28	138.92	-6.63
05-0251	217.60	130.10	40.21	199.25	95.01	52.32
05-0266	483.90	413.40	14.57			
05-0317	140.50	125.90	10.39			
05-0320	120.00	202.60	-68.83			
05-0321	126.40	108.00	14.56			
05-0337	166.20	126.00	24.19			
05-0338	121.90	103.00	15.50			
05-0347	86.80	76.00	12.44	75.13	60.29	19.75
05-0350	153.90	116.10	24.56	150.44	109.14	27.46
05-0365	129.50	97.10	25.02	125.43	95.71	23.69
05-0368	84.50	47.10	44.26	63.74	52.64	17.42
05-0397	120.50	73.40	39.09	97.38	65.93	32.30
05-0399	99.60	57.40	42.37	81.21	51.36	36.76

Table A.3. Continued.

Sample Number	TxDOT			TTI		
	Average Texture		Percent Loss Txtr.	Average Texture		Percent Loss Txtr.
	BMD	AMD		BMD	AMD	
05-0493	79.50			70.14	46.74	33.37
05-0494	122.50			119.90	91.65	23.56
05-0496	82.30	60.60	26.37	59.40	51.60	13.13
05-0519	168.70	114.80	31.95	153.05	89.63	41.44
05-0532	134.90	105.30	21.94	106.48	78.63	26.16
05-0535	454.50	270.80	40.42	436.70	573.99	-31.44
05-0543	150.40			122.26	124.40	-1.76
05-0545	74.70	54.90	26.50	64.70	56.09	13.31
05-0630	111.60			89.24	81.10	9.12
05-0643	133.80	84.29	37.00	122.15	76.21	37.61
05-0649	86.70	51.18	40.97	79.00	47.80	39.49
05-0693	174.70	84.18	51.82	148.43	216.27	-45.70
05-0708	117.80			102.54	92.94	9.36
05-0768	112.56	108.34	3.75	122.45	88.48	27.74
05-0770	115.00	114.69	0.27	116.23	105.29	9.41
05-0771	180.99	111.78	38.24	204.36	142.26	30.39
05-0774	123.73	77.97	36.98	122.39	77.95	36.31
05-0822	167.80	103.28	38.45	193.10	165.05	14.52
05-0824	226.90	156.35	31.09	241.16	168.92	29.96
05-0826	184.90	157.48	14.83	185.32	176.75	4.63
05-0828	145.80	97.86	32.88	133.43	122.85	7.93
05-0832	213.80	111.37	47.91	192.87	114.16	40.81
05-0921	75.70	52.01	31.30	75.21	45.84	39.05
05-0922	103.50	85.78	17.12	111.23	66.51	40.20
05-0938	339.50	217.14	36.04	328.70	305.02	7.20
05-0941	120.20	91.18	24.14	122.21	106.71	12.69
05-0943	99.10	95.11	4.03	92.62	83.75	9.57
05-0946	144.70	78.67	45.63	151.08	111.53	26.18
05-0992	138.10	95.06	31.16	135.81	92.20	32.11
05-0995	122.00	63.71	47.78	115.89	65.10	43.82
05-1002	161.10	110.32	31.52	151.64	101.14	33.30
05-1009	103.35	98.89	4.32	122.98	72.52	41.03

Table A.3. Continued.

Sample Number	TxDOT			TTI		
	Average Texture		Percent Loss Txtr.	Average Texture		Percent Loss Txtr.
	BMD	AMD		BMD	AMD	
05-1183	99.20	64.14	35.34	84.86	49.40	41.78
05-1184	217.00	117.10	46.04	186.29	102.88	44.77
05-1190	90.40	77.59	14.17	84.46	69.42	17.81
05-1201	108.00	72.26	33.09	108.80	61.55	43.42
05-1205	197.60	82.52	58.24	177.88	100.68	43.40
05-1207	96.10	61.83	35.66	86.78	46.97	45.88
05-1210	91.00	77.61	14.72	93.12	62.73	32.63
05-1213	96.20	57.23	40.51	81.79	42.92	47.52
05-1221	104.36	81.37	22.03	98.70	68.79	30.31
05-1222	97.51	84.30	13.55	94.68	71.20	24.80
05-1223	83.73	54.50	34.92	88.77	51.59	41.88
05-1235	113.53	67.48	40.57	102.55	74.16	27.68
05-1236	102.03	62.61	38.64	106.57	57.07	46.44
05-1260	98.55	60.19	38.92	83.00	51.22	38.28
05-1262	142.68	113.14	20.70	147.21	96.43	34.50
05-1269	150.96	65.77	56.43			
05-1274	184.37	185.16	-0.43	218.51	197.25	9.73
05-1319	124.83	79.27	36.49	106.78	77.08	27.81
05-1360	95.49	63.25	33.76	89.16	60.09	32.61
05-1389	208.73	117.56	43.68	207.58	135.41	34.77
05-1419	168.66	93.63	44.49	207.33	107.48	48.16
05-1422	157.82	95.40	39.55	231.54	117.04	49.45
05-1468	234.84	127.72	45.61	234.04	149.27	36.22
06-0009	126.93	80.86	36.30	104.30	60.00	42.47
06-0082	402.52	317.38	21.15	489.76	606.21	-23.78
06-0086	92.45	55.72	39.73	73.18	45.18	38.27

Table A.4. Aggregate Sphericity.

Sample Number	TxDOT			TTI		
	Average Sphericity		Percent Loss Sph.	Average Sphericity		Percent Loss Sph.
	BMD	AMD		BMD	AMD	
04-1205	0.670	0.687	-2.43			
04-1220	0.671	0.694	-3.56			
04-1277	0.651	0.662	-1.67			
04-1283	0.688	0.646	6.12			
04-1285	0.637	0.686	-7.64			
04-1300	0.712	0.707	0.72			
04-1307	0.695	0.690	0.72			
05-0005	0.602	0.654	-8.72			
05-0007	0.683	0.690	-1.00			
05-0009	0.627	0.676	-7.75			
05-0011	0.708	0.717	-1.31			
05-0014	0.687	0.704	-2.38			
05-0017	0.708	0.699	1.29			
05-0020	0.682	0.704	-3.24			
05-0029	0.733	0.718	2.04			
05-0041	0.759	0.738	2.82	0.815	0.750	8.00
05-0048	0.674	0.648	3.80			
05-0077	0.680					
05-0081	0.665	0.672	-0.97			
05-0083	0.668	0.660	1.09			
05-0086	0.709	0.665	6.20			
05-0089	0.649	0.640	1.39			
05-0093	0.684	0.700	-2.37			
05-0109	0.680	0.671	1.31			
05-0129	0.670	0.694	-3.62	0.704	0.773	-9.82
05-0143	0.647	0.672	-3.97			
05-0149	0.690	0.683	1.03	0.674	0.688	-2.17
05-0151	0.673	0.672	0.21			
05-0161	0.692	0.675	2.48			
05-0178	0.640	0.672	-4.99	0.659	0.735	-11.48
05-0213	0.692	0.676	2.35	0.738	0.713	3.33
05-0216	0.637			0.685	0.641	6.37

Table A.4. Continued.

Sample Number	TxDOT			TTI		
	Average Sphericity		Percent Loss Sph.	Average Sphericity		Percent Loss Sph.
	BMD	AMD		BMD	AMD	
05-0231				0.727	0.697	4.07
05-0235	0.695	0.717	-3.03	0.707	0.784	-11.00
05-0238	0.693	0.683	1.44	0.729	0.692	5.06
05-0239	0.689	0.725	-5.24			
05-0245	0.726	0.727	-0.22	0.721	0.755	-4.70
05-0247	0.699	0.711	-1.83	0.676	0.795	-17.66
05-0251	0.684	0.705	-3.16	0.698	0.752	-7.66
05-0266	0.724	0.695	3.96			
05-0317	0.681	0.688	-0.93			
05-0320	0.710	0.716	-0.92			
05-0321	0.625	0.641	-2.55			
05-0337	0.705	0.695	1.55			
05-0338	0.714	0.679	4.84			
05-0347	0.661	0.629	4.91	0.650	0.699	-7.55
05-0350	0.717	0.686	4.27	0.699	0.740	-5.85
05-0365	0.667	0.689	-3.30	0.683	0.733	-7.43
05-0368	0.627	0.635	-1.27	0.668	0.681	-2.02
05-0397	0.695	0.701	-0.88	0.732	0.783	-6.92
05-0399	0.647	0.682	-5.34	0.651	0.730	-12.10
05-0493	0.651			0.664	0.716	-7.96
05-0494	0.667			0.677	0.670	0.99
05-0496	0.590	0.638	-8.11	0.681	0.660	3.00
05-0519	0.673	0.611	9.19	0.681	0.665	2.21
05-0521						
05-0532	0.688	0.686	0.30	0.688	0.673	2.06
05-0534			-			
05-0535	0.699	0.677	3.13	0.716	0.703	1.82
05-0543	0.697			0.699	0.775	-10.82
05-0545	0.644	0.695	-7.83	0.662	0.664	-0.25
05-0630	0.623			0.616	0.647	-5.10
05-0643	0.690	0.705	-2.14	0.683	0.695	-1.82
05-0649	0.685			0.675	0.673	0.35

Table A.4. Continued.

Sample Number	TxDOT			TTI		
	Average Sphericity		Percent Loss Sph.	Average Sphericity		Percent Loss Sph.
	BMD	AMD		BMD	AMD	
05-0693	0.685			0.747	0.696	6.75
05-0708	0.690			0.650	0.748	-15.12
05-0768	0.672	0.669	0.48	0.660	0.668	-1.20
05-0770	0.679	0.655	3.54	0.663	0.668	-0.71
05-0771	0.677	0.671	0.87	0.665	0.706	-6.24
05-0774	0.636	0.643	-1.10	0.673	0.641	4.73
05-0822	0.716	0.691	3.57	0.663	0.696	-5.03
05-0824	0.631	0.603	4.46	0.615	0.659	-7.01
05-0826	0.703	0.672	4.38	0.682	0.693	-1.67
05-0828	0.653	0.651	0.25	0.646	0.677	-4.79
05-0832	0.707	0.703	0.45	0.721	0.684	5.18
05-0921	0.679	0.640	5.85	0.665	0.667	-0.27
05-0922	0.703	0.648	7.91	0.681	0.677	0.60
05-0938	0.660	0.654	1.01	0.617	0.622	-0.87
05-0941	0.720	0.688	4.56	0.695	0.731	-5.24
05-0943	0.687	0.667	2.87	0.669	0.736	-10.06
05-0946	0.670	0.626	6.61	0.623	0.642	-3.13
05-0992	0.735	0.673	8.48	0.686	0.713	-3.98
05-0995	0.683	0.660	3.41	0.631	0.661	-4.68
05-1002	0.727	0.644	11.41	0.702	0.697	0.62
05-1009	0.706	0.676	4.25	0.710	0.725	-2.15
05-1183	0.670	0.638	4.71	0.658	0.667	-1.33
05-1184	0.675	0.655	2.91	0.661	0.654	1.00
05-1190	0.677	0.680	-0.46	0.705	0.673	4.50
05-1201	0.706	0.690	2.32	0.676	0.678	-0.42
05-1205	0.673	0.679	-0.87	0.642	0.668	-4.12
05-1207	0.719	0.670	6.80	0.681	0.684	-0.40
05-1210	0.634	0.629	0.85	0.645	0.662	-2.72
05-1213	0.697	0.668	4.05	0.660	0.713	-8.11
05-1221	0.665	0.666	-0.21	0.633	0.678	-7.10
05-1222	0.668	0.660	1.18	0.649	0.700	-7.96
05-1223	0.678	0.673	0.82	0.655	0.654	0.16

Table A.4. Continued.

Sample Number	TxDOT			TTI		
	Average Sphericity		Percent Loss Sph.	Average Sphericity		Percent Loss Sph.
	BMD	AMD		BMD	AMD	
05-1235	0.679	0.675	0.63	0.683	0.695	-1.75
05-1236	0.668	0.676	-1.26	0.684	0.680	0.49
05-1260	0.689	0.680	1.37	0.709	0.725	-2.25
05-1262	0.660	0.693	-4.88	0.682	0.687	-0.85
05-1269	0.682	0.694	-1.81			
05-1274	0.659	0.679	-3.04	0.713	0.703	1.40
05-1319	0.667	0.650	2.53	0.733	0.672	8.41
05-1360	0.661	0.663	-0.37	0.684	0.655	4.16
05-1389	0.659	0.665	-0.90	0.735	0.659	10.31
05-1419	0.684	0.685	-0.07	0.719	0.696	3.18
05-1422	0.685	0.665	2.95	0.672	0.682	-1.46
05-1468	0.667	0.700	-4.91	0.760	0.686	9.75
06-0009	0.676	0.679	-0.35	0.716	0.586	18.15
06-0082	0.671	0.681	-1.41	0.668	0.687	-2.92
06-0086	0.644	0.624	3.15	0.673	0.639	5.03

Table A.5. Aggregate Durability and Deleterious Materials Test Results.

Sample Number	Percent Loss MD		Mg. Soundness		Percent Loss L.A. Abrasion
	TxDOT	TTI	HMAC	Surface Treatment	
04-1205	17.0	16.9	9	5	
04-1220	18.3	16.3	8	4	
04-1277	17.6	17.0	17	14	
04-1283	24.3	24.4	20	16	
04-1285	20.5	20.6	15	10	
04-1300	21.0	19.5	18	15	
04-1307	30.7	29.5	25	19	
05-0005	13.0	11.7	6	5	
05-0007	12.5	10.5	5	4	
05-0009	11.4	10.8	6	5	
05-0011	7.9	7.2	5	4	

Table A.5. Continued.

Sample Number	Percent Loss MD		Mg. Soundness		Percent Loss L.A. Abrasion
	TxDOT	TTI	HMAC	Surface Treatment	
05-0014	9.3	9.0	8	5	
05-0017	10.9	9.0	9	7	
05-0020	9.2	5.7	7	5	
05-0029	6.2	5.3	13	10	
05-0041	27.6	22.5	10	14	
05-0048	12.0	11.3	7	6	
05-0077	1.8	1.3	2	2	
05-0081	7.2	7.0	3	2	
05-0083	8.6	8.4	5	3	
05-0086	16.3	17.1	18	16	
05-0089	7.2	6.6	6	5	
05-0093	31.1	19.1	20	15	
05-0109	34.9	35.1	42	35	
05-0129	11.0	10.9	8	7	
05-0143	15.5	14.2	7	6	
05-0149	15.9	15.1	11	9	
05-0151	16.7	16.3	18	16	
05-0161	7.3	6.4	11	8	
05-0178	21.7	20.1	25	22	
05-0213	16.7	15.0	8	7	25
05-0216	10.4	10.6	7	7	27
05-0231	8.3	8.2	5	5	21
05-0235	2.7	2.4	3	2	18
05-0238	10.2	9.6	5	4	19
05-0239	7.3		8	5	20
05-0245	2.8	3.2	3	2	18
05-0247	3.7	4.2	3	3	17
05-0251	11.4	11.5	6	5	23
05-0266	23.5	18.0	27	22	
05-0317	2.6	7.6	4	2	11
05-0320	8.1	7.1	11	7	19
05-0321	14.6	13.9	11	7	25
05-0337	11.2		16	14	23

Table A.5. Continued.

Sample Number	Percent Loss MD		Mg. Soundness		Percent Loss L.A. Abrasion
	TxDOT	TTI	HMAC	Surface Treatment	
05-0338	5.2	4.1	9	5	21
05-0347	31.5	29.5	34	27	33
05-0350	15.3	14.6	25	20	33
05-0365	26.4	24.6	30	25	33
05-0368	32.7	28.5	25	22	29
05-0397	19.4	18.4	11	9	27
05-0399	23.1	23.6	20	16	29
05-0493	30.9	29.0	26	21	30
05-0494	26.4	19.1	30	25	31
05-0496	31.2	14.9	57	50	43
05-0519	18.5	18.2	16	15	25
05-0521	19.6		30	20	35
05-0532	19.9	19.5	22	14	27
05-0534			27	18	28
05-0535	22.8	22.5	26	20	
05-0543	4.9	3.5	7	5	19
05-0545	33.7	29.5	27	20	31
05-0630		9.8	19	16	31
05-0643	21.5	19.1			
05-0649		24.9	18	14	30
05-0693	7.9	7.3			
05-0708	8.1	8.0	9	9	26
05-0715	9.1		22	19	32
05-0716			23	20	29
05-0719			29	26	32
05-0768	10.0	9.1	3	3	27
05-0770	9.0	9.3	3	3	22
05-0771	12.0	10.6	6	6	20
05-0774	6.0	6.4	3	3	21
05-0800	16.3		19	17	25
05-0806	11.8		7	7	19
05-0822	6.0	5.4	2	2	18
05-0824	9.0	8.6	3	3	21

Table A.5. Continued.

Sample Number	Percent Loss MD		Mg. Soundness		Percent Loss L.A. Abrasion
	TxDOT	TTI	HMAC	Surface Treatment	
05-0826	8.0	7.7	3	3	33
05-0828	6.0	5.3	5	5	26
05-0832	12.0	11.5	11	10	22
05-0921	24.0	23.3	28	25	29
05-0922	24.0	23.8	23	22	32
05-0938	4.4	4.0	2	2	28
05-0941	3.4	2.9	3	3	19
05-0943	3.0	2.8	4	4	21
05-0946	7.3	6.3	2	2	14
05-0992	17.0	16.7	6	6	31
05-0995	10.0	10.2	3	3	26
05-1002	22.2	19.5	19	13	26
05-1009	18.0	17.9	9	10	26
05-1183	24.1	23.5	23	20	30
05-1184		13.5	5	5	24
05-1190		8.6	20	12	32
05-1194	27.0		24	19	30
05-1201	17.0	14.9	4	4	27
05-1205	8.7	8.2	7	7	18
05-1207	27.0	27.7	30	23	31
05-1210	13.3	12.7	23	18	34
05-1213	26.0	22.9	25	20	30
05-1221	12.0	10.9	19	17	34
05-1222	9.0	8.1	9	9	29
05-1223	27.0	23.6	19	14	29
05-1235	25.8	26.2	19	17	30
05-1236	21.1	20.9	2	9	28
05-1260	21.4	21.7	23	14	29
05-1262	18.2	17.1	2	6	26
05-1274	7.5	7.2	0	6	18
05-1314	11.6		8	6	21
05-1319	22.0		11	7	29

Table A.5. Continued.

Sample Number	% Loss MD		Mg. Soundness		% Loss L.A. Abrasion
	TxDOT	TTI	HMAC	Surface Treatment	
05-1341	22.0		21	16	36
05-1357	20.0		12	11	28
05-1358	22.0		14	13	28
05-1359	22.8		11	9	29
05-1360	24.0	22.7	11	9	29
05-1361	23.0		20	15	30
05-1389		14.4			
05-1412	5.0		9	7	20
05-1419	14.0	12.9	27	24	24
05-1422	13.0	11.4	5	4	23
05-1423	6.0		1	1	13
05-1425	28.0		23	22	30
05-1468		9.2			
06-0004	26.0		17	15	30
06-0009	22.0	19.6	9	9	27
06-0025	10.0		10	8	25
06-0028	23.0		19	17	29
06-0031	5.0		3	4	23
06-0041	26.0		33	30	29
06-0078	20.0		24	16	14
06-0082	19.0	19.8	18	18	33
06-0086	22.0	20.1	21	22	30
06-0087	20.0		17	16	27
06-0107	15.0		16	16	25
06-0116	9.0		6	7	19
06-0121	14.0		8	10	25
06-0136	10.0				34
06-0143	7.0				19
06-0162	24.0		16	13	29
06-0175	7.0		9	10	18
06-0182	23.0		18	12	29
06-0196	20.0		19	17	26
06-0199	9.0		4	4	19

Table A.6. Other AQMP Measurements.

Sample Number	Percent >		Percent CFC>2	Flakiness	PSV	
	3:1	5:1			Initial	Final
06-0257	22.0		17	16	28	
04-1205	1	1		19	39	22
04-1220	1	2		12	43	23
04-1277	5	4		16	42	23
04-1283	3	2		11	46	25
04-1285	2	2		16	49	24
04-1300	1	0		3	47	26
04-1307	2	0		4	50	25
05-0005	9	7		24		29
05-0007	7	4	99	13	42	23
05-0009	5	5		27	41	21
05-0011	3	2		7	50	33
05-0014	2	3	99	15	43	30
05-0017	3	2	97	12	42	31
05-0020	2	1	98	15	47	29
05-0029	2	2	85	11		
05-0041	0	0		2	50	48
05-0048	2	0	66	11		23
05-0077	1	0	94	6	41	25
05-0081	4	4		12		22
05-0083	8	4		20		23
05-0086	4	4		24	46	40
05-0089	6	5		27		24
05-0093	1	0		12		25
05-0109	2	1		9		25
05-0129	1	1		16	42	25
05-0143	2	2		28	40	21
05-0149	2	3		27		24
05-0151	2	0		27		24
05-0161	3	2	89	7	35	23
05-0178	1	1		17	45	27
05-0213	2	0		7	41	21
05-0216	7	0		22	41	25

Table A.6. Continued.

Sample Number	Percent >		Percent CFC>2	Flakiness	PSV	
	3:1	5:1			Initial	Final
05-0231	2	1	86	12	36	24
05-0235	3	2	97	5	42	26
05-0238	2	0	86	7	40	25
05-0239	3	1	96	11	42	27
05-0245	0	0	86	15	42	25
05-0247	0	0	95	9	42	26
05-0251	1	0		4	40	21
05-0266	1	2		10		35
05-0317	1	0		22		29
05-0320	0	0		11		35
05-0321	6	3		33		25
05-0337	1	1	79	16		27
05-0338			61			24
05-0347				10		26
05-0350	1	1		12	45	33
05-0365	1	0		9	46	25
05-0368	1	1		15	48	27
05-0397	0	0		10		24
05-0399	3	1		7	43	26
05-0493	3	1		14		25
05-0494	3	0		10		23
05-0496	5	1		18		35
05-0519	2	1		19	42	23
05-0521	0	0		8	50	35
05-0532	0	0		8	46	28
05-0534					42	25
05-0535	0	0		5	51	35
05-0543	3	1	96	8	42	26
05-0545	3	2		10	46	27
05-0630	4	0		32	50	34
05-0643	1	0		6	45	27
05-0649	0	0		11	45	25
05-0693	0	0		11	46	32

Table A.6. Continued.

Sample Number	Percent >		Percent CFC>2	Flakiness	PSV	
	3:1	5:1			Initial	Final
05-0708	6	1		25	47	35
05-0715					45	26
05-0716					44	25
05-0719					44	25
05-0768	2	0		14	40	23
05-0770	2	1		11		
05-0771						
05-0774	3	2		13		
05-0800			61		41	24
05-0806					44	31
05-0822	2	2		10		
05-0824	7	6		25		
05-0826	2	1		13		
05-0828	3	3		16		30
05-0832	3	2		17		27
05-0921	2	2		12		
05-0922	0	0		9	45	25
05-0938	3	2		19	41	26
05-0941	1	1	98	6	43	30
05-0943	1	1	91	5		
05-0946	8	6		20		
05-0992	1	0		3		24
05-0995	2	1		8		
05-1002	1	1		8	42	37
05-1009	0	0	95	3		
05-1183	2	1		6	43	25
05-1184	2	1		9	43	21
05-1190	5	4		15	48	
05-1194					43	25
05-1201	1	1		8		25
05-1205	3	3		14		31
05-1207	2	1		8		26
05-1210	8	8		25	47	32

Table A.6. Continued.

Sample Number	Percent >		Percent CFC>2	Flakiness	PSV	
	3:1	5:1			Initial	Final
05-1213	1	1		7		26
05-1221	5	4		16	46	
05-1222	4	2		12	49	31
05-1223	1	1		7	43	23
05-1235	1	0		8		25
05-1236	1	1		7		25
05-1260	2	1		3		
05-1262	1	1		7	40	32
05-1269	1	1		15	47	
05-1274	1	1	100	8	45	30
05-1314	2	1		10	20	
05-1319	0	0		5		
05-1341	0	0		4	30	
05-1354						
05-1357	1	0		4		
05-1358	1	1		7		
05-1359	3	3		7		26
05-1360	1	2		9		25
05-1361	2	2		7		26
05-1412	2	4	95	7		
05-1419	1	1	98	4		
05-1422	2	1		8		
05-1423	1	1		1		
05-1425	2	2		8		
06-0004				4		23
06-0009	2	2		6		24
06-0025	1	1		6		
06-0028	2	2		15		20
06-0031		7		16		
06-0041				12		
06-0078		3		19		
06-0082	3	3		6		30
06-0086	8	7		15		21

Table A.6. Continued.

Sample Number	Percent >		Percent CFC>2	Flakiness	PSV	
	3:1	5:1			Initial	Final
06-0087		2		9		21
06-0107	0	0		5		22
06-0116	2	2		9		26
06-0121		9		28		24
06-0136			100	16		
06-0143			90	3		
06-0162				7		25
06-0175		1	92	10		28
06-0182				3		20
06-0196			87	5		22
06-0199				7		26
06-0257				8		

Table A.7. Modified Angularity Summary.

Sample Number	TxDOT			TTI		
	Average Ang Mod		Percent Loss Ang Mod	Average Ang Mod		Percent Loss Ang Mod
	BMD	AMD		BMD	AMD	
04-1205	2723.26	1856.86	31.81	2837.62	1874.87	33.93
04-1220	3000.67	1791.79	40.29	3000.11	1771.93	40.94
04-1277	2909.11	1868.09	35.79	2950.52	1977.80	32.97
04-1283	2967.15	1746.30	41.15	3039.58	1764.14	41.96
04-1285	3508.81	2071.90	40.95	3388.36	2114.35	37.60
04-1300	2938.05	1590.52	45.86	2655.18	1601.09	39.70
04-1307	3320.66	1589.88	52.12	3252.61	1702.94	47.64
05-0005	3131.34	2157.82	31.09	3079.95	2243.34	27.16
05-0007	3048.51	2120.62	30.44	2998.58	2074.90	30.80
05-0009	3168.70	2193.40	30.78	3057.21	2160.89	29.32
05-0011	2567.77	2567.77	0.00	3197.64	2604.69	18.54
05-0014	2950.34	2453.75	16.83	3011.37	2169.38	27.96
05-0017	2664.01	2019.63	24.19	2815.31	2168.95	22.96
05-0020	3132.24	2178.32	30.45	2926.72	2287.43	21.84

Table A.7. Continued.

Sample Number	TxDOT			TTI		
	Average Ang Mod		Percent Loss Ang Mod	Average Ang Mod		Percent Loss Ang Mod
	BMD	AMD		BMD	AMD	
05-0029	2954.28	2143.18	27.46	2915.49	2266.94	22.24
05-0041	2321.05	1285.17	44.63	2332.81	1329.99	42.99
05-0048	2258.98	1766.02	21.82	2371.38	1764.85	25.58
05-0077	3029.10	2984.40	1.48	3091.43	2791.60	9.70
05-0081	3103.15	2186.07	29.55	3194.86	2360.40	26.12
05-0083	3159.67	2275.97	27.97	3059.12	2193.20	28.31
05-0086	2860.95	1900.60	33.57	2734.55	1831.05	33.04
05-0089	3076.53	2217.30	27.93	3169.81	2327.35	26.58
05-0093	2770.51	1770.52	36.09	2818.53	1734.29	38.47
05-0109	2967.75	1958.69	34.00	2900.62	1949.67	32.78
05-0129	2955.22	1997.31	32.41	2797.51	1981.65	29.16
05-0143	2866.36	1826.70	36.27	2994.77	1868.82	37.60
05-0149	2888.83	1844.59	36.15	2763.48	1906.07	31.03
05-0151	2979.70	1898.64	36.28	3049.67	1906.26	37.49
05-0161	2973.44	2836.87	4.59	2879.18	2854.40	0.86
05-0178	3147.99	1835.70	41.69	3101.93	1858.76	40.08
05-0213	3020.90	1911.34	36.73	3002.96	1912.04	36.33
05-0216	3062.77			3029.35	2073.25	31.56
05-0231				2449.73	1652.40	32.55
05-0235	2851.05	2743.04	3.79	2839.87	2657.10	6.44
05-0238	2587.89	1961.69	24.20	2521.39	1852.33	26.54
05-0239	2986.82	2436.17	18.44			
05-0245	2955.66	2650.16	10.34	2847.52	2563.67	9.97
05-0247	3098.83	2561.59	17.34	2953.07	2730.06	7.55
05-0251	2855.27	2757.68	3.42	2654.50	1712.21	35.50
05-0266	3208.41	1712.47	46.63	2970.85	1831.45	38.35
05-0317	3185.17	2225.87	30.12	3212.17	2228.24	30.63
05-0320	3388.00	2389.94	29.46	3192.02	2408.45	24.55
05-0321	3067.77	1998.72	34.85	3086.39	2107.40	31.72
05-0337	3139.09	2676.95	14.72			
05-0338	2692.61	1795.95	33.30	2994.92	2654.59	11.36
05-0347	3176.68	1998.43	37.09	2996.89	2010.38	32.92

Table A.7. Continued.

Sample Number	TxDOT			TTI		
	Average Ang Mod		Percent Loss Ang Mod	Average Ang Mod		Percent Loss Ang Mod
	BMD	AMD		BMD	AMD	
05-0350	2943.91	1851.51	37.11	2900.15	1869.50	35.54
05-0365	3416.27	2072.98	39.32	3430.12	2071.74	39.60
05-0368	3200.20	1881.26	41.21	3023.72	1902.51	37.08
05-0397	2860.36	1740.25	39.16	2897.98	1677.25	42.12
05-0399	3048.91	1698.41	44.29	2906.93	1737.67	40.22
05-0493	3093.18			3070.58	1946.48	36.61
05-0494	3340.45			3197.17	2190.24	31.49
05-0496	2624.19	2083.87	20.59	2684.66	1997.93	25.58
05-0519	2922.91	1955.92	33.08	2803.28	1940.13	30.79
05-0532	3000.46	1555.51	48.16	2880.76	1570.19	45.49
05-0535	3123.44	1628.75	47.85	3032.05	1528.87	49.58
05-0543	2906.21			2820.33	2556.95	9.34
05-0545	3036.73	1923.27	36.67	3052.54	1906.92	37.53
05-0630	2979.95			2958.83	2266.18	23.41
05-0643	2904.03	1703.40	41.34	3031.57	1798.98	40.66
05-0649	2788.92			2923.98	1744.71	40.33
05-0693	3209.55			3307.12	2455.10	25.76
05-0708	2771.35			2725.34	2044.79	24.97
05-0768	3147.85	2282.02	27.51	3158.71	2211.73	29.98
05-0770	3042.83	2224.66	26.89	3135.24	2030.84	35.23
05-0771	2941.58	1859.30	36.79	2936.49	1906.72	35.07
05-0774	3047.41	2416.80	20.69	3069.83	2297.66	25.15
05-0822	3137.25	2670.74	14.87	3008.95	2760.88	8.24
05-0824	3182.12	2345.43	26.29	3157.55	2266.77	28.21
05-0826	3406.05	2767.79	18.74	3523.23	2932.79	16.76
05-0828	2798.92	2040.50	27.10	2806.69	2127.38	24.20
05-0832	2877.08	1999.99	30.49	2890.27	1982.16	31.42
05-0921	3176.90	2050.84	35.45	3017.52	1774.23	41.20
05-0922	2940.30	1910.36	35.03	2888.07	1737.41	39.84
05-0938	3279.25	2681.73	18.22	3278.82	2831.25	13.65
05-0941	2999.88	2628.16	12.39	2994.70	2520.44	15.84
05-0943	2859.53	2479.91	13.28	2830.56	2510.91	11.29

Table A.7. Continued.

Sample Number	TxDOT			TTI		
	Average AngMod		Percent Loss AngMod	Average AngMod		Percent Loss AngMod
	BMD	AMD		BMD	AMD	
05-0946	3257.83	2558.27	21.47	3224.17	2563.01	20.51
05-0992	3298.09			3189.40	1907.88	40.18
05-0995	3051.85	2201.44	27.87	3131.24	1993.28	36.34
05-1002	2976.90			2782.05	1738.58	37.51
05-1009	2491.79			2355.26	1460.55	37.99
05-1183	3008.07	1860.14	38.16	2970.85	1956.66	34.14
05-1184	2807.32	1803.29	35.76	2808.02	1809.77	35.55
05-1190	2733.56	2066.53	24.40	2816.46	2141.05	23.98
05-1201	2851.66	1718.26	39.75	2936.46	1869.29	36.34
05-1205	2910.65	2132.94	26.72	2937.24	2250.02	23.40
05-1207	2940.39	1881.31	36.02	2880.20	1817.08	36.91
05-1210	2802.69	2232.77	20.33	2840.76	2175.40	23.42
05-1213	2984.22	1902.37	36.25	2890.96	1739.55	39.83
05-1221	2748.13	2169.16	21.07	2785.28	2102.91	24.50
05-1222	2687.71	2054.98	23.54	2725.96	1998.00	26.70
05-1223	3053.75	1900.55	37.76	3044.18	1922.25	36.85
05-1235	2905.92	1624.20	44.11	2914.53	1697.84	41.75
05-1236	2804.02	2010.35	28.30	2794.86	1936.00	30.73
05-1260	2969.71	1889.52	36.37	2841.91	1798.38	36.72
05-1262	2906.02	1570.40	45.96	2883.40	1834.20	36.39
05-1269	2934.63	1837.24	37.39			-
05-1274	3275.33	2401.96	26.67	3191.16	2473.88	22.48
05-1319	3111.08	1943.35	37.53	3054.49	1842.97	39.66
05-1360	2938.38	1960.64	33.27	2862.61	1980.36	30.82
05-1389	2823.28	1873.13	33.65	2755.14	1872.14	32.05
05-1419	2943.42	2632.77	10.55	2871.23	2609.94	9.10
05-1422	2867.17	1900.45	33.72	2885.94	1922.83	33.37
05-1468	2872.47	2047.90	28.71	2940.79	2019.49	31.33
06-0009	3076.78	1785.73	41.96	2872.65	1894.10	34.06
06-0082	2766.98	1747.48	36.85	2712.25	1650.99	39.13
06-0086	3092.34	2041.00	34.00	2978.50	2130.01	28.49

Table A.8. Average of Texture Levels 4 and 5.

Sample Number	TxDOT			TTI		
	Average Texture		Percent Loss Txtr.	Average Texture		Percent Loss Txtr.
	BMD	AMD		BMD	AMD	
04-1205	160.61	99.33	38.15			
04-1220	150.64	91.25	39.43			
04-1277	257.41	148.24	42.41			
04-1283	148.71	89.02	40.14			
04-1285	205.27	130.52	36.41			
04-1300	181.23	36.89	79.64			
04-1307	66.29	56.34	15.01			
05-0005	115.25	60.74	47.29			
05-0007	70.23	44.18	37.09			
05-0009	126.51	73.76	41.70			
05-0011	99.94	91.39	8.55			
05-0014	102.57	95.41	6.99			
05-0017	89.00	84.55	5.00			
05-0020	82.64	87.32	-5.66			
05-0029	84.69	87.83	-3.71			
05-0041	110.85	88.18	20.45	113.14	112.55	0.52
05-0048	83.19	78.96	5.08			
05-0077	74.88					
05-0081	55.54	56.46	-1.65			
05-0083	57.90	62.12	-7.29			
05-0086	104.31	92.43	11.39			
05-0089	48.96	49.68	-1.48			
05-0093	39.51	26.67	32.49			
05-0109	39.91	49.51	-24.06			
05-0129	151.12	100.95	33.20	177.19	99.50	43.84
05-0143	57.64	65.32	-13.33			
05-0149	120.65	68.95	42.85	134.12	79.00	41.10
05-0151	74.43	66.34	10.87			
05-0161	86.91	81.22	6.55			
05-0178	59.82	41.42	30.75	62.85	36.31	42.23
05-0213	89.92	61.30	31.83	102.92	72.27	29.78
05-0216	59.23			58.08	36.96	36.37

Table A.8. Continued.

Sample Number	TxDOT			TTI		
	Average Texture		Percent Loss Txtr.	Average Texture		Percent Loss Txtr.
	BMD	AMD		BMD	AMD	
05-0231				117.02	89.86	23.21
05-0235	134.05	105.00	21.67	141.69	100.30	29.21
05-0238	106.73	69.90	34.50	134.03	74.90	44.12
05-0239	140.44	100.72	28.29			
05-0245	177.05	116.15	34.40	167.33	99.58	40.49
05-0247	147.74	102.64	30.53	148.02	107.50	27.37
05-0251	147.31	96.34	34.60	161.17	79.64	50.59
05-0266	381.68	392.58	-2.86			
05-0317	153.50	136.05	11.36			
05-0320	93.23	150.67	-61.61			
05-0321	84.76	77.28	8.82			
05-0337	141.60	93.40	34.04			
05-0338	100.36	75.52	24.75			
05-0347	69.61	59.82	14.07	66.24	55.90	15.61
05-0350	106.62	78.57	26.31	128.45	86.52	32.64
05-0365	89.56	65.30	27.09	99.68	74.39	25.37
05-0368	58.50	39.18	33.03	65.66	52.70	19.72
05-0397	83.04	56.73	31.68	93.07	59.50	36.07
05-0399	69.17	43.37	37.30	74.78	45.68	38.92
05-0493	58.05			61.26	48.97	20.06
05-0494	85.27			96.99	71.08	26.71
05-0496	71.42	50.62	29.13	71.07	54.45	23.38
05-0519	109.58	75.30	31.28	132.23	79.94	39.55
05-0521						
05-0532	90.11	72.46	19.59	86.80	65.56	24.47
05-0534						
05-0535	467.90	216.34	53.76	325.49	357.57	-9.85
05-0543	117.77			115.69	95.90	17.10
05-0545	55.50	41.88	24.54	61.01	53.33	12.60
05-0630	115.17			114.41	94.27	17.61
05-0643	93.73	61.17	34.74	104.57	68.98	34.03
05-0649	61.92			69.15	50.83	26.49

Table A.8. Continued.

Sample Number	TxDOT			TTI		
	Average Texture		Percent Loss Txtr.	Average Texture		Percent Loss Txtr.
	BMD	AMD		BMD	AMD	
05-0693	137.49			131.28	157.09	-19.66
05-0708	129.58			132.77	114.48	13.77
05-0768	75.22	67.08	10.82	84.17	70.44	16.31
05-0770	103.29	82.20	20.42	104.52	94.73	9.37
05-0771	197.46	105.23	46.71	223.05	162.03	27.36
05-0774	138.81	70.98	48.87	141.32	86.88	38.52
05-0822	150.27	85.11	43.36	192.69	154.67	19.73
05-0824	188.19	120.85	35.78	243.54	174.30	28.43
05-0826	137.82	103.70	24.76	146.81	124.45	15.23
05-0828	157.02	96.63	38.46	184.38	152.09	17.51
05-0832	157.79	90.98	42.34	162.46	108.68	33.11
05-0921	47.66	34.09	28.48	56.31	38.26	32.06
05-0922	76.55	59.69	22.03	88.44	64.76	26.78
05-0938	232.15	147.21	36.59	235.66	213.88	9.24
05-0941	91.10	63.25	30.57	105.55	89.55	15.15
05-0943	78.29	64.90	17.10	81.87	68.29	16.59
05-0946	168.29	70.12	58.33	223.58	131.67	41.11
05-0992	91.76	60.83	33.70	96.45	75.35	21.87
05-0995	74.39	42.62	42.72	77.22	50.51	34.59
05-1002	118.68	81.74	31.12	133.35	98.49	26.14
05-1009	81.94	74.18	9.48	112.33	75.31	32.96
05-1183	63.48	42.14	33.61	59.99	45.95	23.40
05-1184	142.10	84.09	40.83	141.62	96.20	32.07
05-1190	89.07	67.07	24.70	101.06	84.45	16.44
05-1201	77.63	50.48	34.98	86.44	59.79	30.83
05-1205	176.04	75.53	57.10	187.75	119.61	36.29
05-1207	61.53	44.03	28.44	65.61	48.15	26.62
05-1210	95.93	71.14	25.84	113.74	77.82	31.58
05-1213	61.43	41.91	31.78	67.59	42.47	37.16
05-1221	101.04	71.57	29.16	119.72	78.45	34.47
05-1222	95.50	76.25	20.16	115.04	88.50	23.07
05-1223	57.89	40.08	30.77	66.90	48.18	27.98

Table A.8. Continued.

Sample Number	TxDOT			TTI		
	Average Texture		Percent Loss Txtr.	Average Texture		Percent Loss Txtr.
	BMD	AMD		BMD	AMD	
05-1235	72.70	47.56	34.59	84.46	64.56	23.56
05-1236	70.30	47.67	32.19	85.70	55.49	35.25
05-1260	66.55	42.66	35.91	68.40	49.44	27.72
05-1262	95.42	80.14	16.02	121.24	91.09	24.86
05-1269	100.25	47.09	53.02			
05-1274	131.06	136.63	-4.24	175.37	153.94	12.22
05-1319	77.78	54.86	29.48	78.04	60.11	22.98
05-1360	69.08	52.12	24.55	75.51	50.79	32.74
05-1389	140.51	96.90	31.04	161.26	106.41	34.01
05-1419	128.58	72.05	43.96	177.96	89.51	49.70
05-1422	134.72	94.50	29.86	246.63	121.75	50.63
05-1468	194.19	113.73	41.43	214.90	143.08	33.42
06-0009	81.30	63.74	21.60	77.38	56.58	26.88
06-0082	279.45	212.72	23.88	344.68	375.79	-9.03
06-0086	64.52	37.33	42.14	60.41	38.39	36.46

VITA

Anthony David Luce was born in Grand Rapids, Michigan. He was awarded a Bachelor of Science in Civil Engineering, Cum Laude, in May 2005 and a Master of Science in Civil Engineering in December 2006 from Texas A&M University. While working toward his degree, he worked as a research assistant at the Texas Transportation Institute (TTI) in College Station, Texas.

He currently resides in Cypress, Texas, and is employed by Brown & Gay Engineers, Inc., in Houston, Texas. His permanent address is 18415 Lodgepole Pine Street, Cypress, Texas 77429.